THE UNIVERSITY OF HULL

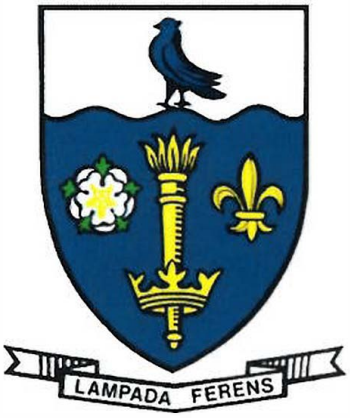

Development of a microfluidic approach to the analysis of carbamate pesticides in drinking water

being a Thesis submitted for the Degree of

Doctor of Philosophy

in the University of Hull

by

Jari Saeed Gery Algethami

BSc (Umm Al-Qura University, Kingdom of Saudi Arabia)

MSc (University of Hull, United Kingdom)

September 2016

Abstract

During the last decade, public concern over carbamate pesticide residues has increased remarkably and their accurate determination in environmental samples is gaining great importance. These compounds are present in environmental samples at low concentration levels; one or several pre-concentration steps are therefore required to isolate the target analytes, bring them to an appropriate concentration level, and remove matrix interference components. This work describes the development of an analytical approach to ultimately allow the combined extraction and detection of eserine, as an example of a carbamate pesticide, within a single microfluidic device.

The current study has been based on the use of the well-known approach using solid-phase extraction (SPE) for eserine sample preparation, with a silica-based monolith used as an SPE sorbent. A silica-based monolith rod was fabricated by the sol-gel process and modified with octadecyl groups for eserine extraction. This sorbent material was found to have a good surface area of approximately 312 $m^2 g^{-1}$ after the modification step. A high extraction efficiency of 96.58% recovery was demonstrated for eserine using the octadecylated silica monolith. The SPE approach was rapid, taking less than 10 min, and used a low volume of sample of 300 µL.

In this study, a very sensitive and rapid microfluidic-chemiluminescence method was developed for the determination of eserine. To the researcher's knowledge, there has been no published data to date in the literature for the determination of eserine by a chemiluminescence method.

The method developed was based on the reaction of luminol with hydrogen peroxide. All the chemical and physical parameters in the reaction system were optimised in

order to obtain the best selectivity, sensitivity, and sample throughput. Under the optimal conditions, the enhanced CL intensity was linear for an eserine concentration over the range 1×10^{-4} to 1×10^{4} μg L^{-1} with a good coefficient of linearity (R^2=0.9901). The limit of detection (LOD) was 0.057 μg L^{-1} and this is below the legal limits (0.1 μg L^{-1}) established by the European Union for drinking water. Intra-day and inter-day coefficients of variation were below 10% over the range studied.

The proposed method was successfully employed to determine eserine in environmental water samples. The average recoveries for UHP water, tap water, and river water were 113.25% with RSD of 4%, 71.25% with RSD of 7%, and 59% with RSD of 13.75%, respectively. The recovery for 1, 10, 100, and 200 μg L^{-1} of tap water were 70.6%, 71.5%, 74.3%, and 68.6%, respectively. The proposed method provides good recoveries in compliance with the EU guidelines for routine analysis.

Dedication

This work is dedicated to

The souls of my great father ***Saeed*** *and great father-in-law* ***Soud*** *both of whom passed away during my PhD study ... May their souls rest in peace.*

My dear mother ***Gazwa*** *and dear mother-in-law* ***Aisha****,*

My beloved and supportive wife ***Manar*** *and my lovely son* ***Talal****,*

My brothers and sisters

For their unfailing love and tremendous support.

Acknowledgements

All gratitude, praise, honour, glory, strength and thanks are due to almighty Allah for giving me the inspiration, patience, and health, lighting my way towards my objective and removing obstacles during every moment in my life. His providence encouraged me to achieve this work.

I would like to express my profound gratitude to my academic supervisors, Dr Kevin Welham and Prof Steve Haswell (previous supervisor) for their encouragement, patience, assistance and invaluable advice throughout the entirety of my PhD. Many thanks are given also to Dr Thomas McCreedy (second supervisor), Dr Steve Clark (microchip manufacturer), Mr Tony Sinclair (SEM technician), Mrs Ann Lowry (TEM technician), and Mr Michael Thompson for their tremendous support.

I am grateful to all colleagues in analytical chemistry research groups and my friends in the department of chemistry, especially the Saudi nationals, for their valuable help.

I also extend my acknowledgement to the Saudi Arabian government, represented by the Ministry of Education (Najran University), for its generous financial support, enabling me to study here in Great Britain.

Special thanks to my brothers and sisters for their good wishes and warm encouragement. I wish to thank my son Talal who has brought happiness and so much joy to my life. Sincere thanks and immense appreciation goes to my great mother and my lovely wife for their unconditional love, endless encouragement, care and prayers. I only hope I can make my beloved family all proud.

Contents

Abstract I

Dedication III

Acknowledgements IV

Abbreviations X

List of figures XII

List of Tables XX

Chapter 1: Introduction 1

1.1 Pesticides 1

1.2 Analytical techniques for pesticides 4

1.3 Pesticides sample preparation 5

1.3.1 Liquid-liquid extraction 6

1.3.2 Solid-phase extraction 8

1.4 Materials used as SPE sorbents 16

1.4.1 Particles 17

1.4.2 Monolithic materials 19

1.5 Inorganic silica-based monoliths 24

1.5.1 Sol-gel reactions of silica 28

1.5.2 Properties of silica-based monoliths 37

1.5.3 Monolith for sample preparation using SPE 38

1.5.4 Chemical modification of silica-based monoliths 41

1.5.5 Physical characterisation of silica-based monoliths 48

1.5.6 Comparison between silica-based and polymer-based monoliths 52

1.6 Miniaturising environmental analysis 56

1.7 Microfluidics 59

1.7.1 Substrates 60

1.7.2 Device fabrication 61

1.7.3 Fluid manipulation 63

1.7.4 Mixing 64

1.7.5 Detection 66

1.8 Chemiluminescence 72

1.8.1 Mechanisms of CL reactions 72

1.8.2 Requirements for CL reactions 73

1.8.3 Factors affecting the CL emission 75

1.8.4 Chemiluminescence detector 75

1.8.5 The luminol reaction 77

1.8.6 CL detection for environmental analysis 79

1.9 Aims of the PhD project 83

Chapter 2: Experimental 85

2.1 Chemicals 85

2.2 Materials 89

2.3 Instrumentation 90

2.4 Fabrication of silica-based monolith 92

2.4.1 Silica-based monolith characterisation 95

2.4.2 Modification of silica-based monolith with C18 96

2.5 Applications of modified silica-based monolith for eserine 97

2.5.1 Study of the performance of C18 silica monolith by HPLC-UV 97

2.5.2 Preparation of stock solution of eserine 98

2.5.3 Preparation of standards for calibration of eserine 98

2.5.4 Solid-phase extraction and pre-concentration procedures 99

2.5.5 Breakthrough volume for SPE 100

2.6 Fabrication of microfluidic device 100

2.6.1 Microfluidic device design 102

2.7 Development of a portable chemiluminescence detection system 106

2.7.1 Design of in-house chemiluminescence detector 106

2.7.2 Preparation of chemiluminescence reagents and oxidants 110

2.7.3 Analysis of environmental water samples 110

Chapter 3: Results and Discussion: Fabrication of Silica-based Monolith 112

3.1 Effect of the basic treatment on the structure of silica monolith 116

3.2 Optimising the starting materials of silica-based monolith 119

3.3 Effect of the period of the basic treatment 124

3.4 Physical characterisation of the C18 modified silica-based monolith 128

3.4.1 Elemental analysis by EDX 130

3.5 Conclusion 134

Chapter 4: Results and Discussion: Applications of Silica-based Monolith for Eserine 136

4.1 Investigation of optimum detection wavelength for eserine 136

4.2 Calibration curve of eserine standards 139

4.3 Effect of flow rate on the extraction efficiency 141

4.4 Extraction efficiency of C18 silica monoliths 143

4.5 Evaluation of the percentage of extraction recovery 146

4.6 The pre-concentration study of eserine 148

4.7 Loading capacity and longevity 154

4.8 Conclusion 156

Chapter 5: Results and Discussion: Detection of Eserine by Chemiluminescence 157

5.1 Optimisation of chemiluminescence parameters 157

5.1.1 Effect of pH on CL intensity 158

5.1.2 Effect of flow rate on CL intensity 159

5.2 Study of different oxidants 161

5.2.1 Effect of potassium permanganate 161

5.2.2 Effect of concentrations of hydrogen peroxide 164

5.2.3 Effect of cerium (IV) sulphate 165

5.2.4 Effect of Cerium(IV) ammonium sulphate 166

5.2.5 Selection of the oxidant 168

5.3 Effect of the concentrations of luminol 169

5.4 Enhancement of the chemiluminescence signal 170

5.5 Effect of the methanol percentage 171

5.6 Analysis of eserine sample using chemiluminescence 175

5.6.1 Calibration curve 175

5.6.2 Comparison with other studies 179

5.6.3 Eserine determination in real samples 181

5.7 Conclusion 185

Chapter 6: Conclusions 187

6.1 Fabrication of silica-based monolithic columns 188

6.2 Extraction and pre-concentration of carbamate pesticide (eserine) 189

6.3 Combination of the microfluidic methodology with chemiluminescence 190

Chapter 7: Future work 192

Chapter 8: References 195

Chapter 9: Presentations and Conferences 206

Abbreviations

BET	Brunauer–Emmett–Teller
BJH	Barrett–Joyner–Halenda
CE	Capillary electrophoresis
CEC	Capillary electrochromatography
CL	Chemiluminescence
DDT	Dichlorodiphenyltrichloroethane
EDX	Energy dispersive X-ray spectroscopy
EOF	Electro-osmotic flow
EU	European Union
FIA	Flow injection analysis
GC	Gas chromatography
HMDS	Hexamethyldisilazane
HPLC	High-performance liquid chromatography
IE	Ion-exchange
ISEC	Inverse size-exclusion chromatography
IUPAC	International Union of Pure and Applied Chemistry
LC/MS	Liquid Chromatography / Mass Spectrometry
LED	Light-emitting diode
LLE	Liquid-liquid extraction
LOD	Limits of detection
LOQ	Limit of quantification
LP	Liquid permeation
microTAS, μTAS	Micro total analysis system
MISPE	Molecularly-imprinted solid-phase extraction
MP	Mercury porosimetry
MRLs	Maximum residue limits
MS	Mass spectrometry
MSPE	Magnetic solid-phase extraction
MTES	Methyltriethoxysilane
MTMS	Methyltrimethoxysilane

NP	Normal-phase
ODS	Octadecylsilane
PAA	Polyacrylic acid
PAHs	Polycyclic aromatic hydrocarbons
PC	Polycarbonate
PDF	Pressure driven flow
PDMS	Polydimethylsiloxane
PEDS	Polyethoxydisiloxane
PEEK	Poly (ether-ether-ketone)
PEG	Polyethylene glycol
PEO	Polyethylene oxide
PMMA	Polymethylmethacrylate
PMT	Photomultiplier tube
PS	Polystyrene
RP	Reversed-phase
SBSE	Stir-bar sorptive extraction
SEM	Scanning electron microscopy
SIA	Sequential injection analysis
SPE	Solid-phase extraction
SPME	Solid-phase microextraction
TAS	Total analysis system
TEM	Transmission electron microscopy
TEOS	Tetraethoxysilane
TEP	Thermoset polyester
THF	Tetrahydrofuran
TMCS	Trimethylchlorosilane
TMOS	Tetramethoxysilane
UV	Ultraviolet
WHO	World Health Organisation

List of figures

Figure 1-1: Global pesticide market from 1992 to 2012; values are expressed in millions of US dollars [6, 8, 9] 2

Figure 1-2: Liquid-liquid extraction (LLE) technique 7

Figure 1-3: Typical solid-phase extraction (SPE) steps 12

Figure 1-4: Polar interactions between a diol-modified silica sorbent and the analyte (phenol) via hydrogen bonding[71] 13

Figure 1-5: Non-polar interactions between bonded silica sorbent and two analytes via van der Waals forces[71] 14

Figure 1-6: Examples of IE interactions: (A) strong cation-exchange sorbent and (B) strong anion-exchange sorbent[71] 15

Figure 1-7: An image of the porous monolith located at the access of the Summer Palace Park in China[93] 21

Figure 1-8: The characteristics of internal structure of (A) particle packed, and (B) monolithic chromatographic beds[95] 23

Figure 1-9: Monolithic silica rod (lower); Monolithic silica columns Chromolith™ cover with PEEK and provided with column end fittings 26

Figure 1-10: Schematic design of a MonoClad column 27

Figure 1-11: Monolith encapsulation mould assembly (A) Silicon release spray lined 20 mL syringe (B) Rubber syringe ends in place, with HPLC fittings inserted (C) Monolith suspended between HPLC fittings 27

Figure 1-12: Scheme of reaction during the synthesis of silica monolith 28

Figure 1-13: The chemical structure and properties of TMOS and TEOS 29

Figure 1-14: The overall steps of preparing silica monolith and the structure of monolithic silica rod with the bimodal pore structure[91] 31

Figure 1-15: SEM image of (A) TMOS monolith prepared from 10kDa MW PEO (100%), (B) TMOS monolith prepared from 10kDa MW PEO (50%) and 100kDa MW of PEO (50%) and (C) TMOS monolith prepared from 100kDa MW PEO (100%) (adopted with a permission from the publisher, Elsevier)[132] 34

Figure 1-16: SEM photograph of the typical porous structure of monolithic silica columns (in the middle), the macropore or through pore (right), and the mesoporous structure of the silica (left)[140] 38

Figure 1-17: An image of commercially available silica monolith spin column and pipette tips presenting the optimum volume of sample and technique of extraction[156] 39

Figure 1-18: Types of silanols on silica available for bonding 41

Figure 1-19: Some types of silanes 43

Figure 1-20: Synthesis of C18 bonded monofunctional phase 44

Figure 1-21: Schematic diagram indicates the porous silica surface, presenting the inaccessibility of some micropores[54]. 45

Figure 1-22: Endcapping of free silanols with TMCS for a C18 sorbent 46

Figure 1-23: Schematic diagram presenting the influence of conditioning process on octadecyl bonded silica: (A) without conditioning (B) partially conditioned (C) totally conditioned[54]. 47

Figure 1-24: IUPAC classification of gas physisorption isotherms. The adsorption and desorption isotherms have six different forms (I-VI): (I) microporous, (II) non-porous or macroporous, (III) non-porous, (IV) mesoporous, (V) mesoporous, and (VI) non-porous. 50

Figure 1-25: SEM photographs of (a) bimodal pore structure silica monolith with macropores and thin skeleton containing mesopores, and (b) typical polymer monolith with globular structures[170] 53

Figure 1-26: Miniaturising and functional integrating laboratory processes on to a microchip device (adopted with a permission from publisher John Wiley and Sons).[201] 58

Figure 1-27: (A) Parabolic flow profile of a fluid as it is passed through a microchannel via hydrodynamic pumping (B) Flat profile generated by electro-osmotic flow (EOF) through a microchannel 64

Figure 1-28: Diagram showing A) well-defined laminar flow, and B) random, turbulent flow. 65

Figure 1-29: Jablonski diagram describing energy levels and possible transitions: A, photon absorption; F, fluorescence; CL, chemiluminescence; P, phosphorescence; S_0, ground state; S_1, S_2, excited singlet state; T_1, T_2, excited triplet state; IC, internal conversion; ISC, intersystem crossing.[241] 71

Figure 1-30: Types of chemiluminescence reactions 73

Figure 1-31: Schematic diagram of PMT 76

Figure 1-32: Mechanism of luminol and hydrogen peroxide reaction[197] 78

Figure 1-33: Some examples of carbamate pesticides 80

Figure 2-1: Pre-functionalised treatment of silica monolith with ammonia hydroxide 93

Figure 2-2: Schematic of silica monolith flow system 94

Figure 2-3: Different lengths of silica monolith rod connected to a borosilicate glass tube or stainless steel tubing by heat-shrinkable tube (PTFE) 94

Figure 2-4: A silica monolith rod connected to the borosilicate tube for surface modification. 95

Figure 2-5: The chemical structure and molecular weight of eserine 98

Figure 2-6: Schematic diagram of the fabrication process of glass microfluidic devices using photolithography and wet-etching technique[271] 102

Figure 2-7: (A) Schematic of a T-shape serpentine channel manifold microfluidic chip (206 mm length, 9 meanders) and (B) Photograph of the microfluidic chip 105

Figure 2-8: Photograph of photosensor module containing a metal casing PMT 106

Figure 2-9: Photograph showing the portable chemiluminescence detection system designed in-house 109

Figure 3-1: The resulting silica monoliths prepared in different cylindrical moulds 113

Figure 3-2: SEM micrographs of internal structure of silica monoliths, consisting of TMOS + poly (ethylene oxide) (100 kDa) + nitric acid (1 M), during the fabrication process (A) before the basic treatment with ammonia hydroxide (1 M) (B) after the basic treatment with ammonia hydroxide (1 M) (C) after the basic treatment and the calcination 114

Figure 3-3: BET isotherm curves obtained for TMOS silica monolith. Isotherm (A) is for the TMOS silica monolith before the basic treatment and isotherm (B) is for the TMOS silica monolith after the basic treatment at 80 °C for 24 hours. 118

Figure 3-4: SEM micrographs of internal structure of silica monoliths of TMOS and TEOS with PEO (200 kDa) at different magnifications 122

Figure 3-5: Morphology changes of the silica monolith with different time periods of ammonia hydroxide treatment. The sample was prepared from TMOS-F127. 126

Figure 3-6: SEM micrograph of the internal structure of TMOS silica monolith; (A) non-modified monolith and (B) C18 modified monolith 129

Figure 3-7: EDX spectra of non-modified silica-based monolith 131

Figure 3-8: EDX spectra of modified silica-based monolith 132

Figure 4-1: Spectra of 20 ppm of eserine detected by UV-VIS spectrometer 137

Figure 4-2: Spectra of 2 ppm of eserine detected by UV-VIS spectrometer 138

Figure 4-3: Calibration curve of eserine standard solutions with the peak areas plotted versus concentration (μg mL^{-1}) 140

Figure 4-4: HPLC chromatogram obtained for the extraction steps. (A) The standard solution of eserine was directly injected into the HPLC, (B) The loading fraction was collected from the loading step, (C) The washing fraction and (D) the elution fraction. The separation column was a Bio Wide Pore C18 column (5 μm, 15 cm × 2.1 mm), the mobile phase was methanol /water (60:40) (V/V) run under isocratic conditions; the UV wavelength was set at 248 nm, the injection volume was 20 μL, and the flow rate was 1 mL min^{-1} 145

Figure 4-5: The extraction profile for 100 μg mL^{-1} of eserine using the C18 silica monolith. The average recovery percentage was obtained from three consecutive experiments (n=3) and the error bars indicate one standard deviation 148

Figure 4-6: HPLC chromatogram shows the peak areas response (A) the standard solution of eserine (10 μg mL^{-1}), (B) the loading fraction, (C) the washing fraction and (D) the pre-concentrated elution fraction. The separation column was Bio Wide Pore C18 column (5 μm, 15 cm × 2.1 mm), the mobile phase was methanol /water (60:40) (V/V) run under isocratic conditions; the UV wavelength was set at 248 nm, the injection volume was 20 μL, and the flow rate was 1 mL min^{-1} 150

Figure 4-7: The pre-concentrated ability for 10 μg mL^{-1} of eserine using the octadecylated silica monolith. The average peak area response was obtained from HPLC three consecutive times and the error bars indicate one standard deviation. 152

Figure 4-8: The pre-concentrated profile for eserine, (n=3). The error bar indicates one standard deviation 153

Figure 4-9: Loading capacities of a C18 silica monolith rod (78.4mg) as measured using breakthrough of eserine 155

Figure 5-1: Schematic diagram of the reaction manifold used for the determination of eserine 157

Figure 5-2: Effect of pH on the luminol chemiluminescence emission within a microfluidic device where the concentration of luminol was fixed at 20 mM, the concentration of H_2O_2 was fixed at 20 mM, and the flow rate was 15 μL min^{-1}. Error bars: one standard deviation (n=5). 158

Figure 5-3: Effect of flow rate on the chemiluminescence reaction signal where the concentration of luminol was fixed at 20 mM, the concentration of H_2O_2 was fixed at 20 mM, and the pH was 10.5. Error bars: one standard deviation (n=5). 159

Figure 5-4: Effect of potassium permanganate concentration on the CL intensity where the concentration of luminol was fixed at 20 mM, the flow rate was 20 μL min^{-1}, and the pH was 10.5. Error bars: one standard deviation (n=5). 162

Figure 5-5: Microscope images of the blocked microfluidic channel with $KMnO_4$. (A) magnification at 3mm and (B) magnification at 10mm 163

Figure 5-6: Effect of the hydrogen peroxide concentration on the CL emission where the concentration of luminol was at 20 mM, the flow rate was 20 μL min-1, and the pH was 10.5. Error bars: one standard deviation (n=5). 164

Figure 5-7: Effect of cerium (IV) sulphate concentration on the CL intensity, where the concentration of eserine was 10 ppm and the concentrations of HNO_3 and H_2SO_4 were 1 M. Error bars: one standard deviation (n=5). 165

Figure 5-8: The effect of cerium (IV) ammonium sulphate concentration on the CL intensity where the concentration of eserine was 10 ppm. Error bars: one standard deviation (n=5). 167

Figure 5-9: Effect of the concentration of luminol on the CL emission where the pH was fixed at 10.5 and the concentration of hydrogen peroxide was 40 mM. Error bars: one standard deviation (n=5) 169

Figure 5-10: The influence of protective surfaces above the microfluidic device on the CL response where the concentrations of luminol and hydrogen peroxide were 30 mM and 40 mM, respectively. Error bars: one standard deviation (n=5) 170

Figure 5-11: The effect of MeOH percentage in eserine solution with Ce(IV) on the CL signal where the concentrations of eserine, Ce(IV), and rhodamine 6G were 10 ppm, 30 mM, and 0.5 mM, respectively. Error bars: one standard deviation (n=5). 172

Figure 5-12: The effect of MeOH percentage in eserine solution with luminol-H_2O_2 on the CL signal where the concentrations of eserine, luminol, and H_2O_2 were 10 ppm, 30 mM, and 40 mM, respectively. Error bars: one standard deviation (n=5). 173

Figure 5-13: Calibration curve showing how the CL intensity changes with the increase in concentration of eserine. Error bars: one standard deviation (n=5) 175

Figure 5-14: Calibrations for the determination of eserine using the luminol-H_2O_2 chemiluminescence reaction. Error bars: one standard deviation (n=5). 176

Figure 5-15: The CL intensity of different concentration of eserine samples (n=5) 181

Figure 5-16: Model structure of humic acid [287] 184

Figure 7-1: Potential designs for a primary off-line pre-concentration step and an integrated microfluidic device..... **Error! Bookmark not defined.**

List of Tables

Table 1-1: Some applications of silica-based monolith as offline SPE 40

Table 1-2: Reactions for the chemical modification of silica 42

Table 1-3: Summary of comparison between silica and polymer monoliths based on the literature review [176] 54

Table 1-4: A number of substrates used for the fabrication of microfluidic devices and the most commonly used technique for fabrication in each substrate 62

Table 2-1: Chemicals, solvents, and reagents used 86

Table 2-2: Materials used 89

Table 2-3: Instrumentation used 90

Table 2-4: The chemical composition of silica monolith rods 92

Table 2-5: Estimated residence times for water within the serpentine channel at different flow rates. Calculation for the residence time (s) = channel length (m) / flow rate (m s^{-1}) 103

Table 3-1: The physical properties of the silica TMOS monolith before and after the basic treatment 116

Table 3-2: A summary of silica monolith compositions and their physical characterisation parameters 120

Table 3-3: The physical properties of the TMOS-F127 monoliths with 1 M NH_4OH treatment over different periods of time 127

Table 3-4: Quantitative EDX analysis for all elements in non-modified silica-based monolith 131

Table 3-5: Quantitative EDX analysis for all elements in modified silica-based monolith 133

Table 4-1: Analytical figures of merit for eserine (n=3) 140

Table 4-2: Effect of flow rate on extraction efficiency 142

Table 4-3: the extraction recovery of eserine runs and the average..... 147

Table 5-1: The result of the background reference experiment. One standard deviation (n=5). 174

Table 5-2: A summary of the optimum values of all the CL parameters studied within a microfluidic device for the determination of eserine 174

Table 5-3: Analytical figures of merit for eserine determination by CL. (n=5) 177

Table 5-4: Analytical performance of FIA-CL applied to the determination of carbamates in water samples 179

Table 5-5: Determination of eserine added to different kinds of waters (n=5)..... 183

Chapter 1: Introduction

1.1 Pesticides

Pesticides are substances used in the environment in order to combat a variety of pests that can destroy crops, as well as to improve the quantity and quality of the food produced and help to limit many human diseases.[1] Among the different ways to classify pesticides, one way is to categorise them according to their type of use. The major pesticide groups are: fungicides, applied to kill fungi; herbicides, employed to eradicate weeds and other unwanted plants; and insecticides, used to kill insects and other arthropods. Algicides, rodenticides, molluscicides, pheromones, acaricides, plant growth regulators, nematicides, and repellents are among the other types of pesticides.[2]

A pesticide can be a biological (e.g. virus or bacteria) or chemical control agent. Since the beginning of agriculture, chemical substances have been employed by humans to control pests, among which inorganic compounds such as mercury, arsenic, lead, and sulphur are included. Paul Müller discovered the use of dichlorodiphenyltrichloroethane (DDT) as an insecticide in 1939, which had an immense effect on pest control and made its use globally prevalent.[3] Effective control of diseases such as malaria transmitted by mosquitoes and the bubonic plague transmitted by fleas which were responsible for the deaths of millions of people over the course of time, is the reason behind the widespread acceptance of pesticides at that time.[4] Following the discovery of some toxic actions of DDT on birds and the publication of the book Silent Spring by Rachel Carson in 1962, acceptance gradually

declined.[5] Globally, particularly in developed countries, the registration and utilisation of pesticides is rigorously regulated at present, owing to their probable toxic actions on human health and on the environment. Pesticides remain crucial for nourishing and shielding the public from diseases despite a little evolution in the biological control and in the development of resistance of plants to pest.[6] It has been estimated that approximately one-third of the world's crop production would be destroyed by pests without the use of pesticides.[7]

During the past few decades the application of pesticides has rapidly increased and the world market of pesticides has doubled.[6, 8, 9] The timeline of pesticide sales during the last years is shown in Figure 1-1 The main market sales of pesticides were herbicides, fungicides, insecticides, and others with 43.8%, 26%, 25.6% and 4.6%, respectively, in 2012.[10] The world agricultural pesticide industry is predicted to expand and achieve US $58.9 billion in 2016.[11]

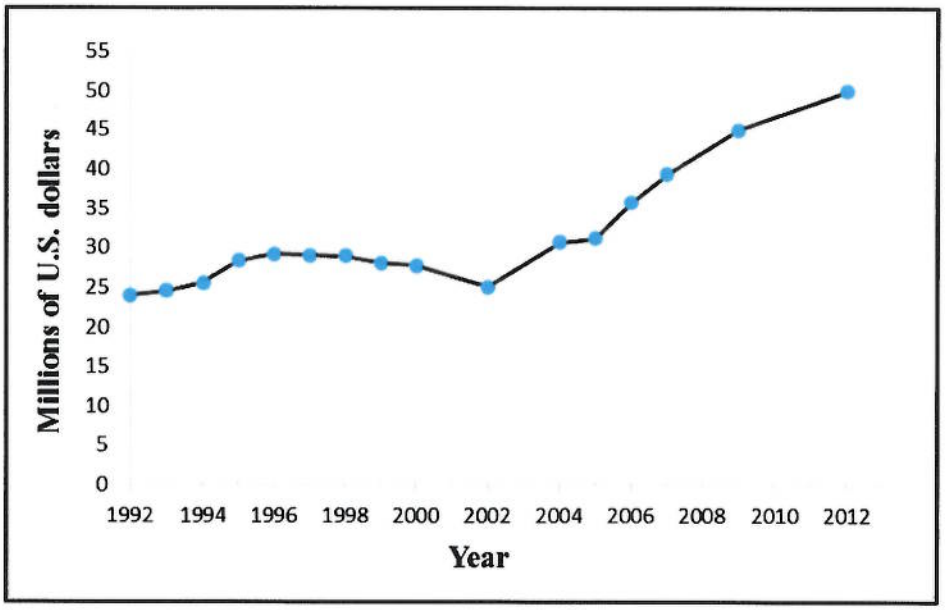

Figure 1-1: Global pesticide market from 1992 to 2012; values are expressed in millions of US dollars [6, 8, 9]

However, this widespread use of pesticides has caused great social and scientific concern all over the world due to the possibility of contamination of water (e.g. ground and surface waters), crops (e.g. fruit and vegetables), soil and air, as well as a consequent potential impact on the environment and public health.[12] According to the World Health Organisation (WHO), there are three million acute cases of pesticide poisoning and 250,000 unintentional deaths each year.[13] Some pesticides are highly toxic, environmentally stable, liable to bioaccumulation, and persist in the environment over long periods of time.[14] Exposure of the public to pesticide residues, comprising both physical and biological degradation products found in water, food and the air, could result from environmental contamination or occupational exploitation.[15, 16]

The majority of pesticides are sprayed over crop fields or applied to soils. Only 1% of the total amount of pesticides reaches the target pests.[17] Pesticide residues have been found in rain, groundwater, foods and drinking water.[18-20] The amount of pesticides in a few samples of river water and groundwater was found by the UK Government to go beyond the values permitted for drinking water.[21] Along with the human food supply, mixtures of pesticides are also found in the aquatic environment, together with the surface waters that sustain aquatic life.[22] Five or more pesticides were found in over 50% of all streams analysed in the United States.[23] Humans would be vulnerable to mixtures of pesticides and their degradation products if the water treatment does not successfully remove pesticide residues, when streams and groundwater are used as a source of drinking water.[20]

As a result, to reduce contamination of surface and ground water guidelines have been formulated, and regulatory limits and guideline levels for residues in drinking water

have been established. Many countries have severely restricted the maximum acceptable concentration of pesticides in water, food, air, and biological materials.[24] For instance, the European Union (EU) has established a maximum permissible concentration of 0.1 μg L^{-1} for individual pesticides, and 0.5 μg L^{-1} is the maximum permissible total concentration of all pesticides in drinking water.[25] Consequently, these legal limitations have given rise to the need for analysis with increased selectivity and sensitivity that merge automation and cost-effectiveness with favourable selectivity, reproducibility, and sensitivity.[26]

1.2 Analytical techniques for pesticides

The monitoring of pesticides in natural water becomes a very important analytical requirement for drinking water quality and to minimise human exposure. The determination of trace and ultra-trace pesticides in complex matrices is always a challenge to analytical chemists. Traditionally, gas chromatography (GC) has been commonly applied for pesticide analysis in environmental, clinical, and food samples due to its high sensitivity and selectivity. However, a number of pesticides, such as carbamate, pyrethroid and some organophosphorus, are not suitable for GC separation because of their high polarity, low volatility, or thermal lability. These drawbacks can be sometimes avoided by derivatisation from earlier GC injection.[27, 28] Moreover, high-performance liquid chromatography (HPLC) is preferred over the GC technique coupled with different detection systems such as mass spectrometry (MS)[29], ultraviolet (UV)[30], and fluorescence[31] for the determination of carbamates.

However, many of the aforementioned techniques are often expensive, time consuming, large in size and lab-based, and they require high consumption of reagents, sample transport, and storage. In addition, in the delay between sampling and analysis, the sample is highly susceptible to losses and contamination. Currently, miniaturisation of analytical techniques, such as lab-on-a-chip, is an effective means to overcome many of the limitations of traditional techniques, with features such as low reagent consumption, small sample size, increased speed of analysis, portability, and remote operation.[32, 33] Miniaturisation of analytical techniques and lab-on-a-chip have been detailed in more depth in Sections 1.6 and 1.7.

1.3 Pesticides sample preparation

The analysis of pesticide residues in environmental water samples involves sample preparation and analytical instruments. Despite the rapid development in analytical instruments, their detection limits, detector noise and final quantification are usually affected by the interferences from complex matrices. Hence, sample preparation has always been considered as the bottleneck in the analytical laboratory for the accurate and effective analysis of trace pesticide residues. Approximately 60%–70% of the total analysis time is currently spent on sample preparation steps.[6, 34, 35] The object of the sample preparation step is to isolate the analytes of interest from a sample matrix and remove the interferences as much as possible. Generally, sample preparation includes extraction, clean-up and pre-concentration steps.[36] The process of extraction and pre-concentration of the environmental samples can be complicated, time consuming, and labour intensive. The ideal sample preparation methods should be fast, environmentally friendly, precise, and accurate. In addition, it should keep sample

integrity and consume little solvent. Typically, pesticide residues from liquid samples (e.g. environmental waters) are isolated and concentrated using two of the most acceptable extraction methods, such as liquid-liquid extraction (LLE) or solid-phase extraction (SPE).[37-39]

1.3.1 Liquid-liquid extraction

Historically, liquid-liquid extraction (LLE) is the earliest sample preparation technique used in analytical chemistry for the extraction of pesticides in aqueous samples. It is dependent on the partition of the analytes of interest between two immiscible liquid phases. Hence, LLE has also been known as immiscible solvent extraction.[40] One phase is generally aqueous, which contains the dissolved sample, whereas the second phase is an organic solvent. In this technique, the aqueous sample is shaken with a suitable volume of an appropriate organic solvent in a separatory funnel that will lead to migrating the target analytes from the aqueous phase to the organic phase [2], as shown in Figure 1-2. For this reason, the analyte should be more soluble in the organic solvent than in water.[41]

In environmental analysis, LLE is mostly used for the extraction of non-volatile and semi-volatile pesticides. Carbamates usually have low solubility in water but are soluble in the more polar organic solvents (e.g. methanol or acetone). Moreover, they are moderately soluble in medium polarity solvents (e.g. dichloromethane or chloroform); they are commonly poorly soluble in non-polar solvents (e.g. petroleum, ether).[36] Sometimes, mixed solvents have been employed to modify the solvent strength. For example, eight carbamate pesticides were extracted from aqueous

environmental samples with chloroform and determined by HPLC with a mean recovery of 71%.[42]

LLE has some advantages such as simple, good extraction recovery, large sample capacity, and low demand on the analyst's skills and reliability. Nevertheless, it also has several serious shortcomings, the most notable being it is an environmentally unfriendly technique due to the large quantities of solvents consumed and the subsequent generation of waste. In addition, it is time consuming, difficult in automation, expensive, labour intensive, and leads to potential loss of analytes. Furthermore, polar pesticides cannot be extracted using this technique. Due to these limitations, LLE has been gradually replaced by SPE.[2, 43, 44]

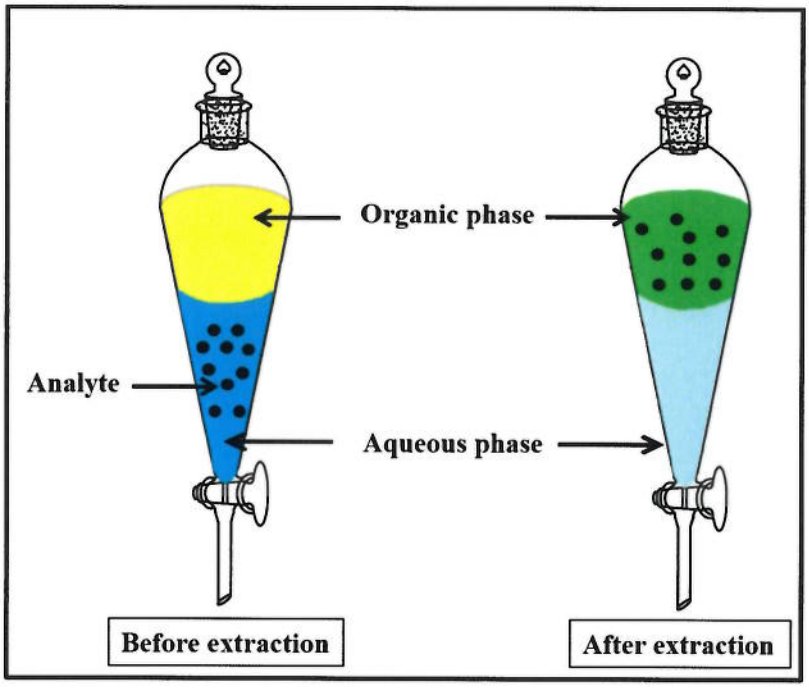

Figure 1-2: Liquid-liquid extraction (LLE) technique

1.3.2 Solid-phase extraction

In the 1970s, solid-phase extraction (SPE) was introduced and shortly became a viable alternative sample preparation approach to LLE. It is now the most popular sampling technique in several areas of chemistry including food [45], pharmaceutical [46], clinical [47], environmental [48], and industrial chemistry.[49] The principle of SPE is analogous to that of liquid-liquid extraction (LLE), involving a partitioning of the analytes of interest between two phases. Nevertheless, as an alternative to the two immiscible liquid phases in LLE, SPE involves partitioning between a liquid (sample matrix containing the analytes of interest) and a solid phase (sorbent). The target analytes, in the liquid sample, are trapped in the solid surface (sorbent), and subsequently eluted by an appropriately selected minimal volume of solvent.[50] SPE has a number of different formats that are commercially available, namely: cartridges, discs, columns, coated stir bars, 96-well plates and micropipette tips.[36]

Due to its high adaptability, the SPE can be used for many purposes, such as trace enrichment (concertation), removal of sample interferences (clean-up), solvent exchange, and sample storage.[36] Sample interferences usually cause problems for the detection of analytes of interest (e.g. overlap band in the chromatogram) that can negatively affect results. In environmental complex samples, a large number of interferences can make it difficult to separate the analyte bands. These interferences can often be reduced or removed by this approach.[51] In addition, SPE can be used to increase the analyte concentration when the sorbent is eluted with a small volume of strong solvent. This process is termed trace enrichment and is frequently used to concentrate sub- part per billion concentrations of target analyte such as pesticides from environmental water samples.[52]

SPE has a variety of distinctive advantages over liquid-liquid extraction. For instance, it is relatively fast, reduces cost and labour, achieves relatively high recovery of the analyte, concentrates the analyte, uses small volume of the sample, is suitable for automation, reduces organic solvent consumption and disposal, reduces potential emulsion formation, completely removes interferences and is environmentally friendly.[36, 53, 54] Nevertheless, there are some disadvantages of the SPE approach such as limited capacity of the sorbent, cracks appearing in the sorbent structure due to dryness through the extraction steps, possible risk of cartridge blockages caused by large particulates in the sample and contamination through manufacturing.[55, 56] In spite of all these disadvantages, solid-phase extraction is still commonly used rather than the LLE approach in environmental analysis.[39]

Typically, the SPE technique can be carried out by two ways: offline or online procedures. In the first procedure, the sorbent is disconnected from the following method of analysis (e.g. HPLC), while in the other the sorbent is directly connected with the following method of analysis. The offline SPE equipment is inexpensive and simple, thus completely appropriate to on-site sampling. Conversely, this approach is time consuming, needs a large amount of the eluted organic solvent, and it could cause a possible contamination or loss of the analyte of interest during the evaporation steps.[39, 57] In environmental analysis, the SPE technique can be easily coupled with an analytical system, such as HPLC [58], liquid chromatography/mass spectrometry (LC/MS) [59] and GC [60], to achieve sample preparation and analysis without the need of an operator. Generally, online SPE techniques are fast (by reducing the analysis time), increase sample throughput, are more beneficial for a limited volume of sample, and improve precision. The online combination of SPE and GC is more complex due to the sensitivity of the GC system to water and the drying process increases the risk of

losing volatile analytes, whereas HPLC is more favourable with SPE since they are both depend on partitioning between a liquid/mobile phase and solid sorbent/column.[39, 54] Despite the demand trend towards online SPE procedures, offline SPE is probably still the most extensively used sample preparation approach to extract pesticides from environmental and food samples. It continues a valuable technique for analysing pesticides in complex matrices due to its high flexibility when the elution solvent is unsuitable for the subsequent method of analysis.[59]

Additionally, there are some friendly miniaturised SPE techniques that have been used for the extraction of carbamate pesticides from environmental water samples such as solid-phase microextraction (SPME), stir-bar sorptive extraction (SBSE), magnetic solid-phase extraction (MSPE), and molecularly-imprinted solid-phase extraction (MISPE). These SPE techniques represent an opportunity to reduce solvent consumption, time of extraction, and overall cost. [61-65]

1.3.2.1 *Solid-phase extraction procedure*

The general SPE procedure has to provide the analyte of interest from the sample that is free from interferences and concentrated enough for detection.[50] The SPE process fundamentally consists of four successive steps, as shown in Figure 1-3: conditioning, application of the sample (loading), washing (removal of interferences) and elution (recovery of the analyte). Initially, the sorbent is activated by flushing an appropriate solvent (e.g. a non-polar sorbent is activated by a polar solvent) that allows the sorbent functional groups to solvate, and remove the air in the voids and any possible impurities present in the sorbent.[36, 66] Then, the sorbent equilibrates with the same solvent in which analytes are dissolved in order to wet the sorbent and make an

appropriate environment to enlarge the adsorption of the analytes in the solid phase. It is essential to keep the solid sorbent wet between this step and loading the solution of sample. Otherwise, the target analytes will not be efficiently trapped and poor recoveries will be achieved.[67]

Following the conditioning step, the solution of sample is loaded into the solid sorbent by gravity, pumping or by an automated system. Hence, the target analytes are retained and concentrated in the sorbent material. In addition, some of the sample constituents may also be retained by the solid sorbent and others may pass through, therefore enabling some purification of the analyte. In the third step (washing), the solid sorbent is rinsed by a suitable solvent, similar to the sample solution, to remove undesired sample constituents without displacing the analytes.[39, 50, 68]

Finally, the target analyte is eluted and removed from the sorbent by a minimum amount of a suitable solvent, and then prepared for further analysis. All the successive SPE steps need careful respect for the nature of the SPE sorbent, the solvent and their influence on the target analyte.[69]

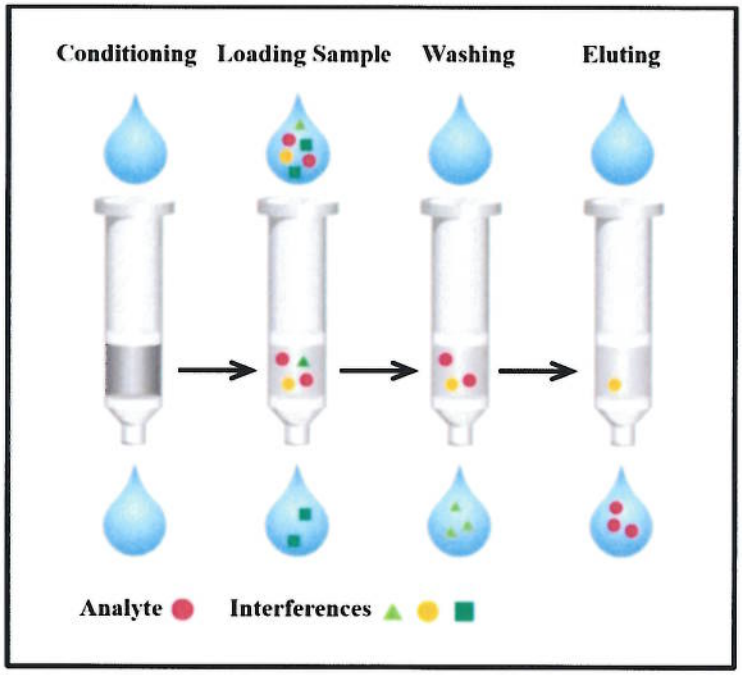

Figure 1-3: Typical solid-phase extraction (SPE) steps

1.3.2.2 *SPE retention mechanisms*

There are several retention mechanisms that are utilised for the interaction of the target analytes with the SPE solid sorbent. Traditionally, solid-phase extraction sorbents can be categorised into three classes: normal-phase (NP), reversed-phase (RP), and ion-exchange (IE).[70] Normal-phase (NP), also known as polar phase, is generally a polar sorbent material (hydrophilic) such as silica $(SiO_2)_x$ and magnesium silicate ($MgSiO_3$), or silica material chemically functionalised with highly polar groups, for example diol groups, cyano, and amino. This phase is especially suitable for the extraction of polar analytes that dissolve in non-polar organic solvents such as hexane (C_6H_{14}), toluene (C_7H_8), and chloroform ($CHCl_3$). The retention mechanism of the target analyte is mainly due to polar interactions (e.g. hydrogen bonding and dipole-dipole interactions) between the polar functional groups of the analyte and the polar groups on the surface

of sorbent. Figure 1-4 illustrates the mechanism of a hydrophilic extraction. The analyte retained by these mechanisms is eluted by passing a polar solvent that broken the binding mechanism.[39, 66]

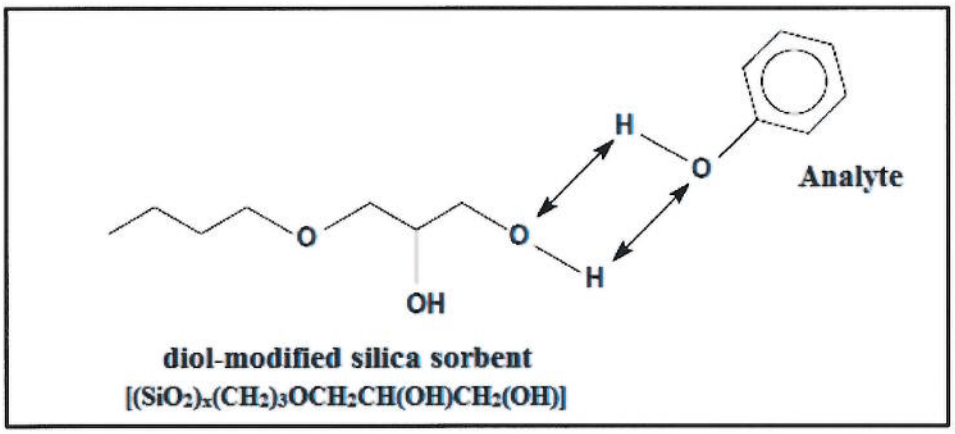

Figure 1-4: Polar interactions between a diol-modified silica sorbent and the analyte (phenol) via hydrogen bonding[71]

Reversed-phase (RP), also known as non-polar phase, is generally a non-polar sorbent material (hydrophobic), which can be polymer-based or silica-based modified with a non-polar functional group (hydrocarbon chains) such as ethyl (C2), octyl (C8), and octadecyl (C18). The RP is more appropriate to extract non-polar or moderately polar organic analytes (e.g. carbamate pesticide) from polar aqueous matrices. Here, the interactions occur between the functional groups on the sorbent and hydrophobic parts on the analyte molecule via van der Waals or dispersion forces. The C18 phase is the most extensively used sorbent in RP for many applications due to the high hydrophobicity and ability to extract many compounds with different chemical properties. However, the main drawback of C18 is that it does not give the best selectivity.[47, 66] The mechanism of a hydrophobic extraction in the case of C18 modified silica sorbent with two non-polar compounds is shown in Figure 1-5. The

elution of retained analyte is mostly made by using a non-polar solvent to disrupt the forces that bind the analyte to the sorbent.

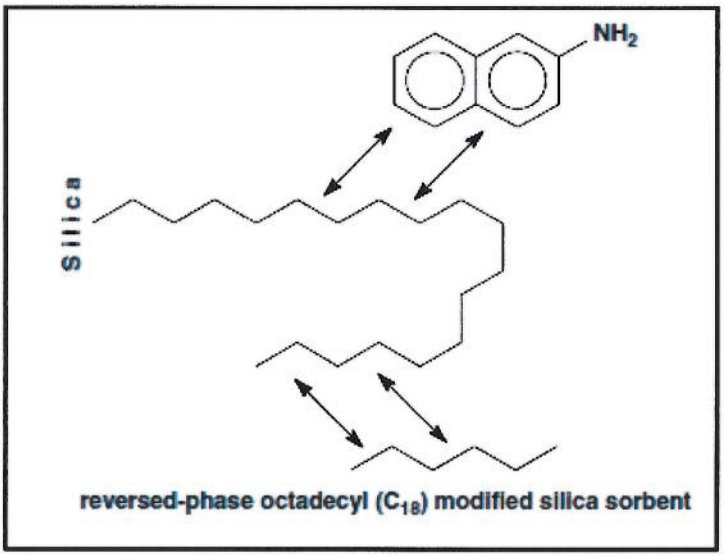

Figure 1-5: Non-polar interactions between bonded silica sorbent and two analytes via van der Waals forces[71]

The ion-exchange (IE) method includes extraction of analytes in solution: negatively charged analytes (anionic) can be extracted using positively charged functional groups that are bonded to the silica surface (such as aminopropyl and quaternary amine), whereas positively charged analytes (cationic) can be extracted using negatively charged functional groups that are bonded to the silica surface (such as benzenesulphonic acid and carboxylic acid). These SPE phases are most appropriate for extraction of charged analytes (such as acidic and basic compounds) from polar or non-polar organic samples. Figure 1-6 shows the mechanism of ion-exchange SPE. The electrostatic attraction occurs between the charged functional groups that are bonded on the sorbent and the charged functional group of the target analytes.[39, 50] The ion exchange sorbent retains analytes of opposite charge depending upon the pH.

These electrostatic attractions can be disturbed by neutralising the sorbent or the analyte with a pH change or by using a solvent with an appropriate ionic strength that contains ions that compete with the target analytes for binding sites on sorbents. Basically, there are three types of ion-exchange: cation exchange, anion exchange, and zwitterion-exchange. The first type is the cation exchange, where the sorbents are negatively charged and interact with positively charged analytes (cations) such as use a resins that a cross-linked with an aliphatic sulfonic acid (- SO_3) functional group. The second type is an anion exchange, where in this case the sorbents are positively charged similar the analyte carries a negative charge, where an aliphatic quaternary amine group (-N^+ $(CH_3)_3$) are commonly used. Also, an ionizable functional group such as amine or carboxylic acid (COOH) can be used for weaker exchange. In zwitterion-exchange, the silica backbone contains molecules which can be negatively or positively charged; therefore the functional group can attach to it, where amino acids group expel of this process.[47,71]

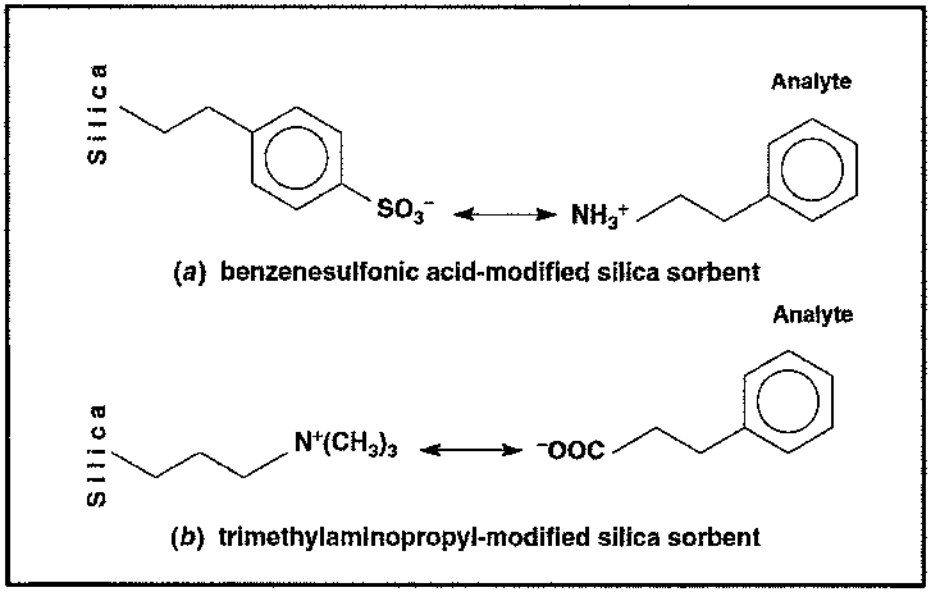

Figure 1-6: Examples of IE interactions: (A) strong cation-exchange sorbent and (B) strong anion-exchange sorbent[71]

1.4 Materials used as SPE sorbents

The SPE sorbent selectivity depends on understanding the knowledge of the chemistry and mechanism of interactions between the functional groups on the sorbent surface and the target analytes, as described in Section 1.3.2. The materials used as sorbents for SPE can be generally categorised based on their nature as organic based, such as natural and synthetic polymers, and inorganic based, such as silica gel (SiO_2) and magnesia (MgO). Materials used as sorbents in SPE are highly analogous to those normally used as stationary phases in typical HPLC.[72] Therefore, the solid-phase materials should rapidly adsorb quantities of the analytes of interest and easily elute the analytes from the solid particles.[54] Overall, successful SPE sorbents should have a number of properties including being porous with large surface areas, offer chemical stability towards the sample matrix and elution solvents during all SPE steps, be free of leachable impurities, and have easily modified surfaces.[53, 73]

Traditionally, at the turn of the twentieth century, Tswett used calcium carbonate as a sorbent to separate plant pigment with petroleum ether as the mobile phase, and he named the process 'chromatography'.[74] In the early 1930s, some inorganic oxide sorbents, including silica gel, alumina, and diatomaceous earth, were applied for normal-phase to clean up samples in organic solvents.[67] Braus *et al.* used metal pipes filled with 1200–1500 g of granular activated carbon for the isolation of organic contaminants from surface waters in the early 1950s.[75] Abel *et al.* introduced a solid reversed-phase (non-polar) polymer by chemically bonding silica surfaces with trichlorosilane.[76] Riley and Taylor, in 1969, were the first who stated the use of

poly(styrene-divinylbenzene) resins as a replacement for active carbon, for the pre-concentration of organic compounds from sea water.[77]

In the mid-1970s, silica-based sorbents chemically modified by C18 were used in solid-phase extraction and introduced in different formats such as disposable cartridges and syringe barrels.[55] The review by Hennion in 1999 reported the most significant features of reversed-phase silica and polymer sorbents in both biological and environmental areas, but they are required to be conditioned with solvent and remain wetted prior to applying the sample solution.[78] Afterwards, Waters Company introduced to the market a polymeric water-wettable sorbent, called Oasis hydrophilic–lipophilic balanced (HLB), used for acidic, basic and neutral analytes which do not necessarily need the conditioning step.[79]

Later, several numbers of sorbents and formats were developed, automated, and miniaturised in solid-phase extraction, but silica is the most widely used material due to its relatively low cost, its different structural forms, availability in a various range of pore sizes and the surface can be simply modified with different functional groups to increase its selectivity towards different desired analytes.[54, 80] Generally, the popular materials that have been applied as solid-phase extraction sorbents are particles (silica-based) and monoliths, which will be described in detail in the next sections.

1.4.1 Particles

As discussed previously, silica-based particles are the most common materials used as sorbents for SPE and offer a number of advantages over other materials. Traditional particle SPE beds, for example columns or cartridges, are created by loading a certain

mass of silica particles into the bottom, and the silica particles are held in place by two polyethylene filters, upper and lower, on each side of the bed. The particle size of the silica particles is typically in the range 40-50 μm. These are much larger than the HPLC column particles (3-5 μm).[66]

These traditional particle SPE columns have some problems with their particles such as a shortage of particles to completely fill the available space; the preparation of particles needs skilled technicians and special instruments since the extraction efficiency is based on the quality of particles packed in the column. In addition, this type of stationary phase requires rigid and highly porous frits that are capable of retaining silica particles in place and avoiding the generation of bubble formations during analysis, which is frequently difficult to achieve.[81]

In fact, the efficiency of the sorbent material for extracting the analytes can be enhanced by improving the surface area, which can be achieved by the decreasing of the size of particle. Nevertheless, this can trigger an increasing in the backpressure, which is inversely proportional to the particle size squared.[82]

In order to prevent the increased back pressure, the bed length should be decreased. However, this can also limit the number of interaction sites on the sorbent surface, leading to a reduction in the sorbent capacity. Furthermore, particle-based SPE cartridges create channels after several usages. This is to allow the analytes to move rapidly through these channels before they interact sufficiently with the sorbent. These drawbacks urge the requirement for more accurate and uncomplicated SPE material which can offer a high surface area and extraction efficiency without any serious problems. As a result of this demand, the use of monolithic material for SPE

application has become a convenient way to overcome the particle-packed problems.[70, 83, 84]

1.4.2 Monolithic materials

During the last 25 years, modern monolithic columns have been attracting attention as they overcome some of the drawbacks of particle-packed columns in terms of analytical performance, time and column efficiency, qualifying them as a strong alternative to particle-packed columns. In chromatographic science, monolithic columns have several properties such as their large through-pores and small skeletons, which provide low backpressure and high efficiency.[85]

The new generation of these materials has had different names in the literature over the years. Historically, Hjerten *et al.* compressed polyacrylamide gel within an LC column for chromatographic separation, and they introduced the term 'continuous beds' in 1989.[86] Afterwards, Svec and Frechet in 1992 fabricated what was known as 'continuous polymer rods', a rigid macroporous polymer formed by a moulding process and utilised as a separation media in the HPLC.[87] Later, several groups of scientists fabricated inorganic silica-based material known as 'porous silica rods'[88], or 'continuous column support'.[89] In 1993 came the first use of the term 'monolith' to define a single piece of functionalised cellulose sponge used for protein separation.[90]

The term 'monolith' derives from the Greek, and it translates into 'a single stone' According to Tanaka and Unger, a 'monolith is a continuous porous object whose morphology and pore structure can be varied over a wide range'.[91] A monolith can be defined generally as a continuous porous structure without interparticle voids.[92] It also

describes a technological or geological characteristic such as a boulder or mountain, involving a single massive stone or rock. An example of a boulder, obtained by a Chinese empress and utilised to embellish the entrance of one of her palaces, is presented in Figure 1-7.[93]

Monoliths have been formatted in different ways such as discs, rods, and membranes. They can generally be divided according to type, for example based on the nature of materials used for the preparation they are organic, polymer-based monoliths and inorganic such as silica-based monoliths. Additionally, depending on the size of the pores, they can be categorised into three groups: microporous (< 2 nm), mesoporous (2–50 nm), and macroporous or through-pores (> 50 nm).[91, 94]

Figure 1-7: An image of the porous monolith located at the access of the Summer Palace Park in China[93]

Each pore has a specific benefit; micropores are the most essential pores with regard to the separation. Nevertheless, large molecules sometimes cannot pass through the micropores; then, they will interact with the mesopores. The main advantage of the macropores is to permit a high solvent diffusion and mass transfer resulting in a reduction of the backpressure of the column. For extraction, mesopores can thus increase the monolith surface area, resulting in increased permeability.[91]

Several papers have compared monolithic materials and packed particles. Most of the authors agreed that monolithic materials have a number of advantages over packed particles, such as high porosity linked to a high permeability and high surface area, robustness, a wide range of flow rate, high separation efficiency and low back pressure. Furthermore, monolithic columns do not require a frit system in comparison with packed particles.[85, 92, 93]

Figure 1-8 illustrates the structural differences between a particle-packed column (A) and a monolithic column, made from a single piece of a porous solid with relatively large channels for convenient flow (B). It can be seen from the SEM micrographs of the two chromatographic columns that the monolithic bed includes a much greater number of channels penetrating the bed compared to the particle-packed column. In addition, the channels' diameter in the monolithic structure is decreased, permitting a significant reduction in the lengths of path necessary for mass transfer between the stationary and mobile phases.[95]

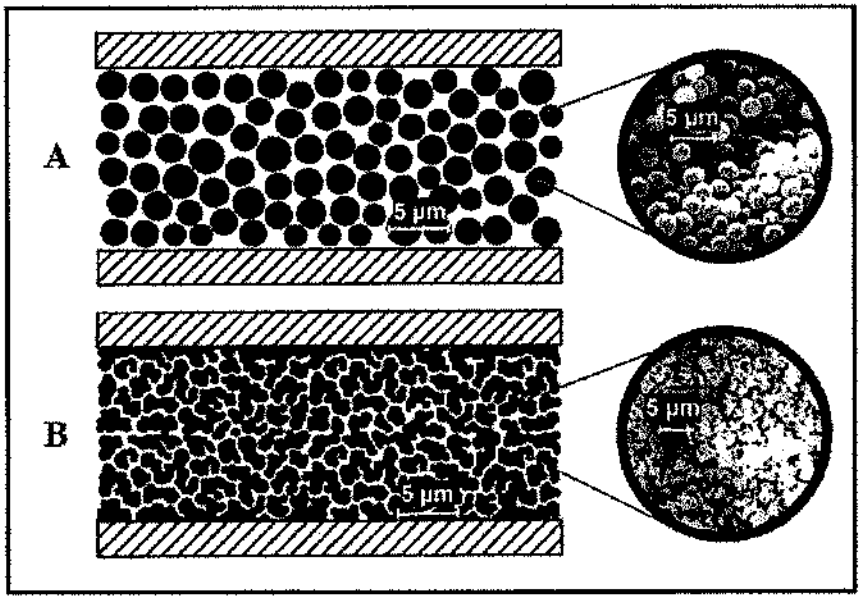

Figure 1-8: The characteristics of internal structure of (A) particle packed, and (B) monolithic chromatographic beds[95]

Owing to the unique characteristics of monolithic materials, they are applied in a diversity range of areas. For instance, monolithic materials have been utilised in various separation science applications, such as gas chromatography (GC), capillary electrochromatography (CEC), and high-performance liquid chromatography (HPLC).[83] These applications have been reported in many reviews.[93, 96-98] As documented previously, monolithic materials can be categorised into organic polymer-based monoliths and inorganic silica-based monoliths. They are different in their preparation chemistry, in which polymerisation is used for the polymer-based monolith whereas hydrolytic polycondensation is used for the silica-based monolith. In this research, emphasis is given to the inorganic silica-based monolith in the next sections.

1.4.2.1 *Organic polymer-based monoliths*

Hjerten *et al.* introduced the first macroporous polymer monolith which is formed by a simple moulding process.[86] These monoliths are polymerised in situ within a tube (e.g. column, capillary or a microchip) in which they remain after the preparation is achieved. Generally, the mould is filled with a mixture of monomer, porogenic solvents, cross linker, and a free radical initiator. Then, the mould is sealed and polymerisation is completed under carefully controlled photo or thermal conditions. After the polymerisation reaction, the polymer monolith is flushed with appropriate solvent, such as methanol or tetrahydrofuran, in order to eliminate porogenic solvents, the initiator, and other unreacted components that remain in the monolith pores. The washing step is performed by using a mechanical pump. Furthermore, the monolith is ready to use for a further experiment. Organic polymer monoliths are mostly based on polystyrenes, polyacrylamides, or polymethacrylates. [93, 97]

1.5 Inorganic silica-based monoliths

Silica monoliths represent an active area of research. According to a SciFinder electronic library search, there have been more than 800 papers published, from 1991 to 2011, describing methods based on silica monoliths. An inorganic silica monolith is prepared as rods from a single-piece structure of porous silica (consisting of skeletons and through-pores), using a sol-gel process. The subsequent surface modification of a silica monolith can also be achieved with relative ease.[51, 99]

Silica monoliths emerged much later than polymer monoliths. In the early 1990s, Nakanishi *et al.* reported a sol-gel approach to making silica-based monoliths. The

earliest paper explaining the successful use of porous silica rods for HPLC was reported by Tanaka and colleagues in 1996, who used a sol-gel process based on the hydrolysis and polycondensation of tetramethoxysilane (TMOS) in the presence of polyethylene oxide (PEO) as a template. This process produced monolithic materials with a continuous silica structure with defined macropores and mesopores. The length of the rods produced was 83 mm with a diameter of 7 mm.[88]

In 1996, Fields *et al.* fabricated a silica xerogel from a potassium silicate solution within a fused capillary and used it to analyse polycyclic aromatic hydrocarbons (PAHs). However, the column possessed very low efficiency (5000 plates/m).[89] In 1998, Horvath and colleagues published a further approach which consisted of packing fused silica capillaries with octadecylated (ODS) 6 μm particles, followed by a thermal treatment, to produce monolithic columns for micro high-performance liquid chromatography (μHPLC) and capillary electrochromatography (CEC). These columns offered good efficiency, characterised by a theoretical plate height of 16 μm for μ-HPLC and 8 μm for CEC.[100]

Additionally, Adam *et al.* used a similar method for the fabrication of monolithic silica capillaries by sintering particles.[101] In 1998, Zare *et al.* fabricated monolithic silica capillaries by incorporating 3–5 μm ODS-particles into a sol-gel solution, which was then placed into a fused silica capillary for CEC. The monolith was investigated with a mixture of aromatic compounds, and it provided efficiencies of up to 80,000 plates/m.[102]

Several scientists have also fabricated monolithic fused silica capillaries by sol-gel bonding of particles using a number of modified methods.[103-105] When silica monoliths were manufactured as rods 4 and 4.6 mm in inner diameter, the challenge was to cover

the silica rods within pressure-stable, leak-tight, cylindrical columns with corresponding fittings.[9i] In 2000, researchers from Merck KGaA, Darmstadt, completed this task by a cladding process using poly (ether-ether-ketone) (PEEK). Since that time, monolithic silica columns have become commercially available in different column dimensions. An example is Chromoliths, which is a trade name manufactured by Merck, as shown in Figure 1-9.[106]

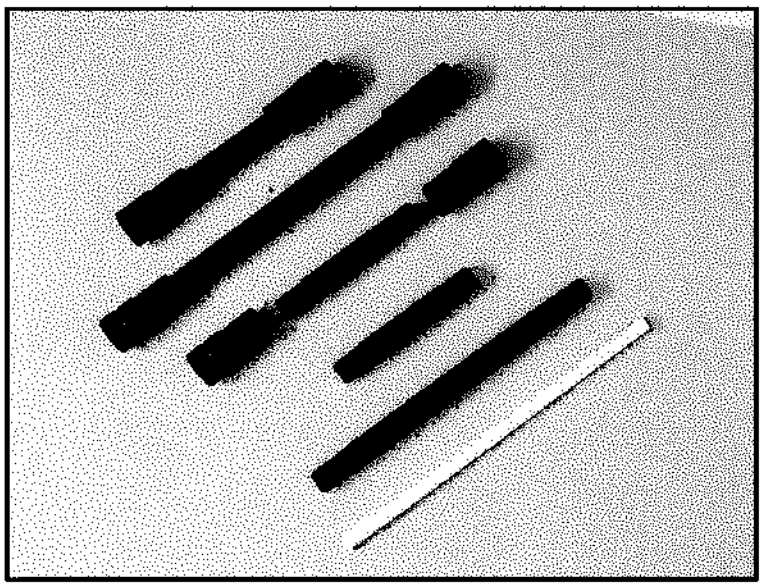

Figure 1-9: Monolithic silica rod (lower); Monolithic silica columns Chromolith™ cover with PEEK and provided with column end fittings

In 2008, Tanaka *et al.* generated 1,000,000 theoretical plates of aromatic hydrocarbons with retention factors of up to 2.4, with a t0 of 150 min. This was accomplished when three 100-μm-i.d. columns were connected to form a 1130–1240 cm column system.[107] In the case of MonoClad columns, Miyazaki *et al.* achieved a higher pressure resistance than with PEEK cladding by covering a silica monolith with two layers of polymer and encasing it in a stainless steel tubing, as illustrated in Figure 1-

10.[108] Recently, Haswell *et al.*, developed a resin silica monolith encapsulation method that enables direct fluidic connection to the monolith using standard union fittings, as shown in Figure 1-11.[109] As the monolith developed in the present work was based on a hydrolysis and sol-gel process, these processes are discussed in more detail the following sections.

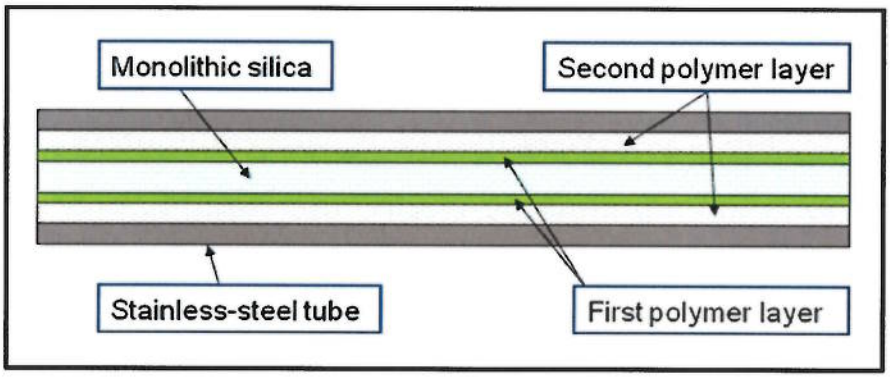

Figure 1-10: Schematic design of a MonoClad column

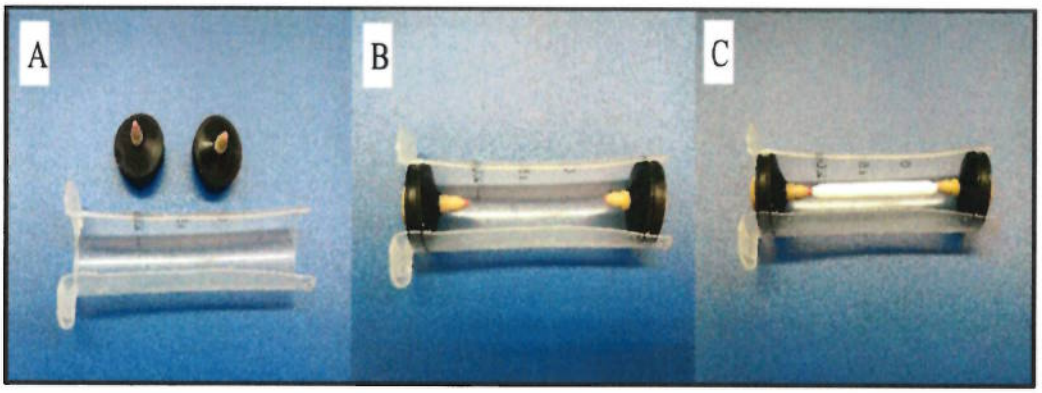

Figure 1-11: Monolith encapsulation mould assembly (A) Silicon release spray lined 20 mL syringe (B) Rubber syringe ends in place, with HPLC fittings inserted (C) Monolith suspended between HPLC fittings

1.5.1 Sol-gel reactions of silica

Silica-based monoliths are prepared by the sol-gel process based on two kinds of reactions: hydrolysis and polycondensation of alkoxides. Normally, the hydrolysis is initiated by mixing water with silicon alkoxide (M-OR) in the presence of alcohol as a co-solvent. The hydrolysis of M-OR produces silanol groups (M-OH), which then condense with one another to produce a polycondensed chain of M-O-M linkages and water. The sequent condensation results in an increase in metalloxane (in the case of silicon, siloxane) oligomers that link together to form a network structure of silica gel skeletons with macropores. Alcohol also can be produced as condensate when the amount of water is limited.[110, 111] The chemical reactions of the sol-gel process are shown in Figure 1-12.

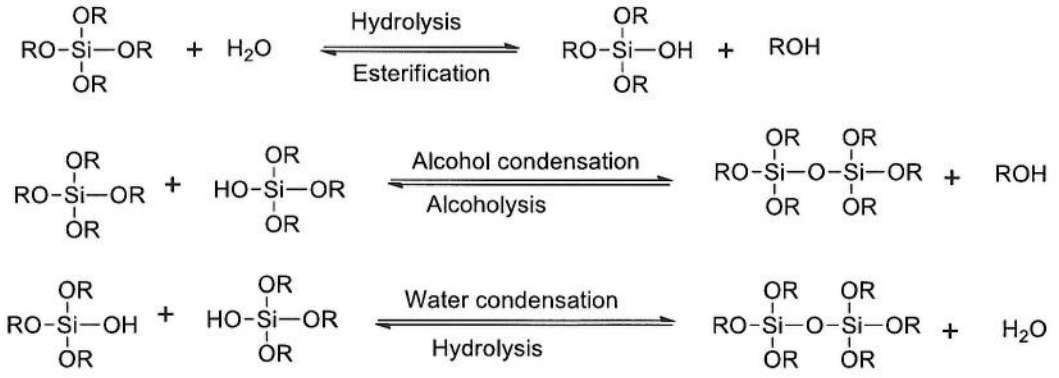

Figure 1-12: Scheme of reaction during the synthesis of silica monolith

1.5.1.1 *Starting material*

The reaction mixture consists of silica gel, an organic additive, a catalyst, and water. There are many choices of silica source that have been used to manufacture silica gel. Water glass (sodium silicate) is employed to prepare macroporous silica monoliths when purity is not required.[112] Silicon alkoxides, mostly tetraethoxysilane (TEOS) and

tetramethoxysilane (TMOS), are commonly used as a silica source according to their purity, low cost, and availability.[91, 93] Figure 1.13 shows the chemical structure and properties of TEOS and TMOS. Nakanishi *et al.* have widely used TMOS to fabricate monoliths for easier hydrolysis; hydrolysis using TEOS is a little slower in making a homogeneous solution from the starting materials.[88, 113] Wagh *et al.* described the use of three kinds of precursors, polyethoxydisiloxane (PEDS), TMOS, and TEOS, to fabricate monoliths, and they found that TMOS produced a higher surface area with narrower and more uniform pores than TEOS; however, PEDS was better than both.[114] Colon *et al.* found that methyltriethoxysilane (MTES) produces a higher surface area than TEOS and a more flexible network. Methyl-modified alkoxides, such as MTES or methyltrimethoxysilane (MTMS), are utilised as minor components. Based on the works of others, such as Harreld *et al.*, a mixture of TMOS and MTES have been used.[115]

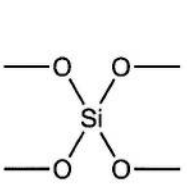

Tetramethoxysilane (TMOS)
Formula : $C_4H_{12}O_4Si$
Molecular weight : 152.22 g mol^{-1}

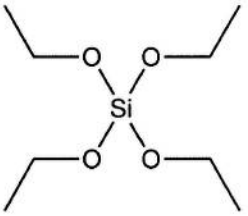

Tetraethoxysilane (TEOS)
Formula : $C_8H_{20}O_4Si$
Molecular weight : 208.33 g mol^{-1}

Figure 1-13: The chemical structure and properties of TMOS and TEOS

Generally, silicon alkoxides offer slow hydrolysis and polycondensation kinetics when compared to other metal alkoxides; thus, a catalyst is necessary to promote the reaction. The catalyst can be a base, such as N-methylimidazole ($CH_3C_3H_3N_2$) or an acid, such as nitric acid (HNO_3) or acetic acid (CH_3COOH), mixed or dissolved in water before

the introduction of the additive. The type and concentration of the catalyst play an important role in determining the macroporous formation of silica monoliths. Furthermore, silicon alkoxides are insoluble in water; therefore, another solvent (polar–non-polar) is required to homogenise the mixture.[91, 116, 117]

Additives: Organic additives are required in the preparation of silica monoliths. They can induce phase separation between silica and water. Polyacrylic acid (PAA) was used as a porogen for first time by Nakanishi *et al.*[118], who later used a water-soluble polymer, polyethylene oxide (PEO), and claimed that the size distribution can be controlled by adjusting the concentrations of TMOS or PEO.[113] Furthermore, Martin *et al.* used polyethylene glycol (PEG) and agreed that low concentrations of PEG lead to a strong solid matrix, and vice versa.[119] Later, Tanaka *et al.* showed that an increase in the concentration of PEG leads to a decrease in the domain size. PEO is broadly applied with a range of molecular weights and is easy to dissolve in water.[120] Shi *et al.* have used triblock copolymer (F127) to fabricate a TMOS silica monolith with continuous textural pores and mesopores, and interconnected skeletons. F127 has been demonstrated to act as a template function and phase separation inducing agent.[121]

1.5.1.2 *Sol preparation and hydrolysis*

The overall steps for preparing macro/mesoporous silica monoliths using the sol-gel process are illustrated in 1.14. The process includes four steps: (i) hydrolysis of silicon alkoxide in the presence of porogen additive; (ii) phase separation and gelation; (iii) ageing and solvent exchange; and (iv) drying and heat treatment.

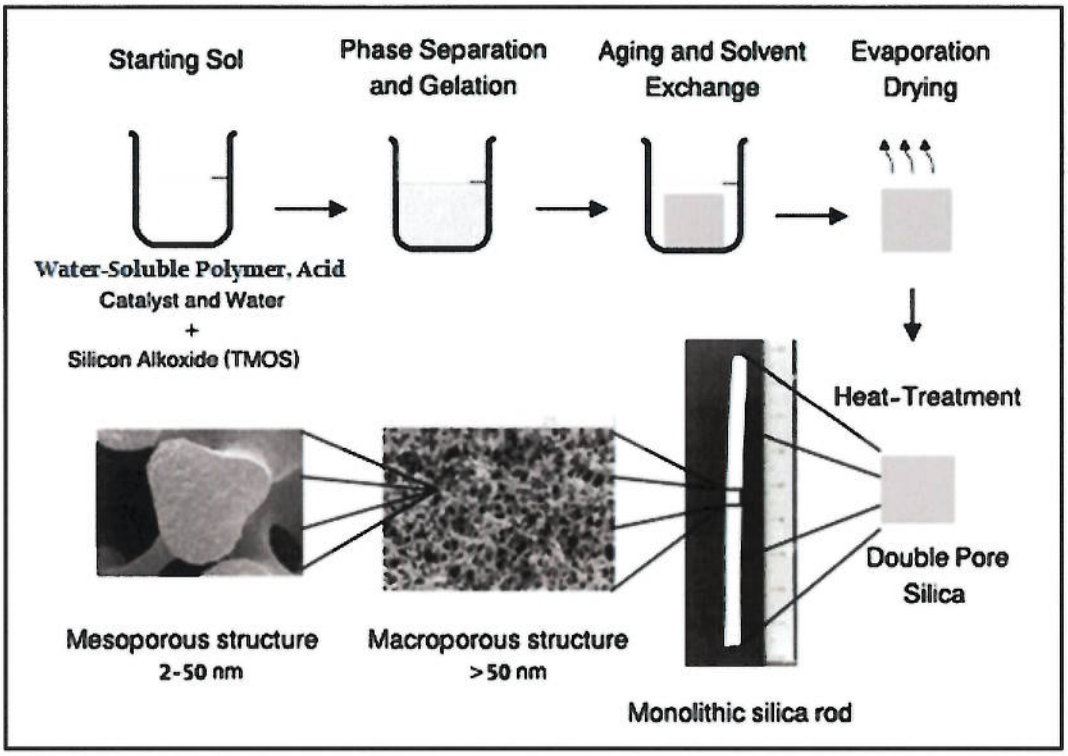

Figure 1-14: The overall steps of preparing silica monolith and the structure of monolithic silica rod with the bimodal pore structure[91]

1.5.1.3 *Hydrolysis and phase separation and gelation*

Hydrolysis is initialised by first mixing water, the catalyst, and the additive. A few minutes are enough to dissolve the additive in water and achieve a homogeneous solution. Next, silicon alkoxide is added to the solution under stirring at ice temperature, as the reaction between water and silicon alkoxide is exothermal. Under mixing, the droplets of silicon alkoxide become dispersed in the solution to form a turbid mixture. Then, after a couple of minutes, the mixture is converted to a transparent solution, and reaction heat is generated. If alcohol is used, the temperature might reach its boiling point. After the transparent solution is obtained, it is poured into a mould as a gel under a constant temperature, before its viscosity becomes too

high.[91, 122] This moulding step can be affected by some factors, including the mould shape (which defines the final shape of the product), cleanliness of the mould to prevent any possible contamination and the type of mould used (to avoid any interaction between the solution and mould).[123]

During the gelation process, the mould should remain stable, avoiding any possible mechanical disturbance. Here, the condensation reactions yield particles that subsequently compose clusters and increase the solution viscosity. In addition, a three-dimensional network will be formed when the hydrolysis and polycondensation reactions are achieved. The gelation temperature is generally in the range of 40–80°C.[91, 122]

The hydrolysis and condensation reactions can be influenced by differences in the processing parameters of the chemical compositions. Motokawa *et al.* examined the influences of using different starting materials and physical parameters during the gel formation process on the structural morphology of silica monoliths. They prepared monolithic fused silica capillary columns by using 18 mixtures of TMOS and MTMS. The fabricated monoliths exhibited a range of skeleton diameters from 1 to 2 μm and macropore diameters from 2 to 8 μm. Silica monoliths with a smaller domain size showed lower back pressure and greater column efficiency.[124, 125]

1.5.1.4 *Ageing and solvent exchange*

Kirkbir *et al.* showed that washing the gel with an aqueous solution of ethanol results in an improvement of the permeability of the sol part of the gel.[126] Einarsrud *et al.* demonstrated that silica gel can be strengthened by ageing it in ethanol solutions, water, and TEOS.[127] Later, they also showed that the permeability of the gel can be increased by washing it in water by dissolution and reprecipitation.[128] During the ageing step the

solvent evaporates, leading to shrinkage of about 25% in the gel network.[120] Dai *et al.* used an ionic liquid, because of its low vapour pressure, which eliminated shrinkage in the gel network.[129] Reichenauer reported that the external microspore surface area could be decreased by washing the gel in water, followed by supercritical drying, leading to no significant shrinkage of the gel.[130]

Following gelation, solvent exchange is required to generate the size of the mesopores required for separation/adsorption. Ammonium hydroxide (NH_4OH) is commonly used to tailor mesopore, as an increase in the concentration of NH_4OH leads to larger mesopores. A higher temperature also can produce larger mesopores, up to 50 nm.[131]

During polycondensation reactions of silica in the presence of water-soluble organic polymer, the phase separation takes place between the silica-polymer system and water. It generates a skeleton with a bicontinuous network of macropores on the silica surface. The sizes of the macropores and skeleton may be controlled by the molecular weight and the concentration of polymers.[110]

Shrinivasan *et al.* synthesised TMOS monoliths using different molecular weights of PEO (10kDa and 100kDa). The morphological structures of the TMOS monolith are different in the presence of variable PEO molecular weights, as shown in Figure 1-15. The SEM image of a TMOS monolith of 10kDa MW PEO shows the diameter of macropores between 5 and 7 μm with surface area of 40 $m^2 g^{-1}$. On the other hand, the SEM image of a TMOS monolith of PEO containing 50% 10kDa MW and 50% 100kDa MW has a macropore diameter between 2 and 4 μm with a surface area of 380 $m^2 g^{-1}$; whereas the SEM image of a TMOS monolith of 100kDa MW PEO has a surface area of 520 $m^2 g^{-1}$ and macropore diameter of less than 1 μm.[132]

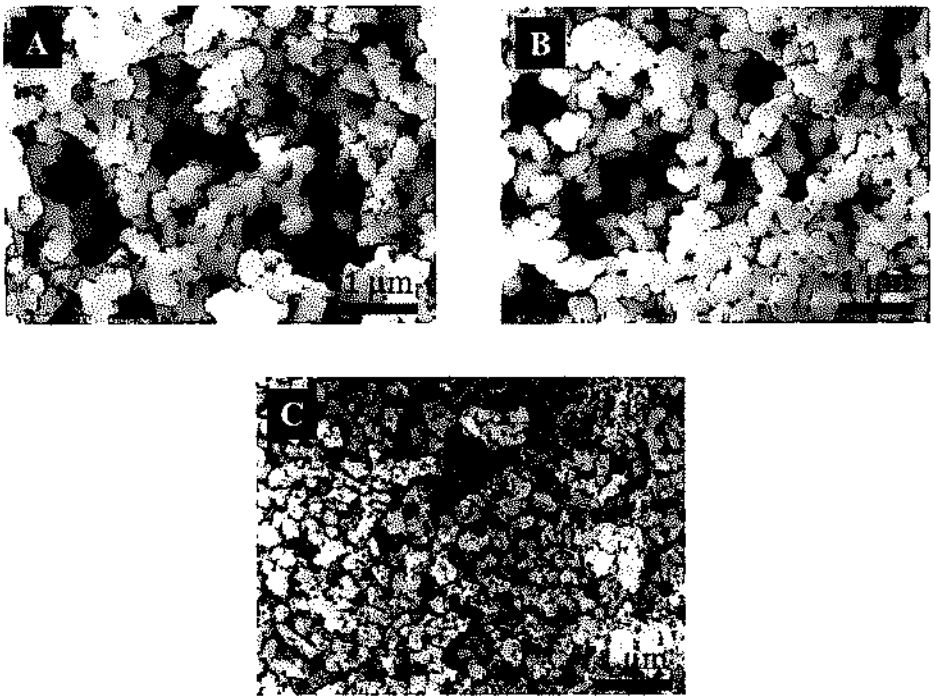

Figure 1-15: SEM image of (A) TMOS monolith prepared from 10kDa MW PEO (100%), (B) TMOS monolith prepared from 10kDa MW PEO (50%) and 100kDa MW of PEO (50%) and (C) TMOS monolith prepared from 100kDa MW PEO (100%) (adopted with a permission from the publisher, Elsevier)[132]

Fletcher *et al.* synthesised the biporous silica monoliths with both macropores (μm) and mesopores (nm) in the skeleton structure. They also found that the sizes of the macropores and skeleton may be influenced by the molecular weight and concentration of the polymers.[133]

Minakuchi *et al.* suggested that increasing the molecular weight and concentration of PEO leads to a delay in phase separation relative to the sol-gel transition. This allows the silica network to grow more in the gelation stage before the structure of the silica monolith is frozen. Hence, increasing the molecular weight and concentration of PEO results in an increase in the thickness and strength of the skeleton structure and so the

porosity and permeability of the monolith decrease. The shrinkage in the wet gel enabled the monolith to be removed from the mould for the basic treatment.[82, 120]

To increase the surface area of the monolith, the well-aged form with basic treatment was produced by thermal decomposition of ammonium hydroxide or urea solution at a temperature near to 100°C to form the mesoporous structure. These mesopores are shaped inside the silica skeleton by a dissolution–reprecipitation process, where dissolution of the silica occurs on the convex surface and reprecipitation occurs on the concave surfaces by adjusting pH and temperature.[134, 135]

Numerous experiments suggested that the experimental parameters such as the basic treatment period, pH, and temperature may influence the performance of monolithic material and the pore size distribution.[131, 136-139]

1.5.1.5 *Drying and heat treatment*

Drying is the last process in the preparation of a monolith. This step is critical, as shrinkage of the gel can lead to damage and cracking of the monolith. It has a minimal influence on the monolith structure. During drying, shrinkage of the gel is driven by the capillary pressure, Pc, which is described by equations (1-1) and (1-2).

$$Pc = (2\ \gamma LV\ \cos\theta)\ rh^{-1} \qquad (1\text{-}1)$$

Where, γLV is the surface tension of the pore liquid at the liquid vapour interface.

θ is the contact angle.

r is the pore radius.

$$rh = 2Vp\ Sp^{-1} \qquad (1\text{-}2)$$

Where, Vp is the pore volume.

Sp is the surface area.

Drying removes the majority of the organic compounds from the wet gel monolith.[91, 113] In general, the temperatures applied are between 40 °C and 80 °C, depending on the starting materials. Subsequently, a heat treatment is performed at high temperature from 500 °C to 650 °C to remove the organic residues without causing any possible deformation on the structure of the monolith. Furthermore, the mechanical stability on the silica monolith improved due to the heat treatment whereas the surface area and the pore volume decreased.[111, 133]

1.5.2 Properties of silica-based monoliths

Monolithic silica materials represent a three-dimensional network structure and exhibit bimodal pores, through-pores, and mesopores (see Figure 1-16). The through-pores, also called macropores, enable flow paths through the column and allow the analyst to enter the mesopores. The mesopores contribute mainly to the surface area. The term 'skeleton size' denotes the average thickness of the silica network, whereas the term 'domain size' denotes the total size of both skeleton and through-pores. The sizes of the mesopores and macropores can be controlled independently.[91, 140] Mesopores are formed in the skeleton in the 10–20 nm range, and they can be adjusted after the formation of the network structure by the basicity of an etching solution, reaction time, and temperature, whereas the sizes of the silica macropores and skeletons can be adjusted by the composition of the starting mixture.[141] The size of macropores is usually larger than the size of the skeleton, leading to (macropore size to skeleton size) ratios of up to 4.0. This porosity is greater than that of a particle-packed column.[116, 125] The total porosity of a monolithic column is about 85%, which is 15–20% higher than a particle-packed column with 5 μm particles. This porosity can be divided into 80% macroporous, 10–15% mesoporous, and a small percentage of microporous. High porosity leads to high permeability or a low pressure drop.[140, 142, 143]

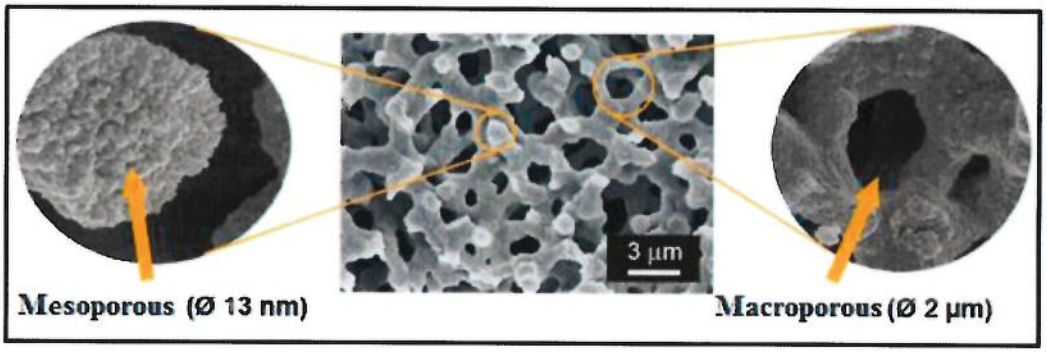

Figure 1-16: SEM photograph of the typical porous structure of monolithic silica columns (in the middle), the macropore or through pore (right), and the mesoporous structure of the silica (left)[140]

1.5.3 Monolith for sample preparation using SPE

Solid-phase extraction (SPE) has become one of the most widespread extraction techniques used in the extraction and pre-concentration of analytes in matrices of environmental, clinical, food, and biological samples, because it is simple and versatile. In SPE, the analyte of interest is transferred from the aqueous phase to a sorbent phase and subsequently eluted in an appropriate solvent. SPE can offer the benefits of reducing analysis time, sample volume, organic solvent consumption and disposal, cost, and labour.[71]

Monoliths are becoming increasingly popular as a sample preparation tool which is apparent in a number of publications.[144-147] Historically, monoliths were first used as extraction sorbents for SPE of polar organic compounds in 1998,[148] and as sorbent material in a microfluidic device to extract peptides and proteins in 2001.[149] These

materials have several advantages over more conventional particulate materials. For example, they offer low backpressure and high permeability, depending on their structure, and ease of preparation and automation; in addition, they form adjustable shapes and can be modified with any chemical functionality. On the other hand, monolithic sorbents have some limitations, such as a small surface area, narrow column dimensions, and limited commercial suppliers.[150]

Various applications have been revealed for online SPE coupled with LC[148, 151, 152] and inline pre-concentration with monoliths with capillary electrophoresis (CE),[153-155] and many types of offline devices have been designed (e.g. attaching the monolith to a syringe, stir bar, pipette tip, or spin column). Figure 1-17 illustrates some examples of commercially available SPE formats.[147, 156] Some applications of silica monoliths as offline SPE are shown in Table 1.1.

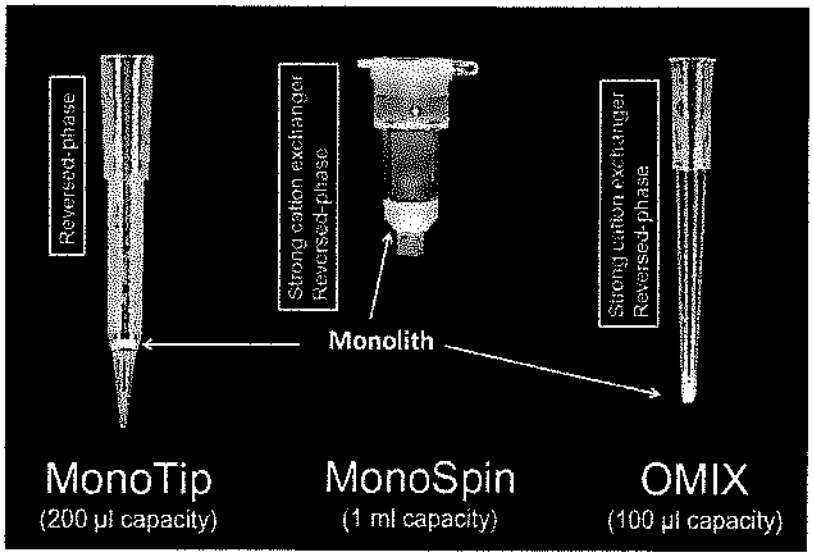

Figure 1-17: An image of commercially available silica monolith spin column and pipette tips presenting the optimum volume of sample and technique of extraction[156]

Table 1-1: Some applications of silica-based monolith as offline SPE

Packing type	Material	Analyte	Sample	Ref. no.
Fused silica capillary with syringe device (40 mm x 0.2 mm id)	TEOS-PEO-C18	Methamphetamine	Urine	157
Silica rod in pipette tip (2.8 mm id, 1 mm thickness)	TEOS-PEO-C18	Peptides/proteins	Aqueous sample	158
Stir bar (SBSE) 40 mm (without magnetic stir)	TMOS-PEG	Polycyclic aromatic hydrocarbons (PAHs)	Aqueous sample	159
Silica disc in spin column (4.3 mm id, 1.5 mm thickness)	TEOS-PEO-C18	Pesticides (Amitraz)	Serum	160
Silica disc in spin column (4.3 mm id, 1.5 mm thickness)	Silica-C18	Pesticides (Cyromazine)	Bovine milk	161
Silica rod in plastic syringe (2mL)	TMOS-PEG	Epinephrine, normetanephrine, and metanephrine	Urine	83
	TMOS-PEG	Morphine and codeine	Serum	162
	TMOS-PEG	Ketamine	Urine	163

1.5.4 Chemical modification of silica-based monoliths

The surface chemistry of silica is polar and displays different configurations of silanol groups (SiOH). The silanol groups are the points of attachment for the bonding of different ligands to silica. These groups can be presented in three forms: isolated (single hydroxyl groups) where the surface silicon atom has three bonds into the silica backbone and the fourth to an OH group, vicinal or bridged silanols (two isolated silanol groups attached to two adjacent silicon atoms are bridged by an H-bond), and germinal (two hydroxyl groups attached to one silicon atom). The three types of silanols available for bonding are shown in Figure 1-18.[47, 67, 164]

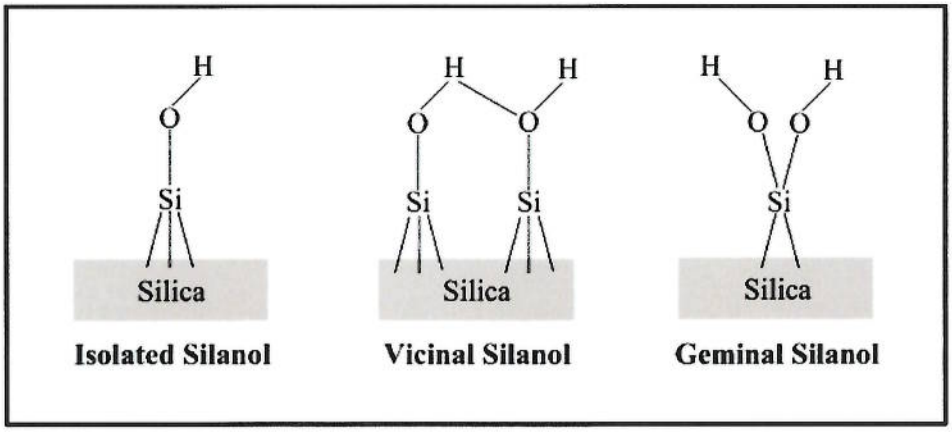

Figure 1-18: Types of silanols on silica available for bonding

Moreover, the silanol groups can retain compounds on to the silica surface by hydrogen bonding due to the strong energies of absorption for these groups. An isolated silanol group has an absorption energy of 7.9 kcal mol^{-1}, while vicinal and geminal silanol groups have absorption energies of 13 kcal mol^{-1}.[47]

The surface of the silica-based monolith can be chemically functionalised by bonding the silica surface with another chemical species to obtain the required stationary phase through an appropriate chemical reaction. Generally, the chemical modification of the silica surface can be performed by three types of reactions, as shown in Table 1-2.[54]

Table 1-2: Reactions for the chemical modification of silica

Type of reaction	Surface linkage
Organosilanisation	Si-O-Si-C
Esterification	Si-O-C
Chlorination	Si-Cl

In this project, the chemical modification of the silica monolith is based on organosilanisation, to achieve a stationary phase for reversed-phase SPE. Organosilanisation is the most common reaction for the modification of silica, which is based on using a derivatisation reagent such as chlorosilanes or alkoxysilanes, to generate a more or less hydrophobic surface on the silica. The two types of derivatisation reagents differ in their reaction rates.

$$R\text{-}SiCl_3 > R\text{-}Si(OCH_3)_3 > R\text{-}Si(OCH_2CH_3)_3$$

Trichlorosilane > Trimethoxysilane > Triethoxysilane

Alkoxysilanes are less reactive than chlorosilanes. Chlorosilanes react immediately upon contact with reactive groups. Alkoxysilanes react slower than chlorosilanes and can be used to avoid chloride ions or to achieve an additional reactive functional group such as amines. The produced bonded phase can be greatly influenced by the type of substitution on the silane. Figure 1-19 illustrates some of the typical silanes.[47, 66]

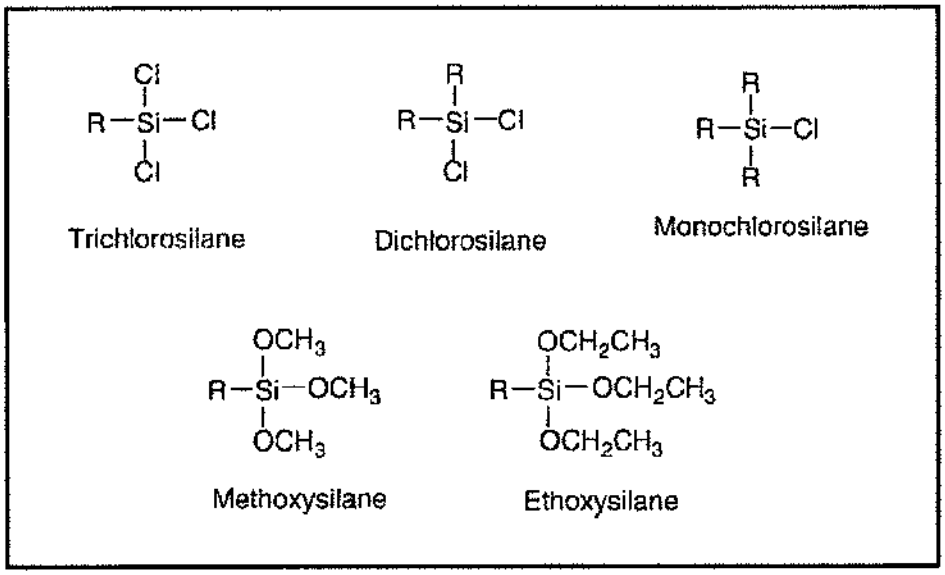

Figure 1-19: Some types of silanes

Monochlorosilanes are commonly applied for the modification of a silica surface or the endcapping of active sites with phases normally having 2, 4, 8, or 18 carbon atoms attached. These phases are mainly known as C-2, C-4, C-8, and C-18 phases, respectively. Trichlorosilanes and dichlorosilanes can be employed for modification as well. Nevertheless, the presence of water in trichlorosilane and dichlorosilane reactions can result in cross-linking and decrease the permeability of the silica monolith. Moreover, three-dimensional polymers and linear polymers are difficult to produce and manufacture.

Thus, in this work monochlorosilanes (octadecyl, C18) was used to modify the surface of the silica-based monolith, due to factors such as its ability to retain non-polar and moderate polar pesticides from a liquid sample, offering high permeability with better extraction efficiencies. [6, 47]

Octadecyl (C18) is the most hydrophobic phase and also known as octadecylsilane (ODS) materials. Figure 1-20 shows derivatisation of silica with a chlorosilane reagent (octadecyldimethylchlorosilane). The degree of surface loading by the R group of the monochlorosilane (C-2 to C-18) will vary from 5% to 19% by weight as carbon for the packing material. The octadecyl type (C18) sorbents have the greatest capacity due to the longer chain alkyl groups. The sorbent capacity is stated in milligrams of analyte sorbed per gram of sorbent.[66, 67]

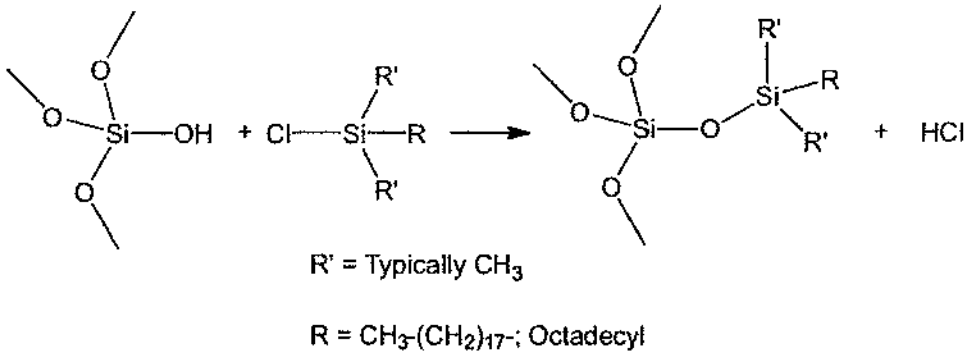

Figure 1-20: Synthesis of C18 bonded monofunctional phase

The functionalisation of the silica surface generally takes place in the silanol groups of the mesopores (2–50 nm) since the mesopores are more accessible to the analytes of interest as well as the derivatisation reagents (octadecyl groups). Conversely, the

silanol groups in the micropore (>2 nm) are generally inaccessible due to the blockage that occurs by the bonded moieties in the mesopores, as can be seen in Figure 1-21.[54, 67]

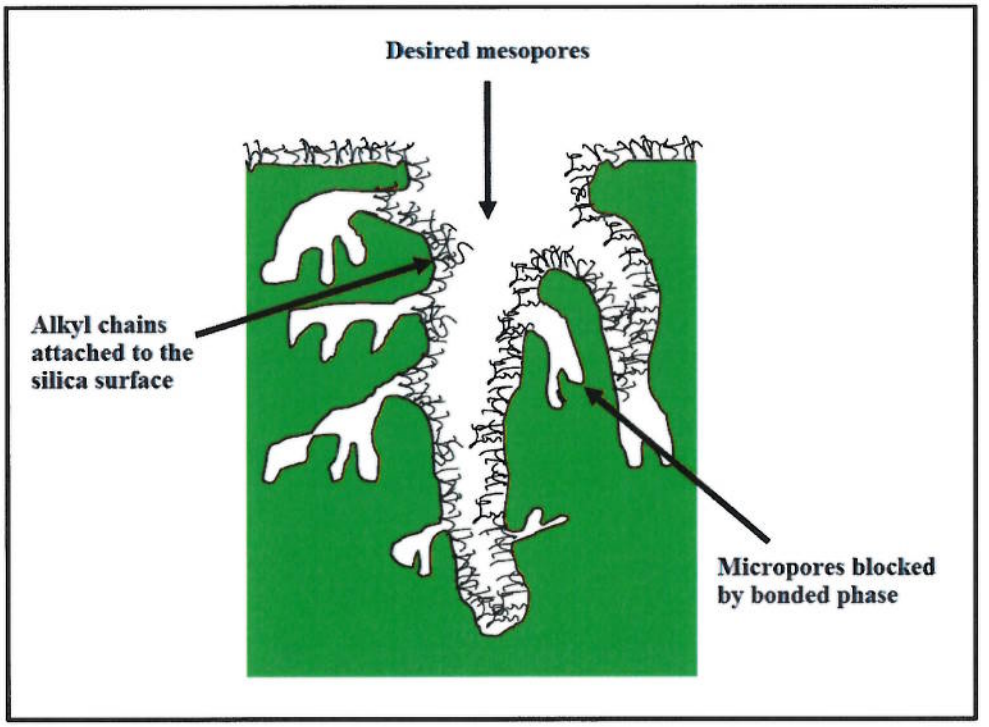

Figure 1-21: Schematic diagram indicates the porous silica surface, presenting the inaccessibility of some micropores[54].

Some of the silanol groups on the silica surface can be left unreacted after derivatisation due to reaction conditions and steric hindrance. For a small alkyl group, the movement is very restricted and the nearby silanols are not blocked. However, when the attached bonded organic moieties are large (e.g. octadecyl groups), their movement can block the neighbouring silanol groups, hinder other organic moieties from reaching the surface, and retain a considerable number of free silanols.[54, 71]

The presence of free silanol groups on the derivatised surface may have a negative influence on the sorbent performance because they can cause polar interaction with

the sample and make the elution of the analyte more difficult. In order to minimise the number of free silanol groups remaining on the modified silica sorbent, a further reaction known as endcapping can be performed by treating the derivatised sorbent with a small silane molecule such as trimethylchlorosilane (TMCS) or hexamethyldisilazane (HMDS), as can be seen in Figure 1-22. The endcapping process allows a more hydrophobic surface to be produced and generates a more uniformly non-polar stationary phase.[67, 71, 165]

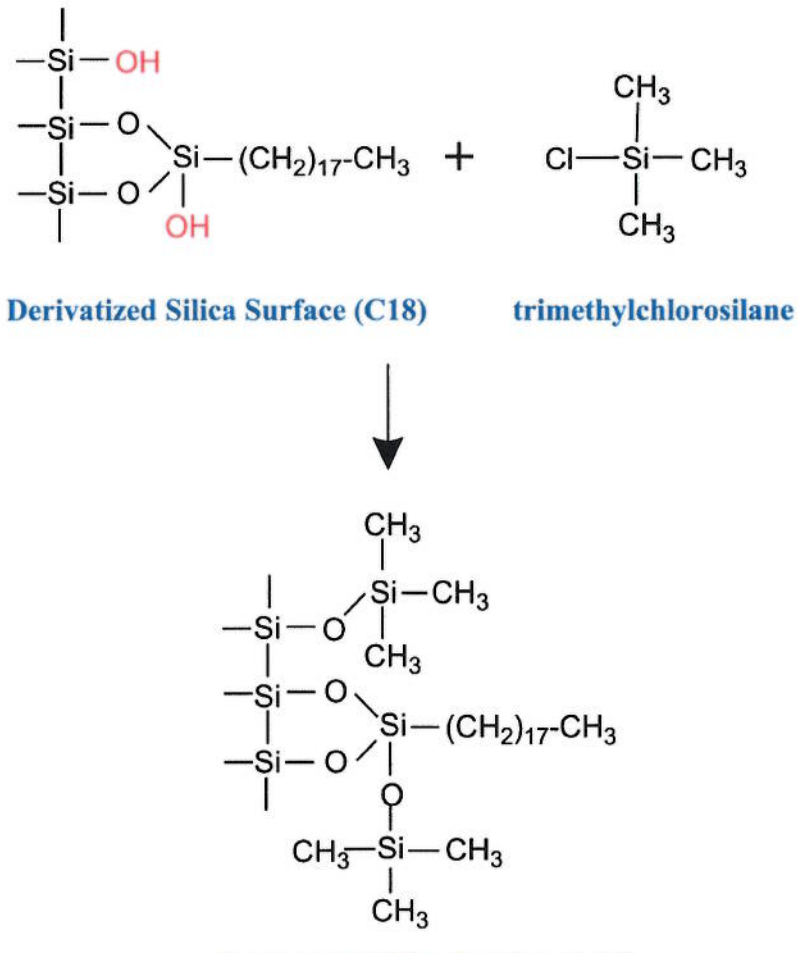

Figure 1-22: Endcapping of free silanols with TMCS for a C18 sorbent

Conditioning of the bonded silica sorbent before applying the solution to the sample is a common operation significant to achieving the promised performance of the sorbent. When the C18 sorbent is unconditioned and dry, the orientation of the octadecyl bonded phase material on the sorbent surface is random. Water is often used as a solvent for the sample. If the solution of the sample is loaded on the sorbent, the environment neighbouring the bonded organic moiety would be highly polar and this environment is not appropriate with octadecyl groups. The alkyl groups have the tendency to aggregate among themselves in order to minimise the exposure of the high polarity medium, as can be seen in Figure 1-23 (A).

To overcome this problem, the octadecyl chains required to be conditioned with an organic solvent such as acetonitrile, methanol, or tetrahydrofuran before the use of the sorbent. The conditioning step makes the octadecyl bonded phase less aggregated and fully opened, and also allows the sorbent to have maximum interaction with the target analyte, as can be seen in Figure 1-23 (B) and (C).[54, 67, 72]

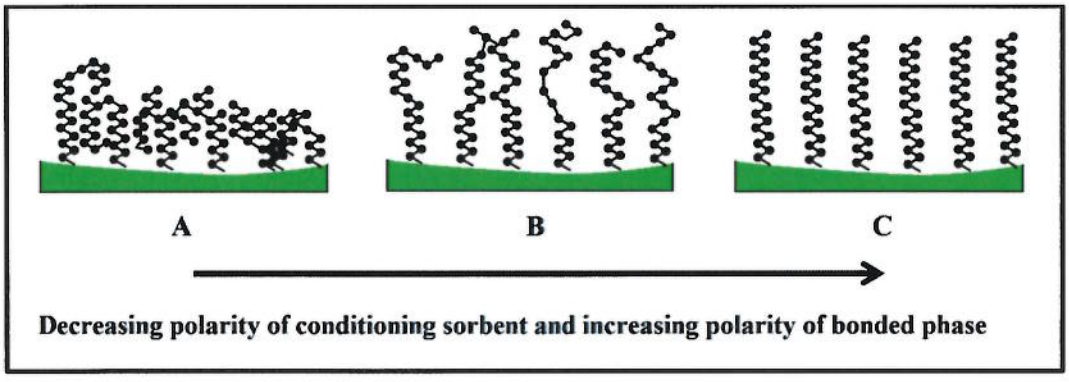

Figure 1-23: Schematic diagram presenting the influence of conditioning process on octadecyl bonded silica: (A) without conditioning (B) partially conditioned (C) totally conditioned[54].

1.5.5 Physical characterisation of silica-based monoliths

Silica monoliths are physically characterised to establish their flow and surface area properties in order to design new and efficient separation media. Various techniques have been employed to investigate the pore structure of silica monoliths containing through-pores (pores of width > 50 nm) and mesopores (pores of width between 2 and 50 nm). Some of these methods are mercury porosimetry (MP), liquid permeation (LP), nitrogen sorption, microscopy and image analysis, and inverse size-exclusion chromatography (ISEC). Inverse size-exclusion chromatography (ISEC) is applied for the assessment of mesoporous structures based on the size separation of polymers. This approach obtains mesopore size distribution and the porosity from a relationship between the silica mesopore size and the molecular size of the polymer standards.[91, 97, 142]

In this research, the following techniques, (i) nitrogen sorption and (ii) microscopy and image analysis, were selected to investigate and characterise the pore structure of the fabricated silica-based monoliths.

1.5.5.1 *Nitrogen sorption*

One of the most common methods for mesoporous analysis is the nitrogen sorption isotherm at 77 k, which provides information about the physical properties of silica monoliths including the specific pore volume, the specific surface area, and mesopore size distribution.

In this technique, the amount of adsorbate (nitrogen gas) is adsorbed in the solid adsorbent (silica-based monolith) at a constant temperature depending on the applied pressure. The adsorption process is called physical adsorption (physisorption) when

the interactions between the adsorbate and the adsorbent are relatively weak (van der Waals) and there are no chemical bonds formed. Moreover, this adsorption process usually produces reversible changes.

At a certain pressure, defined as equilibrium pressure (P), the progress of gas adsorption stops and the number of atoms or molecules being adsorbed equates to the number of atoms or molecules desorbed from the surface. The surface area of the solid then can be measured by the physical adsorption of adsorbate molecules. The most commonly used expression to quantify the amount of the adsorption phenomenon is the adsorption isotherm.

In general, the measurement of the adsorption isotherm curve is achieved from plotting the amount of gas adsorbed (preferably in $cm^3\ g^{-1}$), (y-axis) against the equilibrium relative pressure (p/p_0), (x-axis), where p_0 is the saturation pressure of adsorptive gas (N_2) at the temperature of the measurement. There are six various types of adsorption isotherms categorised by the International Union of Pure and Applied Chemistry (IUPAC), which are illustrated in Figure 1-24.[91, 166, 167]

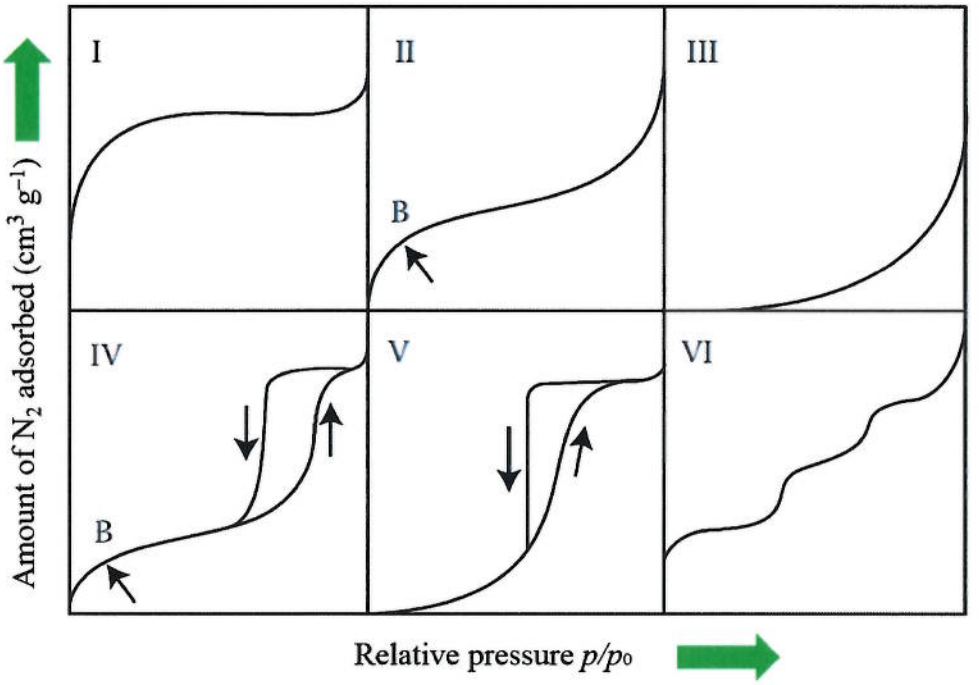

Figure 1-24: IUPAC classification of gas physisorption isotherms. The adsorption and desorption isotherms have six different forms (I-VI): (I) microporous, (II) non-porous or macroporous, (III) non-porous, (IV) mesoporous, (V) mesoporous, and (VI) non-porous.

From the IUPAC classification of the sorption isotherms, the type I isotherm shows a steep increase in the adsorbed amount with rising pressure up to the saturation pressure. This type of isotherm is obtained when adsorption is restricted to a monolayer or adsorbents containing micropores, which have a relatively small pore diameter not wider than 2 nm.

Type II isotherms are obtained with non-porous or macroporous absorbents (with pores larger than 50 nm). This type of isotherm describes unrestricted monolayer-multilayer adsorption. In Figure 1-24 (II), point B, which is the start of the almost

linear middle section of the isotherm, shows the step at which monolayer coverage is finished and multilayer adsorption is about to begin.

The type III is convex to the relative pressure axis over its entire range and thus does not offer a point B. It results in very weak adsorbate-adsorptive interactions for non-porous materials.

The type IV isotherms have a characteristic feature which is a hysteresis loop. This feature is related to the filling and emptying of mesopores (pores with a size of range between 2nm and 50nm) by capillary condensation and limited uptake over a range of high relative pressures (p/p_0). The initial point (B) of the type IV isotherm is referred to as a monolayer-multilayer adsorption as it pursues the same direction as the corresponding part of a type II isotherm found with the given amount adsorbed on the same surface area of a non-porous solid. Type IV isotherms are observed in numerous mesoporous industrial adsorbents.

The type V isotherm is comparable to type III isotherms, not only do they simulate very weak adsorption interactions, but they also include a hysteresis loop due to the presence of mesopores. Finally, type VI isotherms, known as stepped isotherms, correspond to the formation of multilayers of non-porous solids which appear as a stepwise multilayer adsorption on a uniform solid surface.[166, 167]

1.5.5.2 *Electron microscopy and image analysis*

The two most widespread electron microscopy techniques used for studying the physical aspects of silica-based monoliths are scanning electron microscopy (SEM) and transmission electron microscopy (TEM). SEM has been employed to investigate

the morphology of monoliths after the drying step, and it can be used to assess the skeleton and flow-through pore diameters of the silica monolith.

In addition, this technique can be combined with energy dispersive X-ray spectroscopy (EDX) to offer a valuable instrument to determine the elemental composition of the fabricated silica monolith as part of the analysis. SEM-EDX is therefore a powerful tool, particularly when comparing the morphological merits of two products and examining product quality. Nevertheless, SEM-EDX requires the solid sample to be destructed as a part of the preparation prior to establishing an analysis. TEM is a more powerful method than SEM, which gives excellent images of tiny structures down to the Ångstrom scale.[91, 168]

1.5.6 Comparison between silica-based and polymer-based monoliths

Numerous studies have compared the main classes of monolithic materials, inorganic silica-based and organic polymer-based, and have confirmed that each monolith has its own unique characteristics and weaknesses. The substantial difference between silica and polymer monoliths is their internal structures and porous properties. Figure 1-25 shows the differences in pore morphology between the two types of monoliths. Nevertheless, both types of monolith include one feature in common, which is the presence of macropores.[169]

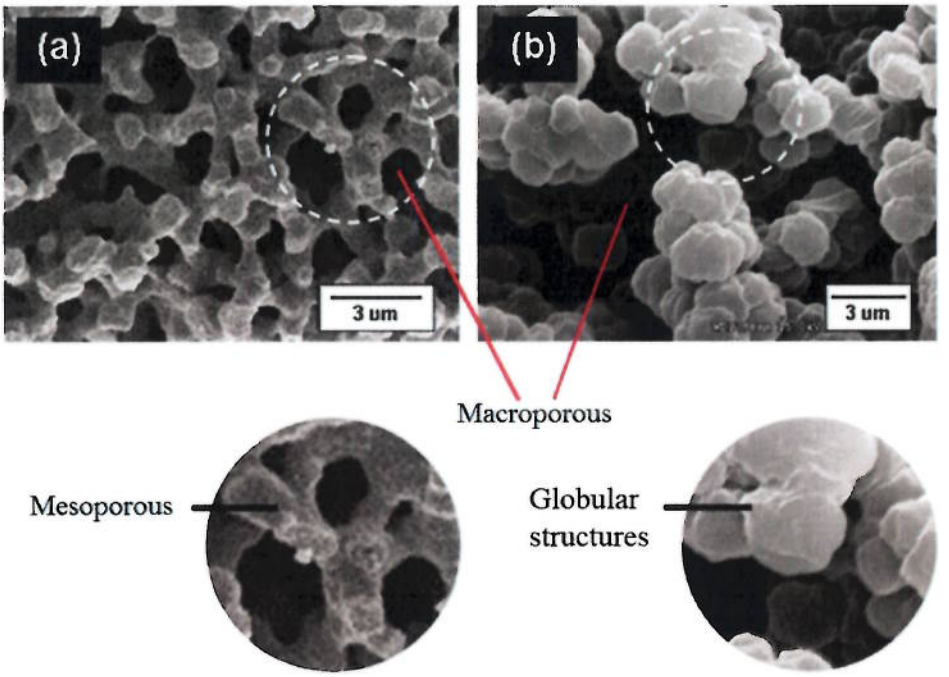

Figure 1-25: SEM photographs of (a) bimodal pore structure silica monolith with macropores and thin skeleton containing mesopores, and (b) typical polymer monolith with globular structures[170]

Silica-based monoliths possess a bimodal pore structure, macropores (through-pores) and mesopores, with relatively high surface area of several hundred m^2 g^{-1}. The macropores offer the sorbent a high hydrodynamic permeability, while the mesopores on the surface of the thin skeleton present a high surface area and increase the number of sites available to interact with the target analyte. [170-172]

The bimodal structure allows easy penetration of the small molecules to interact with the adsorption sites, and offers fast diffusion. These pore structures give improved efficiency of extraction and are generally utilised for low and medium molecular mass substances such as pesticides and drugs. However, silica monoliths show relatively lower performance for extraction of macromolecules, for example proteins and other

biopolymers, because the macromolecule needs wide pores to allow easy access and good penetration.[171, 173]

In contrast, organic polymer monoliths have a globular structure (Figure 1-25, b), which consists of soft matter composed of cross-linked polymer. Moreover, the absence of mesoporous structures in the polymer monoliths results in significantly lower surface area compared to the silica monoliths. Hence, organic monoliths have shown low efficiency for the extraction and separation of small molecules. The morphology of this type is more appropriate for extraction and separation of macromolecules.[174, 175] A further extensive comparison between silica and polymer monoliths is summarised from the previous monolith literature in Table 1-3.

Table 1-3: Summary of comparison between silica and polymer monoliths based on the literature review [176]

Comparison	Silica monolith	Polymer monolith
Preparation method	Simple	Simple
Preparation time	Long[93]	Short[177, 178]
Surface area	High (200–800 m^2g^1) [78, 179, 180]	Limited surface area (100–400 $m^2 g^{-1}$)[148, 181]
Permeability	High[78, 179, 180]	Moderate[182, 183]
Chemical and thermal stability	They have high mechanical strength and high thermal stability.[184]	They can shrink or swell when exposed to various organic solvents, and are affected by temperature. [182, 183]

Stability over pH range	Not stable at high pH values[49]	Stable over a wide range of pH values[185]
Surface modification of the monolith	They can be simply modified with several functional moieties resulting an additional efficiency and selectivity.[54, 164]	They have many cross-linking bonds, which need hours to reach equilibrium for the activation of surface.[164]
Fabrication inside microchip	Complicated, since the position of the monolith inside the microchip cannot be defined due to their fabrication based on using thermal initiation.[116, 186]	Simple, since the initiation of a polymerisation reaction can be achieved by photoinitiation (light).[187, 188]
Extraction efficiency	A number of papers demonstrate their use as materials for extraction with high efficiency.[189]	A number of papers demonstrate their use as materials for extraction with relatively good efficiency.[190]

1.6 Miniaturising environmental analysis

Over the past few decades, massively increased production in the pharmaceutical, industrial, biochemical, and medical fields has resulted in an increasing list of contaminants and a rise in environmental guidelines. As the number of potentially harmful pollutants increases, extensive calls are made on environmental analysis. Monitoring of contaminants in the water, soil and air is an effective element in understanding and controlling hazards to human health and the environment. Given this need as well as the cost and time involved in conventional analytical methods for environmental samples (e.g. chromatographic methods), there is an urgent requirement for portable, robust, and accurate monitoring methods.[191, 192]

In this context, chemical sensors become a suitable approach for the development of portable systems for environmental monitoring. These systems transform chemical information into an electrical or optical signal. The sensors have some positive features such as rapid analysis and cost-effectiveness; nevertheless, they are often limited regarding selectivity.[193-195]

The advancement of automated flow injection analysis (FIA) offers another solution for portable systems in the field of environmental analysis. FIA was first invented by Rutzicka and Hansen in the mid-1970s.[196] FIA, being a continuous flow system, is based on the injection of a sample into an unsegmented carrier stream of reagents, which in turn transports it into a detector. The use of this approach has assisted towards the design of a 'total analysis system' (TAS), involving the entire analysis carried out within a single system.[32]

The basic advantages of FIA are simple instrumentation, large throughput, high sensitivity, and reduction of sources of contamination. However, besides a number of advantages, FIA also exhibits some disadvantages such as high reagent consumption, large sample volumes, and consequently large waste production.

Sequential injection analysis (SIA) is an alternative approach to overcome the problems found in FIA. In this method, the solutions (e.g. sample and reagents) are aspirated into a holding coil by valves and reverse flow is used to stack the sample and reagents before detection. However, one drawback of SIA is its tendency to run slower than FIA.[197-199]

The shortage of aforementioned methods in the field has led to the miniaturisation of analytical methods, which has been an interesting research area during the last few years. Manz *et al.* first introduced the concept of the 'micro total analysis system' (microTAS, μTAS) in the early 1990s, whereby all the steps of chemical analysis such as sample preparation, separation and detection are miniaturised and performed in one automated system (a few square centimetres).[200]

This analytical miniaturisation concept can be termed in different ways, for example lab-on-a-chip or microfluidic devices. Figure 1-26 illustrates the concept of miniaturisation and functional integration of these laboratory processes on to a microchip. Microfluidics technology will be discussed in greater detail in Section 1.7.

Figure 1-26: Miniaturising and functional integrating laboratory processes on to a microchip device (adopted with a permission from publisher John Wiley and Sons). [201]

1.7 Microfluidics

Microfluidics refers to the behaviour and manipulation of low volumes of fluids (typically nanoliters or less) in channels with micrometre dimensions. In addition, microfluidic devices offer a variety of distinctive benefits for environmental monitoring applications, such as low consumption of samples and reagents, low waste production, low expense, portability, rapid analysis time, minimised risk of contamination, and incorporation of multiple analytical processes.[202, 203]

In recent years, numerous researchers have focused on the use of microfluidic technology for environmental analysis. Marle and Greenway studied the use of microfluidic devices in the area of environmental monitoring. They described microsystems with different detection methods such as absorbance, fluorescence, chemiluminescence, and electrochemical detection.[32] Chen *et al.* covered the wide application of microchip electrophoresis coupled with electrochemical detection for environmental pollutants.[204] Li *et al.* presented a review of the current development of the applications of microfluidic systems for real environmental samples in 2009.[203] In 2012, Jokerst *et al.* reviewed the published literature over the past three years on advances in integration of the three analytical processes: sample preparation, separation methods, and detection, in microfluidic analysis for environmental samples.[191] Due to their favourable properties and wide-ranging applications, microfluidic devices have been examined in order to develop portable approaches for the monitoring of environmental pollutants.

1.7.1 Substrates

Since microfluidic devices have been widely used in various areas of applications, the properties of the fabrication material can play an essential role in the achievement of the application and this has resulted in a wide diversity of substrate materials being introduced.[205] The substrate materials utilised for the production of microfluidic devices can be divided into three major groups: inorganic, polymeric, and paper.[206]

Inorganic materials can include silicon and glass. Silicon was one of the earliest materials used to fabricate microfluidics devices and has contributed to the rapid development of microfluidic technologies. Silicon possesses high thermal conductivity, excellent surface stability, and solvent compatibility.[206-208] However, silicon is relatively expensive, is incompatible with electro-osmotic flow (EOF) and is not transparent in visible light (inappropriate for systems that use optical detection). To overcome these drawbacks, transparent materials such as glass or polymer can be bonded to silicon in order to generate a hybrid system.[206, 209]

Different glass materials such as fused silica, soda-lime, and borosilicate glass have been widely utilised in microfluidic device fabrication. These substrates have good optical transparency, EOF compatibility, excellent thermal stability, and high resistance to several chemical solvents. However, glass has shortcomings such as a high cost of fabrication (require clean rooms), easy to fracture, and high temperature bonding processes (≤ 650 °C).[209, 210]

Polymer-based materials are an attractive alternative for the fabrication of microchip devices, because they include a wide range of substrates. Polymeric materials can be divided into two main classes: elastomers such as polymethylmethacrylate (PMMA) and thermoset polyester (TEP), and thermoplastics such as polydimethylsiloxane

(PDMS), polycarbonate (PC) and polystyrene (PS). They are relatively inexpensive, disposable, easily manufactured and have good mechanical flexibility. Nevertheless, polymers have some disadvantages; for example, low resistance to organic solvents, limited operation-temperature range, and gas permeability. [209, 211, 212]

Recently, paper has been suggested as an alternative material used for the fabrication of microfluidic devices. Paper is inexpensive, biocompatible with many biological samples, available in an extensive range of thickness, is lightweight, and is disposable.[205, 213] As no substrate is well suited for all microfluidic applications, hybrid materials have also been established in order to take advantage of their comparative benefits to the full, for example polymer/glass. [214]

Nevertheless, for carbamate pesticides monitoring in environmental samples, it can be easy to choose a material based on the most appropriate properties. Moreover, several studies have successfully utilised glass microfluidic devices for the detection of carbamate pesticides.[215-217] As a result, glass was used as the substrate material for the fabrication of microfluidic device in this study.

1.7.2 Device fabrication

There are several aspects to consider when selecting the most suitable method for microfluidic device fabrication such as process time and costs, the availability of fabrication equipment, the preferred substrate materials, the device design and reproducibility of the fabrication method.[218, 219]

1.7.2.1 *Photolithography and wet etching*

The earliest and most widely used technique for glass and silicon chip fabrication is photolithography and wet etching. The substrate (glass or silicon) is covered with two

layers; the first layer is metal (e.g. chromium) and the other layer is a photoresist. The required channel design is generated in a mask form. The mask is placed above the layers and exposed to UV light. The exposed photoresist layer is then removed, and the uncovered metal layer removed using a metal etchant. Finally, the whole device is etched using an appropriate etching solution, such as hydrogen fluoride (HF), followed by thermal bonding to close the substrate microstructures.[218, 220] The process of this fabrication technique will be detailed in Section 2.5. Table 1-4 illustrates some substrate materials that have been utilised for μTAS chips and relevant applicable fabrication methods.[205, 221]

Table 1-4: A number of substrates used for the fabrication of microfluidic devices and the most commonly used technique for fabrication in each substrate

Material	Fabrication technique
Glass	Photolithography and wet etching, laser cutting, deep reactive ion etching (DRIE)
Silicon	Dry etching, LIGA
Elastomers	Soft lithography
Thermoplastic	Hot embossing, injection moulding
Paper	Photolithography, wax printing, PDMS application, plasma treatment

1.7.3 Fluid manipulation

Fluid movement in microfluidic devices requires low flow rates and minimal pulsation. Numerous methods are available for pumping fluids within a microfluidic channel, and two of the most common methods are pressure driven flow (hydrodynamic) and electro-osmotic flow (EOF).[218]

Pressure driven flow (PDF) can be generated due to off-chip pressure (e.g. syringe pumps coupled to a microchip via connectors and tubing) to move aqueous and non-aqueous solutions through a microchannel. The hydrodynamic flow depends on the microchannel geometry and the viscosity of the liquid, and is mostly laminar resulting a characteristic parabolic flow profile, as shown in Figure 1-27 (A). Syringe pumps are selected over traditional peristaltic pumps for flow injection analysis (FIA) due to the low flow rates required within the micro fluidic devices.[221, 222]

In contrast, the working mechanism of electro-osmotic flow (EOF) is based on the movement of bulk fluid with an electrical field. Depending on the charge and size of ionic and non-ionic particles, they move towards the cathode with different rates of flow.[218] Microfluidic devices are fabricated from glass or silica that permits a negatively charged surface at pH > 4 because of the deprotonation of silanol groups (≡Si-O-). The outer negative ions (anions) are aligned with inner positive ions (cations) and form double rigid stern layers. Although, these cations are not capable of neutralising anions completely, therefore a diffuse layer is formed in the system. When the electric current is applied, the cations of the diffuse layer move towards the cathode.[223]

This motion causes a flat flow profile with homogeneous velocity across the width of the channel with slow movement close to the internal surface wall, as shown in Figure

1-27 (B). There are couple of disadvantages of this system: (a) it generates Joule heat causing band broadening and loss of separation resolution; (b) it is related to electrokinetic movement that generates gas bubbles in the system as the result of electrolysis causing the break of the flow rate.[224] In this research, PDF was applied for precise control of the flow rate and to prevent the EOF shortcomings.

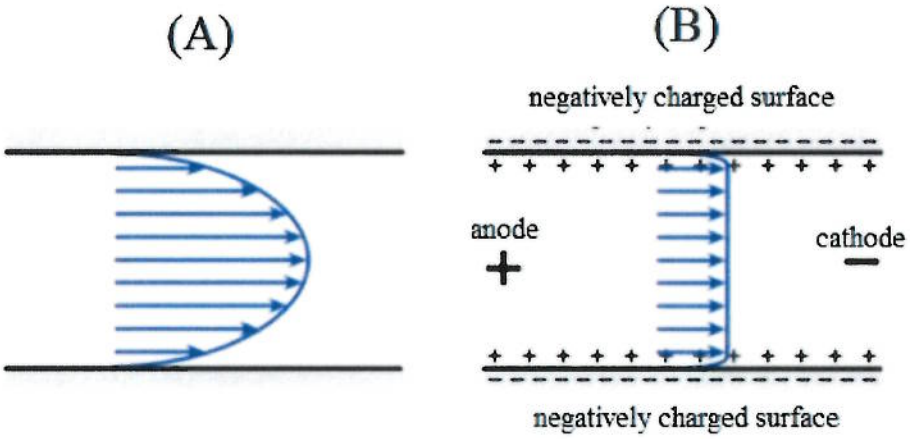

Figure 1-27: (A) Parabolic flow profile of a fluid as it is passed through a microchannel via hydrodynamic pumping (B) Flat profile generated by electro-osmotic flow (EOF) through a microchannel

1.7.4 Mixing

Rapid mixing of the sample and reagents is essential for analytical purposes. The small channel size within a micro fluidic device means that the flow of liquid within this is predominantly laminar due to the dominant viscous forces. The dimensionless parameter, the Reynolds number (Re) gives the ratio of viscous and inertial forces and is utilised to identify whether flow of the fluid is laminar or turbulent (equation 1-

3).[225] At low Reynolds numbers (<2000) laminar flow occurs, where fluid motion is smooth and constant. At high Reynolds numbers (>2000), inertial forces are dominant generating eddies and turbulent flow. Figure 1-28 shows both laminar and turbulent flow.

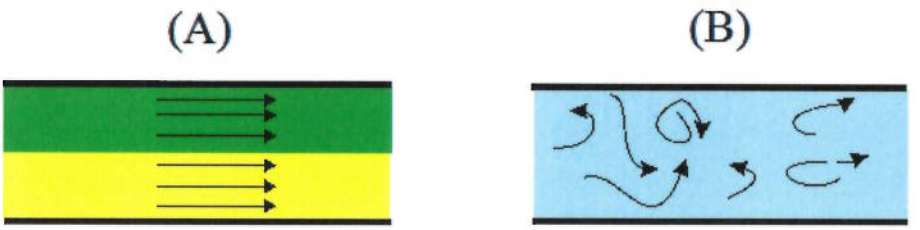

Figure 1-28: Diagram showing A) well-defined laminar flow, and B) random, turbulent flow.

$$R_e = \frac{\rho v L}{\eta} \qquad (1\text{-}3)$$

Where, R_e is the Reynolds number.

ρ is the density of the liquid (kg m^{-3}).

v is the velocity of the liquid (m s^{-1}).

L is the channel diameter (m).

η is the viscosity (Ns m^{-2}).

Laminar flow can be expected when the channels' diameters are very small in microfluidic devices. Therefore, in the presence of a concentration gradient between adjacent parallel laminar streams, molecules are transported across their common interface only by the mechanism of diffusion.[226] The Einstein-Smoluchowski equation can be utilised to measure the extent of molecule diffusion, as can be expressed in Equation 1-4.[214]

$$X = \sqrt{2Dt} \qquad (1\text{-}4)$$

Where, X is distance to be travelled (cm)

D is the diffusion coefficient ($cm^2\ s^{-1}$)

t is the time required (s)[227]

From equation 1-4, it can be shown that when the diffusion coefficient is large (i.e. with a small molecule) the diffusion time is rapid. For the same molecular size (the same diffusion coefficient), a decrease in the dimension of channels can also reduce the time required for diffusive mixing. For instance, scaling down the channel width from 1 mm to 50 μm considerably decreases the time taken for a water molecule to mix fully by 400 times (from 200 s to 500 ms).[228]

1.7.5 Detection

Microfluidic devices have been employed in a wide range of analytical applications such as environmental,[229, 230] pharmaceutical,[231, 232] forensic,[233] and clinical

applications.[234, 235] One of the most important components of the microfluidic technology is a highly sensitive detector. This component has the ability to identify low concentrations of the analyte of interest within small sample volumes. Electrochemical and optical techniques are the most popular detection systems used in microfluidic devices for environmental analysis due to their portability and cost.[191, 203] This section will be focused on optical detection methods generally used in the field of study.

Optical detection

Optical techniques of detection, including ultraviolet-visible spectrophotometry, fluorescence and chemiluminescence, have been employed for environmental applications.

Ultraviolet-visible spectrophotometry

UV-VIS spectrometry is one of the oldest detection methods to be applied in microfluidic devices; it has been used in a wide variety of analytes. Nevertheless, the short optical path length of microchannels (mostly 5 to 50 nm) significantly hinders sensitivity and detection limits and reduces the absorbance signal,[191] according to the Beer–Lambert Law (equation 1-5).

$$A = \varepsilon c l \qquad (1\text{-}5)$$

Where, A is the absorbance

ε is the molar absorptivity coefficient ($dm^3\ mol^{-1}\ cm^{-1}$)

c is the concentration ($mol\ dm^{-3}$)

l is the path length (cm)

A further drawback to UV-VIS spectrometry is the requirement for a light source which can increase the complexity of the detection method for microchips. Despite these disadvantages, several researchers are working to develop this detection method on microfluidic devices. This development focuses on miniaturisation of spectrophotometers by reducing the size of light sources, as known light-emitting diodes (LEDs). LEDs can be easily incorporated into microfluidic devices.[203]

Diamond *et al.* designed three layered 'T' microchips containing UV-LED as the light source. The colorimetric reagent of hydrochloric acid, ammonium metavanadate and ammonium molybdate reacted with phosphate to form yellow vanadomolybdophosphoric acid, which showed absorbance at 380 nm. The yellow method was used to determine phosphorus in river water. The LOD of this method in the microfluidic system was 0.2 mg L^{-1} and the dynamic linear range was 0–50 mg L^{-1}.[236, 237] They developed an autonomous microfluidic sensor with an incorporated UV-LED detector. The incorporation of reagent and waste storage, sampling, wireless communication, colorimetric detection, and the power supply produced a miniaturised and portable sensor, which could measure phosphate for seven days.[238]

Ueno *et al.* developed a portable microfluidic device with UV absorbance for the detection and identification of atmospheric aromatic volatile organic compound gases, specifically benzene, toluene, and xylenes (BTX). A fibre optic link moved light from a UV lamp to the microchip. They achieved a 0.05 mg L^{-1} detection limit for toluene gas in a sampling time of 30 min.[239]

Fluorescence

Fluorescence is the ability of some organic and inorganic components (fluorophores) to absorb light at a specific wavelength and subsequently emit light at a different wavelength. The emitted wavelength is always longer than the initial incident wavelength, revealing the fact that electromagnetic radiation is partly absorbed by the material and partly emitted by lower energy photons.[240] Fluorescence is a detection technique belonging to the photoluminescence technique, along with phosphorescence.[241] The fluorescence intensity is described by equation 1-6:

$$I = kP_0c \qquad (1\text{-}6)$$

Where, I is the intensity of the incident light

k is a constant

P_0 is the radiant power of the incident light

c is the concentration of the emitting species (mol dm^{-3})[242]

According to Equation 1-6, the intensity of light is proportionate to the radiant power, which means it can use to detect the analyte at very low concentrations depending on a powerful light source which led to being very sensitive technique.

Fluorescence detection is an excellent option for detection in microfluidic systems because of its high sensitivity accompanied by low detection limits. These benefits overcome the typical limitations related to absorbance due to the limited path length in a microchip.[191, 206]

Nevertheless, fluorescence is not without its own disadvantages, including the limited number of substances that show native fluorescence for environmental analytes and

the complexity and large size of optical instrumentation. The supplement of a fluorophore to environmental analytes involves further sample preparation steps and leads to increases in the cost of the experiment. Regardless of these drawbacks, fluorescence detection has been utilised effectively for environmental analysis with microfluidic technology.[191]

The process of luminescence is demonstrated by the Jablonski diagram, as illustrated in Figure 1-29. The Jablonski diagram shows that a molecule will absorb a photon which produces the excitation of an electron to an excited singlet state (S_2). The excited electron through internal conversion (IC) will relax to another excited singlet state (S_1). The electron can take place in one of two routes.[197, 241]

The first route is when the electron returns to the ground state (S_0) and emits light through fluorescence (F) or chemiluminescence (CL). The lifetime of the process is very short, approximately 10^{-9} to 10^{-7} seconds. The second route is when intersystem crossing (ISC) occurs in an excited triplet state (T_2), and then the electron relaxes back to the ground state (S_0) emitting light through phosphorescence. This process is slower than the singlet state and can take up to 10 s. In photoluminescence, fluorescence and phosphorescence, the source of excitation is energy from absorbed ultraviolet or visible light, while chemiluminescence energy is from chemical reactions.[243, 244]

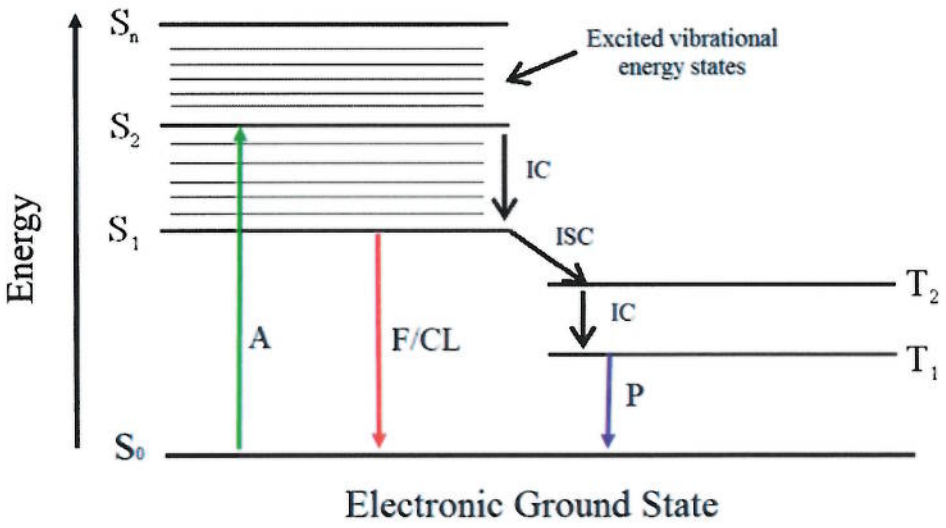

Figure 1-29: Jablonski diagram describing energy levels and possible transitions: A, photon absorption; F, fluorescence; CL, chemiluminescence; P, phosphorescence; S_0, ground state; S_1, S_2, excited singlet state; T_1, T_2, excited triplet state; IC, internal conversion; ISC, intersystem crossing.[241]

1.8 Chemiluminescence

Chemiluminescence (CL) is a luminescent phenomenon, clarified as the emission of light produced during the process of a chemical reaction. The pathway of light emission in chemiluminescence is similar to that in fluorescence except for the excitation source, as discussed in Section 1.7.5. CL does not required a light source, in contrast to adsorption and photoluminescence techniques, and it has been known as a dark-field detection technique. This feature can reduce the background signals, lead to improvement in the detection limit, and offer wide dynamic ranges. Owing to its high sensitivity and selectivity, simplicity, and low cost, CL detectors can be easily coupled and miniaturised with flow-based approaches.[241, 245]

1.8.1 Mechanisms of CL reactions

Generally, there are two basic mechanisms of CL reactions, specifically direct and indirect CL, as shown in Figure 1-30. In the situation of direct CL, two reagents, a substrate (usually a chemiluminescence precursor) and an oxidant in the presence of some cofactors, react to give an intermediate or product, sometimes in the presence of a catalyst. Some fraction of the intermediate or product is generated in an electronically excited state, which consequently returns to the ground state with photon emission. The catalyst, which could be an enzyme or metal ions, works to decrease the activation energy or to process an oxidant. A cofactor is sometimes required to modify the substrate into a form eligible to interact with the catalyst. On the contrary, indirect CL is based on the excited product transferring its energy to a fluorophore. The fluorophore then becomes excited and emits light.[241, 246]

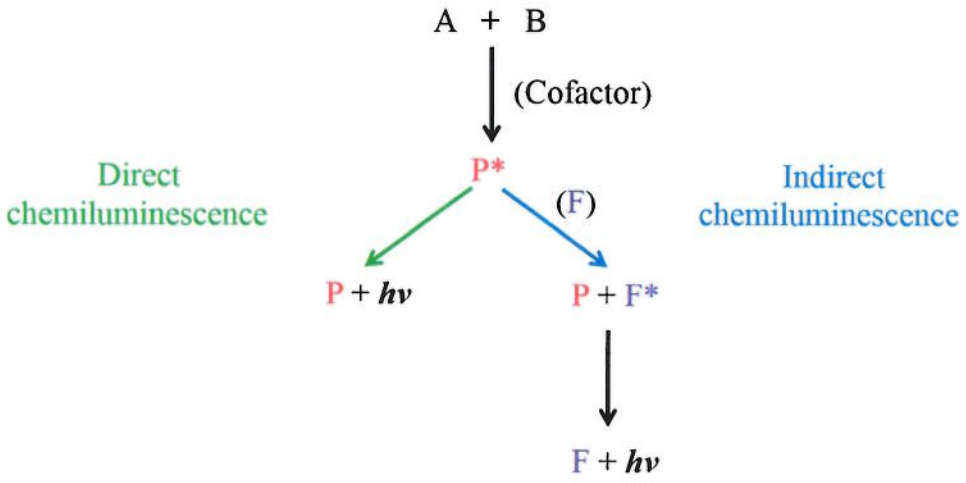

A, Chemiluminescence precursor
B, Oxidant
P, Intermediate or Product
F, Fluorophore

Figure 1-30: Types of chemiluminescence reactions

1.8.2 Requirements for CL reactions

There are some important requirements for light to be produced from the CL chemical reaction. An exothermic reaction is necessary to produce sufficient energy, around 40–70 kcal mol^{-1}. The free energy requirement can be calculated using:

$$-\Delta G \geq \frac{hc}{\lambda_{ex}} = \frac{28600}{\lambda_{ex}} \qquad (1\text{-}7)$$

Where, $-\Delta G$ is free energy

λ_{ex} is the long wavelength limit for excitation of the chemiluminescent species

The pathway of reaction has to be of sufficient energy to form an electronically excited state. The reagents of chemiluminescence are generally associated with redox reactions using similar potential oxidants or oxygen and hydrogen peroxide.[197] The analyte can be identified by CL detection only if it has one of the next three characteristics, such as it is chemiluminescent when mixed with a particular reagent or works as a catalyse, or suppresses CL between other reagents.[247]

In chemiluminescence reactions, the intensity of emission is based on the efficiency of producing molecules in the excited state, which can be represented by the quantum yield (quantum efficiency). The intensity can be calculated from Equation 1-8.[241]

$$I_{CL} = \Phi_{CL} \frac{-dA}{dt} \tag{1-8}$$

Where, I_{CL} is the chemiluminescence emission intensity (photons/second)

Φ_{CL} is the chemiluminescence quantum yield

$\frac{-dA}{dt}$ is the rate at which the CL precursor A is consumed

Therefore, the CL quantum yield (the efficiency of CL reaction) can be expressed in Equation 1-9.[197]

$$\Phi_{CL} = \Phi_C \times \Phi_{ES} \times \Phi_F \tag{1-9}$$

Where, Φ_{CL} is the CL quantum yield

Φ_C is the chemical yield of the reaction

Φ_{ES} is the fraction of the product that enters the excited state

Φ_F is the fluorescence quantum yield

1.8.3 Factors affecting the CL emission

Chemiluminescence measurement is significantly dependent on some of the experimental parameters that can have an effect on the CL efficiency and the rate of reaction. These parameters include the CL precursor chemical structure, the concentration and nature of other substrates that could influence the CL route, the selected catalyst, the pH, the presence of metal ions, temperature, ionic strength, and the hydrophobicity of the solution composition and solvent.[241]

1.8.4 Chemiluminescence detector

The CL emission is always achieved in a dark environment; it demands a detector for collecting the emission. There are some basic requirements for the detector, such as the ability to detect light over several ranges of intensity, highly sensitive over the spectral range 400–600 nm, the speed of the response of the detector has to be faster than the rate of the CL reaction to provide a true light signal, and the signal output should be immediately associated with the light intensity.[241]

The two common detectors employed to measure the chemiluminescence emission are the photomultiplier tube (PMT) and the charge coupled device (CCD). CCD is usually applied in combination with a camera, it has high sensitivity, and allows for multiplexing. [197]

Photomultiplier tube (PMT)

PMT is photodetector device more extensively used in CL due to its portability and high sensitivity leading to the measuring of low light-level detection. A PMT involves a photosensitive cathode and a collection anode that are divided by dynodes (electrical electrodes), which offer electron multiplication or gain. A schematic diagram of PMT is shown in Figure 1-31.

The photon reacts with the photocathode, which is normally fabricated from antimony with a range of various metals.[248] After the process of reaction, a photoelectron is released as a result of the transfer of light energy to the electron. As these electrons passes through the PMT they are amplified via a series of dynodes at increasing voltages until the anode is reached; the current that has been generated through the system is then measured.[197]

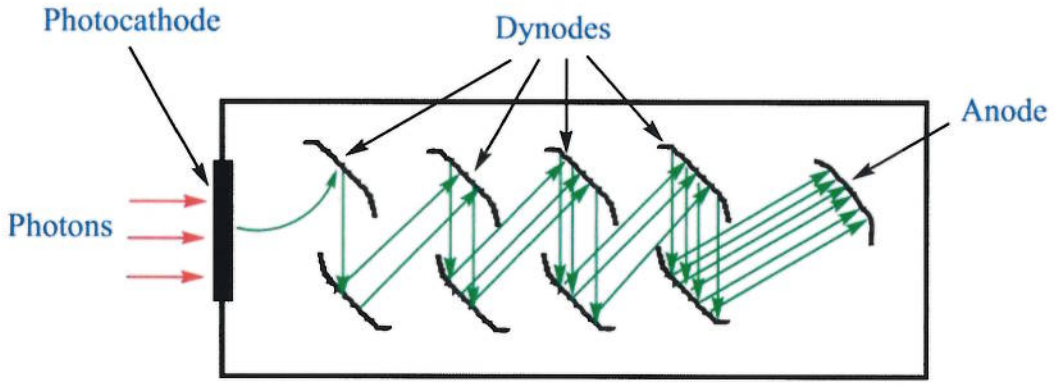

Figure 1-31: Schematic diagram of PMT

1.8.5 The luminol reaction

Several types of molecules are used to offer an increase of the CL reaction, such as luminol, oxalyl chloride, lophine, and peroxylates. Luminol has been extensively employed in most chemiluminescence applications, because it is low cost, commercially available, and can be easily applied in the aqueous condition. In contrast, the other molecules mostly require organic solvents which may lead to interference of the analyte or forming an insoluble product which can cause blockages in the microchannels.[241]

Luminol must be prepared in the alkaline medium, and it reacts with a variety of oxidants such as permanganate, periodate, hydrogen peroxide, and hexacyanoferrate (III). The luminol solution is highly sensitive to light and thermally unstable, thus it must be kept at the dark at low temperature.[2, 244] Luminol is mostly utilised to react with hydrogen peroxide (H_2O_2) to emit light at 425 nm, where H_2O_2 works as an oxidising reagent. The mechanism of luminol and hydrogen peroxide reaction is shown in Figure 1-32.

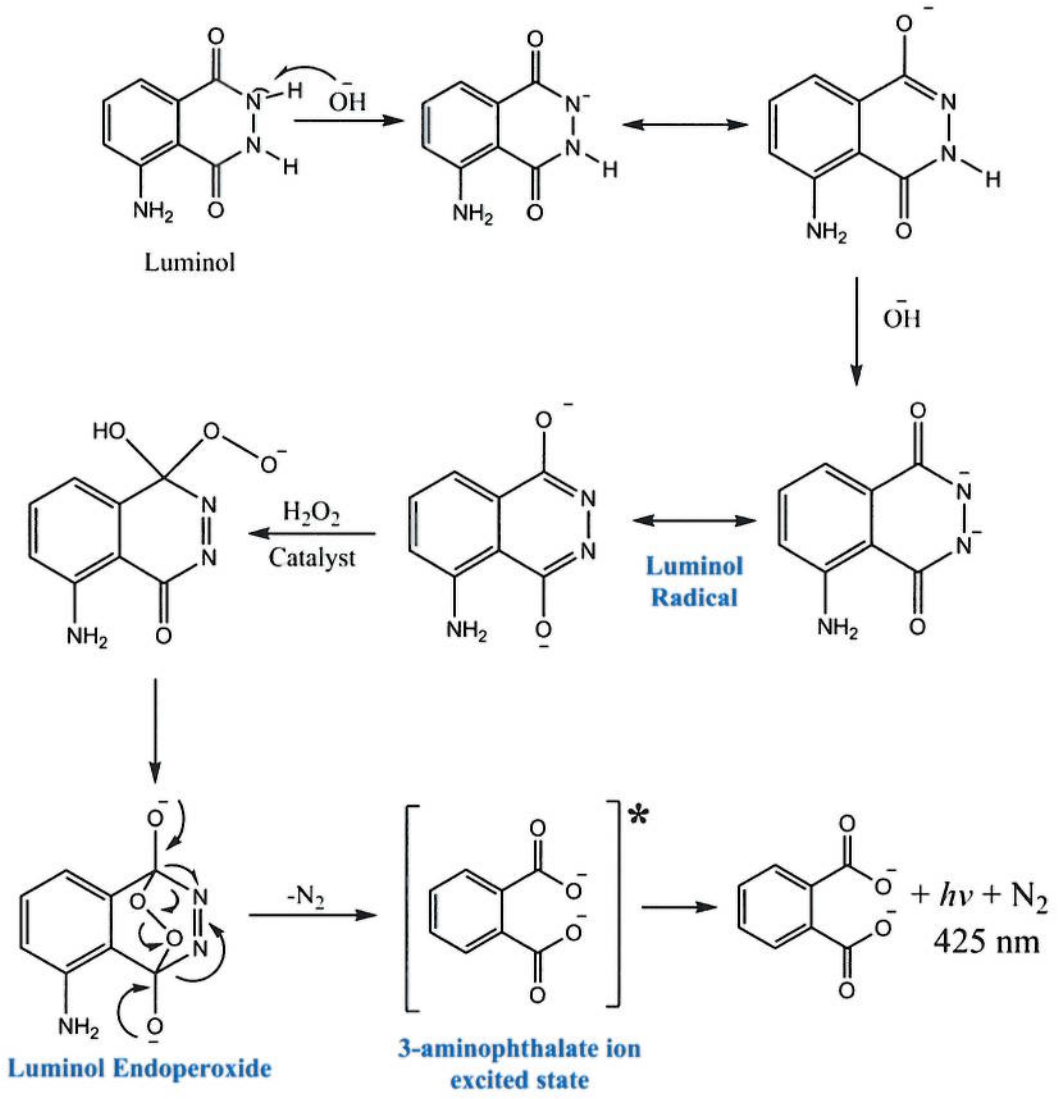

Figure 1-32: Mechanism of luminol and hydrogen peroxide reaction[197]

1.8.6 CL detection for environmental analysis

1.8.6.1 *CL detection for flow injection analysis (FIA)*

Carbamate pesticides are mostly applied for agricultural and non-agricultural objectives due to their great effectiveness and broad-action spectrum. The majority of the carbamates have low vapour pressures and high melting points. They are commonly expanded in environmental water samples due to their high solubility in water. Studies have revealed that carbamates and their degradation products are threaten human health and potential source of environmental contamination.[249, 250] Some examples of carbamate pesticides are shown in Figure 1-33.

Some of these pesticides have been investigated by direct oxidation with strong oxidants, for example permanganate or cerium (IV) in an acidic medium.[26] In those cases, the CL signal is sometimes sensitised by the use of some substances, for instance sulphite, rhodamine 6G, or quinine.

Waseem *et al.* found a strong CL signal was generated when carbaryl and carbofuran were mixed with sodium sulphite and potassium permanganate in a sulphuric acid medium. The limits of detection were 10 and 50 μg L^{-1} for carbaryl and carbofuran, respectively. The FI-CL method was used to determine these pesticides in fresh water with satisfactory results.[251]

The same oxidant was used by Palomeque *et al.* for the determination of aldicarb in mineral waters, which produced recoveries higher than 91%. The CL emission was enhance by adding quinine. This method had sample throughput of 17 h^{-1} over the range 2.2–100. μg L^{-1} with LOD of 0.069 μg L^{-1}.[252]

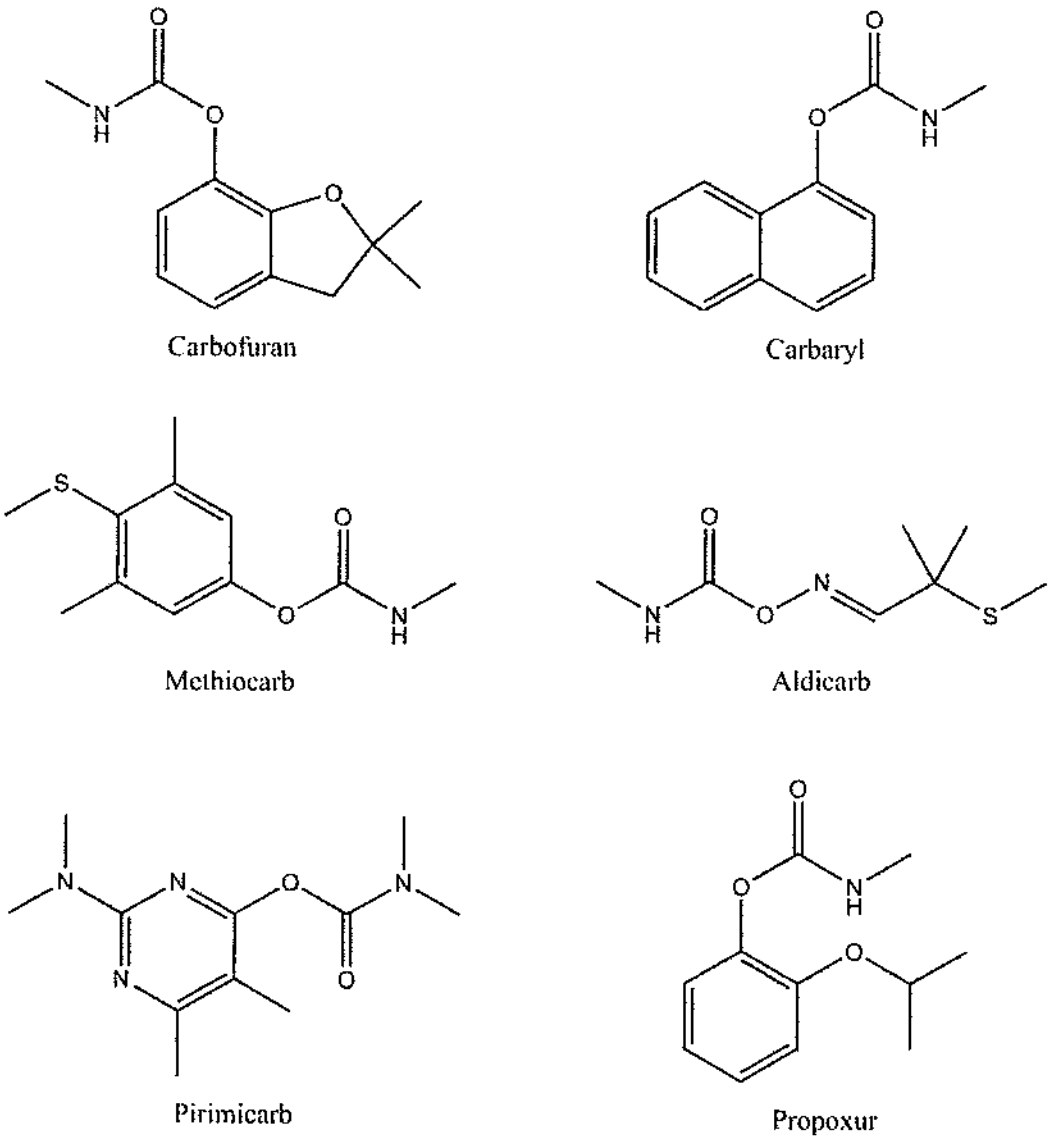

Figure 1-33: Some examples of carbamate pesticides

Murillo Pulgarin *et al.* used the oxidant cerium (IV) in the FI-CL system for the determination of carbaryl in various types of matrices, including water, commercial formulations, soil, and grain samples with recoveries higher than 93%. The limit of detection is 28.7 $\mu g\ L^{-1}$. In this case, Ce(IV) was prepared in nitric acid and rhodamine 6G used as the sensitiser to enhance the CL emission.[253]

The luminol oxidation in basic medium has been also utilised for the determination of carbamate pesticides. Huertas-Pérez *et al.* revealed that carbaryl can show a great improvement of the CL emission from the oxidation of luminol when is oxidised by potassium permanganate. The CL intensity was linear over the range of 5–100 μg L^{-1} with a LOD of 4.9 μg L^{-1}.[254] The same research group also employed the same approach, luminol with $KMnO_4$, to carry out carbofuran analysis.[255]

On the other hand, some carbamates can act as both inhibitors of the CL emission and as substances that are easily oxidised and act as interferents in the luminol reaction, being indirectly determined by calculating the reduction resulting from the CL emission.[256] Waseem *et al.* found carbaryl can inhibit the CL emission when hydrogen peroxide as an oxidant and cobalt (II) nitrate as a catalyst are present. This method has been developed for carbaryl determination in water and shows a sample throughput of 120 h^{-1}. The dynamic range is 100–400 μg L^{-1} with a limit of detection of 48 μg L^{-1}.[257]

Diaz *et al.* found that pirimicarb can enhance the CL signal from luminol with the presence of hydrogen peroxide and horseradish peroxidase (HRP). This method was successfully employed for the determination of pirimicarb in tap water and the mean recoveries were 98.3–118.5%.[258]

1.8.6.2 *CL detection for micro flow injection analysis (μFIA)*

To the researcher's knowledge, there is no published data to date on the determination of carbamate by μFIA-CL. Chemiluminescence has been integrated within microfluidic devices in environmental applications.

Numerous groups have demonstrated microfluidic systems with luminol-CL detection for the determination of metal ions, including chromium (III), nickel (II), cobalt (II), and copper (II), and detection limits down to the subnanomolar range have been accomplished.[259-262] Jorgensen *et al.* employed a CL detection microfluidic device to determine hydrogen peroxide based on the luminol-CL reaction.[263] Greenway *et al.* applied CL detection microchips to determine micromolar levels of H_2O_2 in rainwater. They fabricated a reflective surface above the device to improve the CL signal and employed cobalt to sensitise the luminol reaction.[264]

Som-Aum *et al.* established CL detection for the determination of arsenate, in drinking, mineral, and tap water samples, based on luminol-CL with a heteropoly acid complex.[265]

1.9 Aims of the PhD project

The precise determination and actual time measurement of results is an essential topic in environmental analyses. Pesticides analysis requires many necessary processes, including sampling, sample pre-treatment and detection. By optimising these processes, reproducible and more accurate outcomes can be obtained, however the process can be very labour intensive and time consuming. Currently, miniaturisation of analytical techniques, such as lab-on-a-chip, have been applied for the detection of some pesticides, and have demonstrated increased speed of analysis, reduced sample size, low reagent consumption, portability, and remote operation.

The aim of the present study is to develop a reliable detection device based on the combination of SPE and CL detection using a limited volume of sample in a single experimental process. Carbamate pesticides are widely applied in agriculture owing to their powerful biological activity, however exert high and acute toxicity. Eserine has not been extensively studied before and was selected as a model compound belonging to the carbamate family.

The first objective was to develop a method to extract the eserine from the environmental water sample, for example drinking water. From the literature, it was decided that a silica-based monolith, chemically functionalised through in situ covalent attachment of phases such as a C18 phase, would provide a promising approach for the extraction and pre-concentration of the eserine.

The second objective was to design an approach for using a microfluidic based system for pesticide analysis in drinking water. This necessitated a third objective, to develop a simple, portable, and sensitive detection method suitable for incorporation with a

microfluidic device. After searching the literature, it was decided that an approach using chemiluminescence detection would provide the high sensitivity and selectivity required for pesticide analysis. Once confirmed for eserine, this approach would be suitable for the simultaneous detection of several pesticides.

The fourth objective was to miniaturise the detection by integrating the CL with a microfluidic device. This would make the system sufficiently portable and minimise the use of reagents.

Chapter 2: Experimental

This chapter offers a general overview of the chemicals, materials and procedures utilised for the work reported in this thesis. All chemicals were of analytical grade and used as supplied, without further purification. Water utilised for preparation of the solutions was deionised using the Elgastat Prima 3 reverse osmosis water system [Elga Ltd., High Wycombe, UK].

The main procedures employed in this work are detailed including: fabrication and characterisation of a silica-based monolith, modification of the monolithic materials, and the application of the silica-based monolith in pesticide extraction.

For pesticide detection, a chemiluminescence detection system was used. This process includes some steps such as design of in-house chemiluminescence detector, design of fluid manipulation, preparation of reagents and standards of chemiluminescence reactions, and optimisation of chemiluminescence parameters. Moreover, the design of the microfluidic device and the device set-up for the detection experiments are described.

2.1 Chemicals

Many chemicals were used for the fabrication and modification of silica monolith, extraction of pesticide, fabrication of microfluidic devices and chemiluminescence reactions. All these chemicals used were purchased from the suppliers as shown in Table 2-1.

Table 2-1: Chemicals, solvents, and reagents used

Chemical	Supplier	Purity/grade
Silica monolith fabrication and modification		
Poly(ethylene oxide) (PEO)	Sigma-Aldrich Company Ltd. (Poole, UK)	-
Triblock copolymer pluronic (F127)	Sigma-Aldrich Company Ltd. (Poole, UK)	-
Tetramethoxysilane (TMOS)	Sigma-Aldrich Company Ltd. (Poole, UK)	98%
Tetraethoxysilane (TEOS)	Sigma-Aldrich Company Ltd. (Poole, UK)	99%
Octadecyldimethylchlorosilane	Sigma-Aldrich Company Ltd. (Poole, UK)	95%
Ammonium hydroxide (5 N)	Fisher Scientific (Loughborough, UK)	Analytical grade
Nitric acid (HNO_3)	Fisher Scientific (Loughborough, UK)	70%
Acetic acid (CH_3CO_2H)	Fisher Scientific (Loughborough, UK)	$\geq$ 99%
Methanol	Fisher Scientific (Loughborough, UK)	99%
Toluene	Fisher Scientific (Loughborough, UK)	95%

Tetrahydrofuran (THF)	Fisher Scientific (Loughborough, UK)	99%
Silicon oil	Alfa Aesar (Lancashire, UK)	-
Pesticide extraction		
Eserine	Sigma-Aldrich Company Ltd. (Poole, UK).	99%
Acetonitrile	Sigma-Aldrich Company Ltd. (Poole, UK).	99.9%
Ammonium acetate	Sigma-Aldrich Company Ltd. (Poole, UK).	98%
Microfluidic devices fabrication		
Hydrofluoric acid	Fisher Scientific (Loughborough, UK)	40%
Hydrochloric acid	Fisher Scientific (Loughborough, UK)	37%
Sodium bicarbonate	Fisher Scientific (Loughborough, UK)	99%
Ammonium fluoride	Sigma-Aldrich Company Ltd. (Poole, UK).	40%
Chrome Etch No1	Microchem (Westborough, UK)	-
Microposit Developer Concentrate	Chestech Ltd (Warwickshire, UK)	-
Microposit remover 1165	Chestech Ltd (Warwickshire, UK).	-

Chemiluminescence reactions		
Luminol	Fisher Scientific (Loughborough, UK).	97%
Hydrogen peroxide	Fisher Scientific (Loughborough, UK)	Analytical grade
Sodium hydroxide	Fisher Scientific (Loughborough, UK)	Analytical grade
Potassium permanganate	Fisher Scientific (Loughborough, UK)	-
Cerium(IV) sulphate	Sigma-Aldrich Company Ltd. (Poole, UK)	98%
Cerium(IV) ammonium sulphate	Sigma-Aldrich Company Ltd. (Poole, UK)	99%
Rhodamine 6G	Sigma-Aldrich Company Ltd. (Poole, UK)	95%
Sulphuric acid	Sigma-Aldrich Company Ltd. (Poole, UK)	95%

2.2 Materials

There is a range of various materials that have been utilised throughout this research (see Table 2-2).

Table 2-2: Materials used

Material	Supplier
Heat-shrinkable tube poly (tetrafluoroethylene) (PTFE) with a shrinkage ratio of 4:1, 0.94 and 1.27 mm i.d.	Adtech Polymer Engineering Ltd. (Stroud, UK)
Polytetrafluoroethylene (PTFE) thread seal tape	ARCO Ltd. (Hull, UK)
Disposable plastic syringes (1 and 2 mL)	Scientific Laboratory Supplies (Nottingham, UK)
An adapter straight/standard bore (1.5mm), female luer lock adapter, fingertight fitting, stainless steel tubing, and union assembly PEEK	Kinesis (Cambridgeshire, UK)
Borosilicate glass tubes (2.10 mm i.d. and 3.90 mm o.d.)	Smith Scientific (Kent, UK)
B270 glass	Telic Company (Valencia, USA)
Photomask	JD Photo-Tools Company (Oldham, UK)
Conical centrifuge tubes (50mL)	Fisher Scientific (Loughborough, UK)
Gas-tight Luer lock syringe	Sigma-Aldrich Company Ltd. (Poole, UK)
Micropipettes	Eppendorf Limited (Stevenage, UK)
A pH meter	Thermo Scientific Orion (Beverly, USA)

2.3 Instrumentation

The instrumentation used for all experiments is listed in Table 2-3.

Table 2-3: Instrumentation used

Instrumentation	Supplier
BabyBee™ syringe pump	Bioanalytical Systems Inc (West Lafayette, IN, USA)
Hot plate-stirrer	VWR International LLC (West Chester, PA, USA)
HPLC-UV system	PerkinElmer, California, USA
Bio Wide Pore C18 column (5 µm, 15 cm × 2.1 mm)	Phenomenex (Cheshire, UK)
Ultraviolet-visible (UV-Vis) spectroscopy	PerkinElmer (California, USA)
Brunauer–Emmett–Teller (BET)	Micromeritics Ltd (Dunstable, UK)
A Cambridge S360 scanning electron microscope (SEM)	Cambridge Instruments (Cambridge, UK)
Ultraviolet lamp	Mega Electronics (Cambridge, UK)
Diamond drill	Drill Service Ltd (Surrey, UK)
Photosensor	Hamamatsu Photonics Ltd (Hertfordshire, UK)
A KERN ABJ 220-4M balance	Kern & Sohn GmbH (Balingen, Germany)

Minor sonicator	Decon Laboratories Ltd (East Sussex, England)
MINO/50 oven	Genlab Thermal Engineers (Cheshire, UK)
MAS 700 microwave furnace	CEM Microwave Technology Ltd (Buckingham, UK)
A Fusion 100 syringe pump	Chemyx Inc (Stafford, TX, USA)

2.4 Fabrication of silica-based monolith

Silica monolith rods were fabricated following a procedure similar to those reported by Nakanishi [110] and Fletcher *et al.*[133] The silica monolith mixture was prepared from the composition of four reagents, as shown in Table 2-4. The chosen amount of water-soluble polymer (PEO or F127) was added to the chosen amounts of water and acid catalyst (HNO_3 or CH_3CO_2H) in a plastic tube, after which the mixture was cooled in an ice bath and stirred with a magnetic flea until the polymer totally dissolved in the acidic water. This stirring step took about 20 minutes to dissolve the polymer and form a homogeneous solution. The required amount of silicon alkoxide (TMOS or TEOS) was then added to the homogeneous solution under stirring and ice-cooled conditions for 30 min until a transparent solution was formed.

Table 2-4: The chemical composition of silica monolith rods

Mon	Water-soluble polymer (g)	Water (mL)	Acid catalyst (mL)	Silicon alkoxide (mL)
1	PEO 100kDa (0.282)	0.291	HNO_3 1 M (2.537)	TMOS (2.256)
2	PEO 200kDa (0.282)	0.291	HNO_3 1 M (2.537)	TMOS (2.256)
3	PEO 100kDa (0.282)	0.291	HNO_3 1 M (2.537)	TEOS (2.256)
4	PEO 200kDa (0.282)	0.291	HNO_3 1 M (2.537)	TEOS (2.256)
5	F127 (0.432)	CH_3CO_2H 0.02 M (4)		TMOS (2)
6	F127 (0.432)	CH_3CO_2H 0.02 M (4)		TEOS (2)

During stirring, a 1 or 2 mL plastic syringe was sealed at the thin end using PTFE thread seal tape and used as a mould. Subsequently, the solution was transferred slowly

into the mould. The other open end was then closed with a small lid. The mould was placed in an oven at 40 °C for three days, during which time a wet, semi-solid gel monolith was formed. Some shrinkage occurred, and the wet gel monolith was carefully removed from the mould and washed with copious amounts of distilled water to remove any residue. The wet silica rod formed was treated with an aqueous solution of 20% ammonium hydroxide NH_4OH (1 M) in an autoclave at 85–90 °C for 24 h (see Figure 2.1) in order to generate the required mesoporous structure. The monolith was then washed again with copious amounts of distilled water before drying in an oven at 40 °C for one day and at 90 °C for a further day. Finally, the dried monolith rods were transferred to a furnace and calcined at 550–650 °C for three hours to remove any remaining organic material.

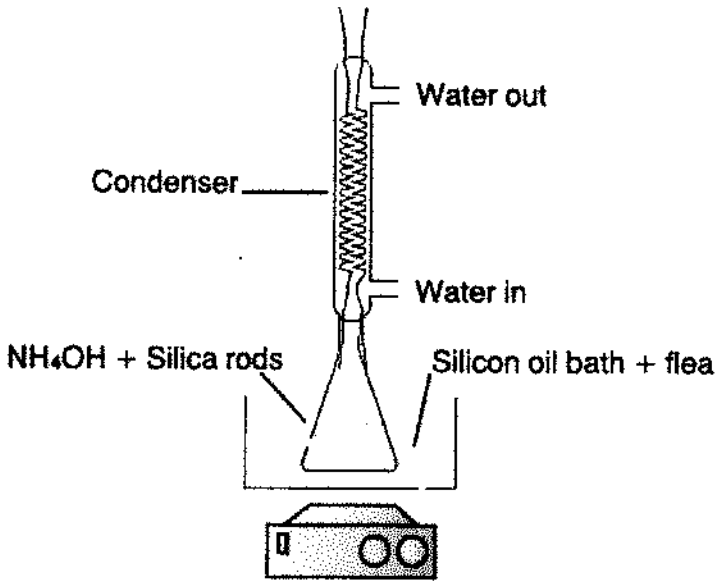

Figure 2-1: Pre-functionalised treatment of silica monolith with ammonia hydroxide

After calcination, the silica rod was cut to an appropriate length, covered with a heat-shrinkable tube (PTFE), and connected to a borosilicate glass tube or stainless steel tubing, as shown in Figure 2-2.

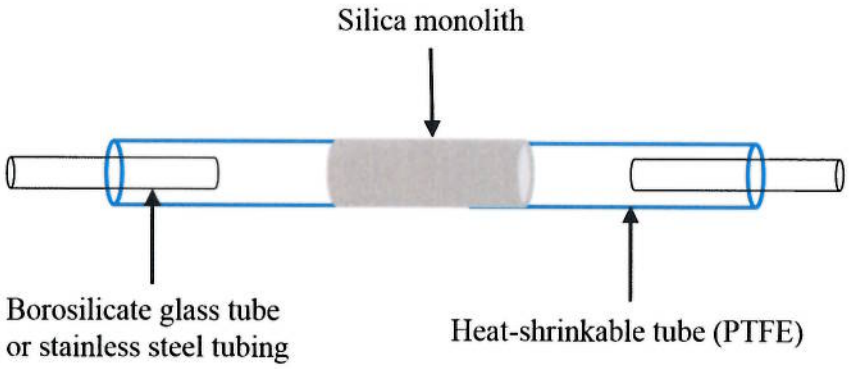

Figure 2-2: Schematic of silica monolith flow system

The silica rod was then heated at the appropriate temperature (340 °C) for 2 h in a furnace to shrink the PTFE tube to fit tightly to the monolith, as shown in Figure 2-3.

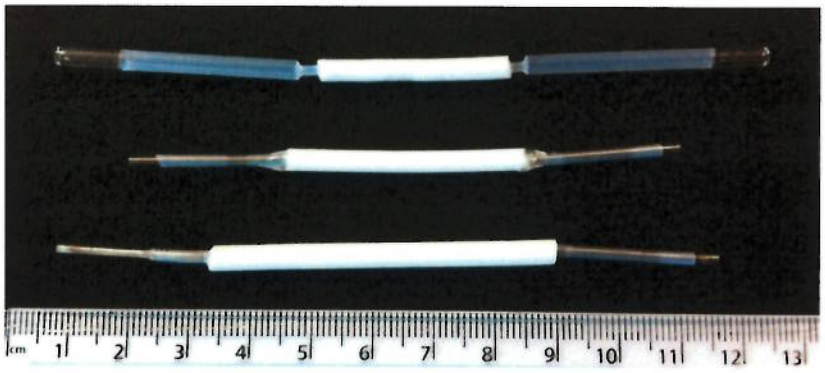

Figure 2-3: Different lengths of silica monolith rod connected to a borosilicate glass tube or stainless steel tubing by heat-shrinkable tube (PTFE)

Finally, the silica monolith rods were ready for the modification of the surface and the syringe pump was connected to the tubing using a two-piece finger-tight fitting, as shown in Figure 2-4.

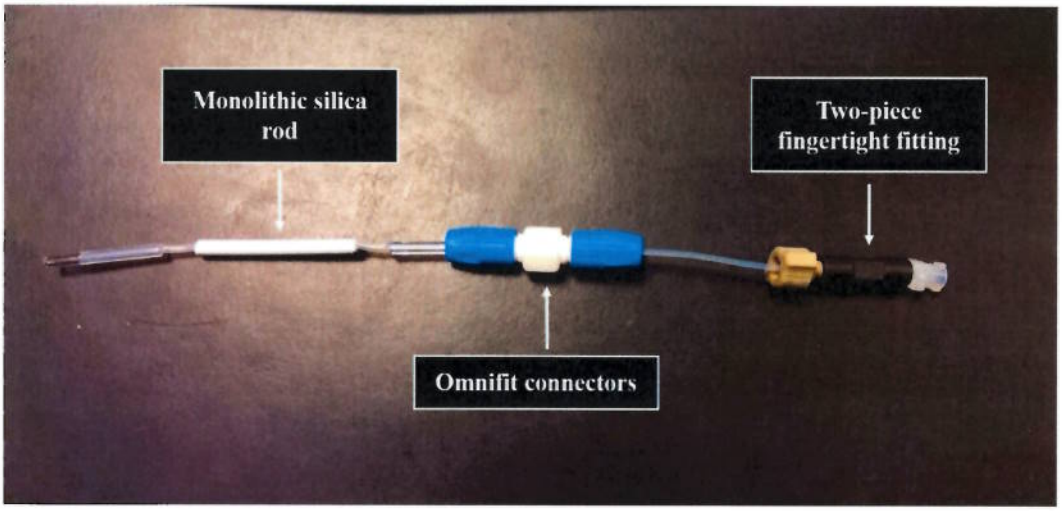

Figure 2-4: A silica monolith rod connected to the borosilicate tube for surface modification.

2.4.1 Silica-based monolith characterisation

2.4.1.1 *SEM analysis*

The morphology of the fabricated silica monolith was characterised using scanning electron microscopy (SEM) with a Cambridge S360 scanning electron microscope to measure the macropores followed by averaging 20 pore diameters. The samples for SEM analysis were coated with a thin layer of gold-platinum (thickness around 2 nm) using a SEMPREP 2 Sputter Coater [Nanotech Ltd., Sandy, UK]. The SEM images of silica-based monoliths were achieved using an accelerating voltage of 20 kV and a probe current of 100 pA in high vacuum mode.

2.4.1.2 *BET analysis*

A Brunauer–Emmett–Teller (BET) instrument was employed to identify the physical properties of the monolith, including the surface area, pore size, and pore volume, using nitrogen adsorption and desorption isotherms at 77 K. The volume of pore volume and pore size distribution inside silica monoliths were also identified from isotherms using the Barrett–Joyner–Halenda (BJH) model. A small piece of the silica monolith rod was weighed and placed into the BET instrument for analysis. The BET instrument was utilised to investigate the surface changing during the monolith fabrication process in the necessary step to generate mesopores with the basic treatment. Isotherms of the silica monolith rod before and after basic treatment were achieved.

2.4.1.3 *EDX analysis*

Energy dispersive X-ray (EDX) analysis was employed to determine the chemical composition of monolithic materials before and after modification of the silica-based monolith with C18. EDX analysis was achieved using an INCA 350 EDX system.

2.4.2 Modification of silica-based monolith with C18

The silica monolith rods were modified following a procedure similar to that reported by Kang *et al.*[266] The surface of the monolithic silica was chemically modified by C18 in order to make the sorbent hydrophobic. The silanisation solution contained 10% (w/v) octadecyldimethylchlorosilane in toluene. Surface modification of the monolithic silica was accomplished by continuously delivering silanisation solution

through the column, at a flow rate of 30 μL min^{-1}, for 6 h at 80 °C. Then, the monolith was sequentially flushed with toluene, tetrahydrofuran (THF), methanol, 50/50 (v/v %) methanol/water, and methanol, using a syringe pump at a flow rate of 50 μL min^{-1} for 30 min. Finally, the derivatised silica monolith was placed in an oven for 24 h at 40 °C prior to use.

2.5 Applications of modified silica-based monolith for eserine

2.5.1 Study of the performance of C18 silica monolith by HPLC-UV

HPLC was employed to investigate the extraction and pre-concentration performance of the modified silica monolith. All eluted samples were analysed directly by a HPLC-UV detector to obtain the peak area for eserine and to compare them with the peak areas of eserine standard solutions, to measure the extraction efficiency. To detect eserine, chromatographic analysis was achieved using HPLC with a UV detector consisting of an LC 200 series binary pump, a PerkinElmer 785A UV/visible detector, and a Bio Wide Pore C18 column.

The mobile phase was methanol /water (60:40) (V/V) run under isocratic conditions; the flow rate was 1 mL min^{-1}.[267, 268] A predetermined λ_{max} wavelength was set at 248 nm, and the injection volume was 20 μL. The extraction recovery (ER) was calculated (see Equation 2-1) and defined as the percentage of the total analyte (n_0) which was extracted to the eluent (n_{set}).[269]

$$ER = (n_{set} / n_0) \times 100 \quad (2\text{-}1)$$

2.5.2 Preparation of stock solution of eserine

A stock solution of eserine at 1 mg mL^{-1} (1000 ppm) was made by weighing out accurately to 4 decimal places approx. 1 mg of eserine into a 1.5 mL microcentrifuge tube and dissolving it in 1 mL water, solubility in water at 25 °C (7760 mg L^{-1}). Then, the sample solution was mixed well, protected from sunlight and stored in a refrigerator at 4 °C. The chemical structures and the molecular weight of eserine, the target analyte, are shown in Figure 2-5.

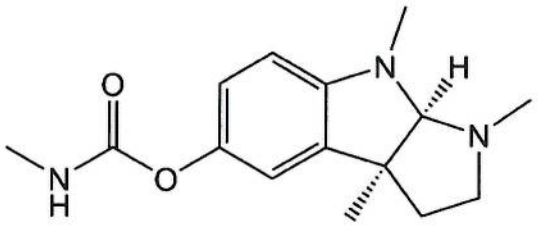

Chemical Formula: $C_{15}H_{21}N_3O_2$
Molecular Weight: 275.35

Figure 2-5: The chemical structure and molecular weight of eserine

2.5.3 Preparation of standards for calibration of eserine

The stock solution (1 mg mL^{-1}) of eserine was serially diluted. The working standard solutions contained 5, 10, 20, 30, 40, 50, 60, 70, 80, 90, and 100 µg mL^{-1}. These working standard solutions were analysed directly by HPLC-UV three times at each concentration level. Peak areas were obtained from a chromatogram of the eserine, and the peak areas were plotted against each concentration. The limits of detection

(LOD) and quantification (LOQ) were determined from linear regression of the calibration curve. The LOD and LOQ can be expressed as:

$$LOD=3 \times SD/S \quad (2\text{-}2)$$

$$LOQ=10 \times SD/S \quad (2\text{-}3)$$

Where SD is the standard deviation of the response

S is the slope of the calibration curve

2.5.4 Solid-phase extraction and pre-concentration procedures

Before extraction and pre-concentration, the C18 silica monolith rods were conditioned with 3 ml methanol and then equilibrated using 3 mL of purified water at a flow rate of 400 μL min^{-1}. All the solutions were injected with a syringe pump. All steps for extraction and pre-concentration were repeated three times. For extraction, a 300 μL sample from the standard solutions (100 μg mL^{-1}) was loaded through the C18 silica monolith sorbent at pre-determined optimised flow rate. Then, the monolith sorbent was washed with 3 mL of purified water to remove any possible impurity, and the eluate was collected for further analysis. After washing, the analytes were eluted from the C18 silica monolithic sorbent with 300 μL of methanol/water (60:40) (V/V) into a glass tube at a flow rate of 400 μL min^{-1}, and stored for further experiments.

For pre-concentration, a 4 ml sample (10 μg mL^{-1}) was loaded through the C18 silica monolith sorbent at a flow rate of 400 μL min^{-1}. The monolith sorbent was then washed

with purified water twice. The analytes were eluted with 400 μL of methanol/water (60:40) at the same flow rate from the C18 silica monolithic sorbent.

2.5.5 Breakthrough volume for SPE

To determine the capacity of the fabricated silica-based monolith, constant volumes of the sample (300 μL), containing concentrations of 30 μg, were loaded through the monolith sorbent at 400 μL min^{-1}. These steps were continued up to the point where the analyte mass exceeded the retention capacity of sorbent. Each fraction was then collected separately and measured directly by a HPLC-UV detector.

2.6 Fabrication of microfluidic device

The glass microfluidic devices were fabricated by Dr Steve Clark (University of Hull, UK) and prepared using photolithography and a wet-etching technique, as shown in Figure 2-6. AutoCAD LT® (2010) software was utilised to draw the design of the microfluidic device channels and the design was then printed using JD Photo-Tools as a photomask film. The mask was then placed above the top of borosilicate glass (B270) pre-coated with chrome layers and photoresist. The channel manifold design was transferred by exposing the photoresist layer to the UV light for 60 seconds under darkroom safelight conditions. The wafer was then submerged in Microposit© Developer Concentrate diluted in a 1:1 ratio with purified water for 60 seconds, followed by immersion in a Chrome Etch 18 solution for a further 60 seconds to remove the exposed photoresist layer and etch away uncovered chrome.

The glass was then chemically etched using a solution consisting of 5% ammonium fluoride (NH_4F) and 1% hydrofluoric acid (HF) at 65 °C was then utilised to etch the exposed glass isotropically to the required depth, which was 65 μm in current work.

Microposit© Remover 1165 and Chrome Etch 18 solution were used to remove the remaining photoresist and chrome layers. Diamond drill bits were used to drill the access holes into the top glass cover plate. The etched base and drilled glass cover plates were thermally bonded together at 585 °C for two hours to complete the fabrication process.[218, 270]

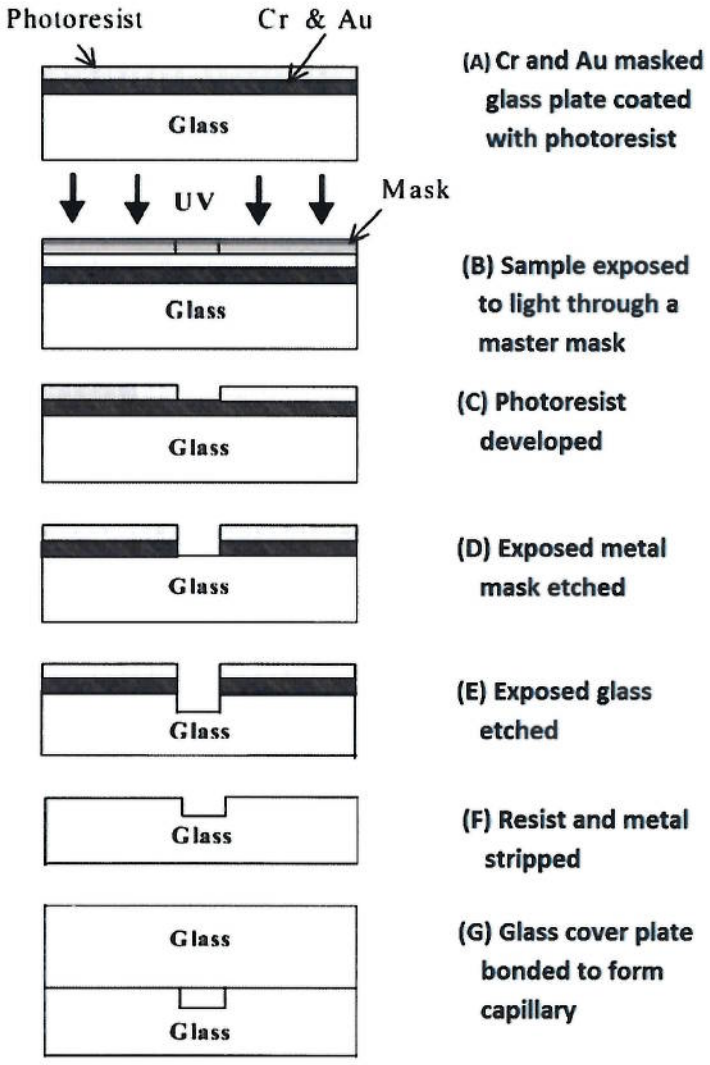

Figure 2-6: Schematic diagram of the fabrication process of glass microfluidic devices using photolithography and wet-etching technique[271]

2.6.1 Microfluidic device design

For chemiluminescence reactions, efficient mixing of the reagents is important for the detection sensitivity. This results in design microfluidic manifolds with longer channel lengths. The channel length had to be in the form of a serpentine in order to fit the microchannels within an area that would sit above the PMT for detection. The

microfluidic chip designs used were obtained from a previous project carried out at the University of Hull.[222]

The serpentine channel dimensions were 200 μm wide and 65 μm deep with a channel length of approximately 206 mm with 9 meanders as shown in Figure 2-7. Three reservoirs holes of diameter of 1.5 mm were drilled in the top glass plate to permit the microfluidic chip to be connected to Teflon tubes which support transmission of the pushed liquid inside the channels.

Taking into consideration the flow rate of the fluid and the cross sectional area of the channel, the residence time of the fluid over the channel length can be estimated (see table 2.5).

Table 2-5: Estimated residence times for water within the serpentine channel at different flow rates. Calculation for the residence time (s) = channel length (m) / flow rate (m s^{-1}).

Flow Rate (μL min^{-1})	**Velocity (m s^{-1})**	**Residence Time (s) Channel length (206 mm)**
1	1.3×10^{-3}	160
5	6.4×10^{-3}	32
10	0.013	16
15	0.019	10.7
20	0.026	8
25	0.032	6.4
30	0.038	5.35

The volume of regents used in the channel was 2.678 μL. The chemiluminescence reagent was passed through one channel of the T piece (inlet 1) and the sample and oxidant were passed through the other channel (inlet 2). The chemiluminescence intensity was determined using the portable chemiluminescence detection system.

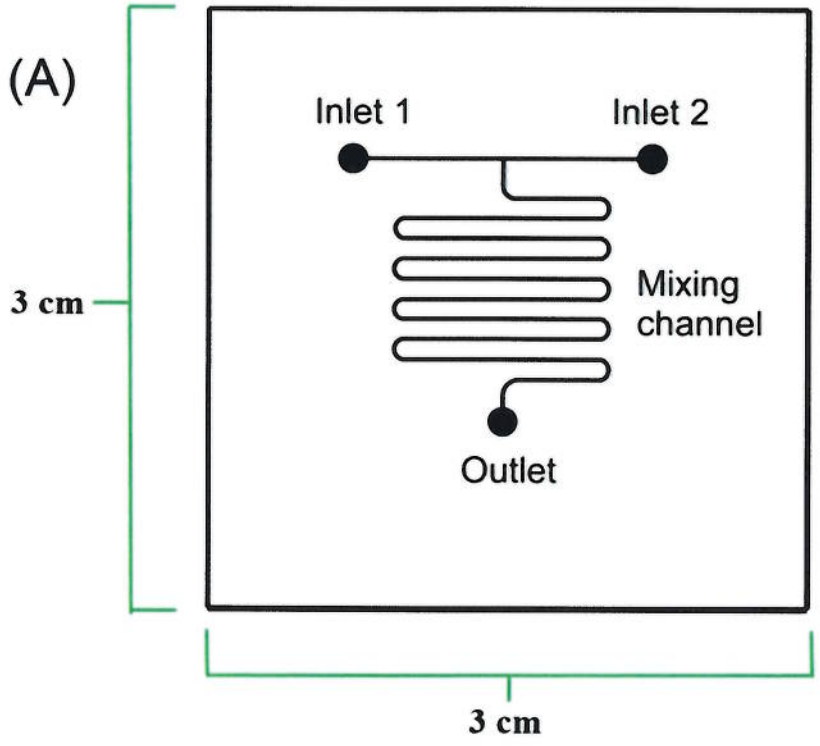

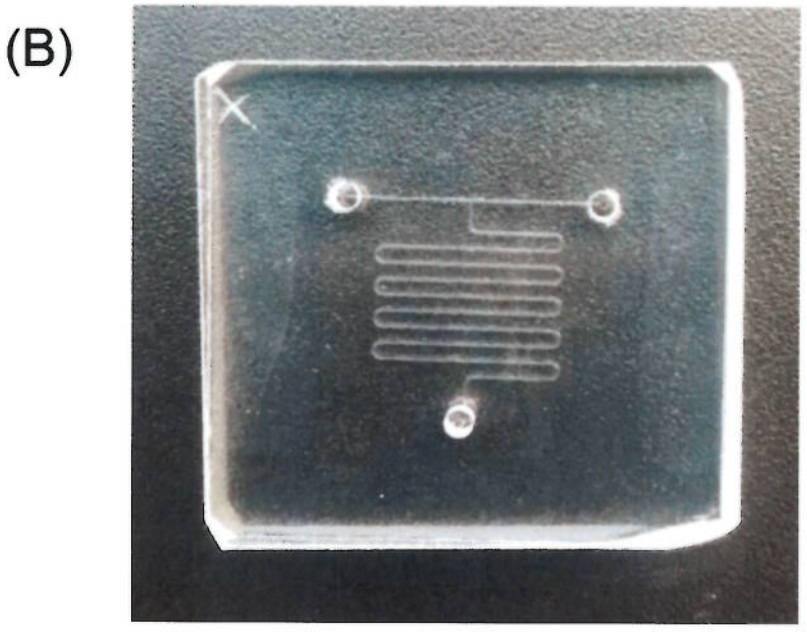

Figure 2-7: (A) Schematic of a T-shape serpentine channel manifold microfluidic chip (206 mm length, 9 meanders) and (B) Photograph of the microfluidic chip

2.7 Development of a portable chemiluminescence detection system

2.7.1 Design of in-house chemiluminescence detector

2.7.1.1 *Selection of photodetector*

The low power consumption photosensor module (H10722-20) was purchased from Hamamatsu Photonics Ltd (Hertfordshire, UK), as shown in Figure 2-8. The photosensor module combines a 'head-on' photomultiplier tube (PMT) with a high voltage power supply and signal processing electronics in a metal casing (dimensions 22 x 22 x 60 mm). The effective area of PMT is 8 mm in diameter, providing a spectral response of 230–920 nm, with a peak sensitivity wavelength of 630 nm. A 5V power pack (SPU45E-301) was obtained from RS Components Ltd (Northants, UK) and connected to the PMT. The system was designed with a variable gain dial, allowing the gain of the PMT and therefore the sensitivity of the PMT to be adjusted.

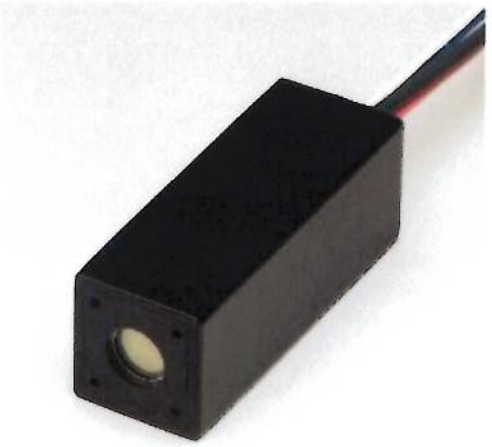

Figure 2-8: Photograph of photosensor module containing a metal casing PMT

2.7.1.2 *Design of light-tight housing*

The CL detection system was located inside a dark (light-tight) box which was fabricated by the workshop of Chemistry Department at Hull University. The light-tight box was made of steel with dimensions of 180 mm x 165 mm x 10 mm. The box size allowed CL detection to be achieved inside the box and examinations to proceed outside the laboratory if required for collecting data.

To make the system portable and amenable to field use, the system was designed with a protective shutter, with a diameter of 2.55 cm^2, for the PMT. This allows access to the samples and the microfluidic device while preventing it from being exposed to external light. A shutter mechanism was constructed in-house and was designed such that it could only be opened when the box is properly shut and sealed from external light, due to the position and configuration of the thread on the closing mechanism which turns the direction of the shutter; likewise, when the box is open the shutter remains closed.

An oscilloscope (PicoScope PS2202 OAT01/70, Pico Technology, UK) was connected to a computer. Data acquisition software (PicoLog Recorder®) was also used to collect, analyse and display the signal.

2.7.1.3 *Position of microfluidic device*

The reaction cell must be situated as close as possible to the detector to maximise optical efficiency. The designed microfluidic device is placed on top of the PMT shutter, while the area of the serpentine shape is placed exactly on the light-tight shutter over the PMT to ensure all the light produced from the reaction is obtained.

Two holes were placed on the right-hand side of the box cover. These holes are for inserting microtubes from the syringe pump to the microfluidic chip which is housed inside the light-tight box. The microtubes are the same size as these holes in order to prevent any light escaping from the box. The waste produced from the reaction between the reagents is collected via a beaker placed at the end of the waste hole, so preventing any spillage inside the box. The portable chemiluminescence detector is shown in Figure 2-9.

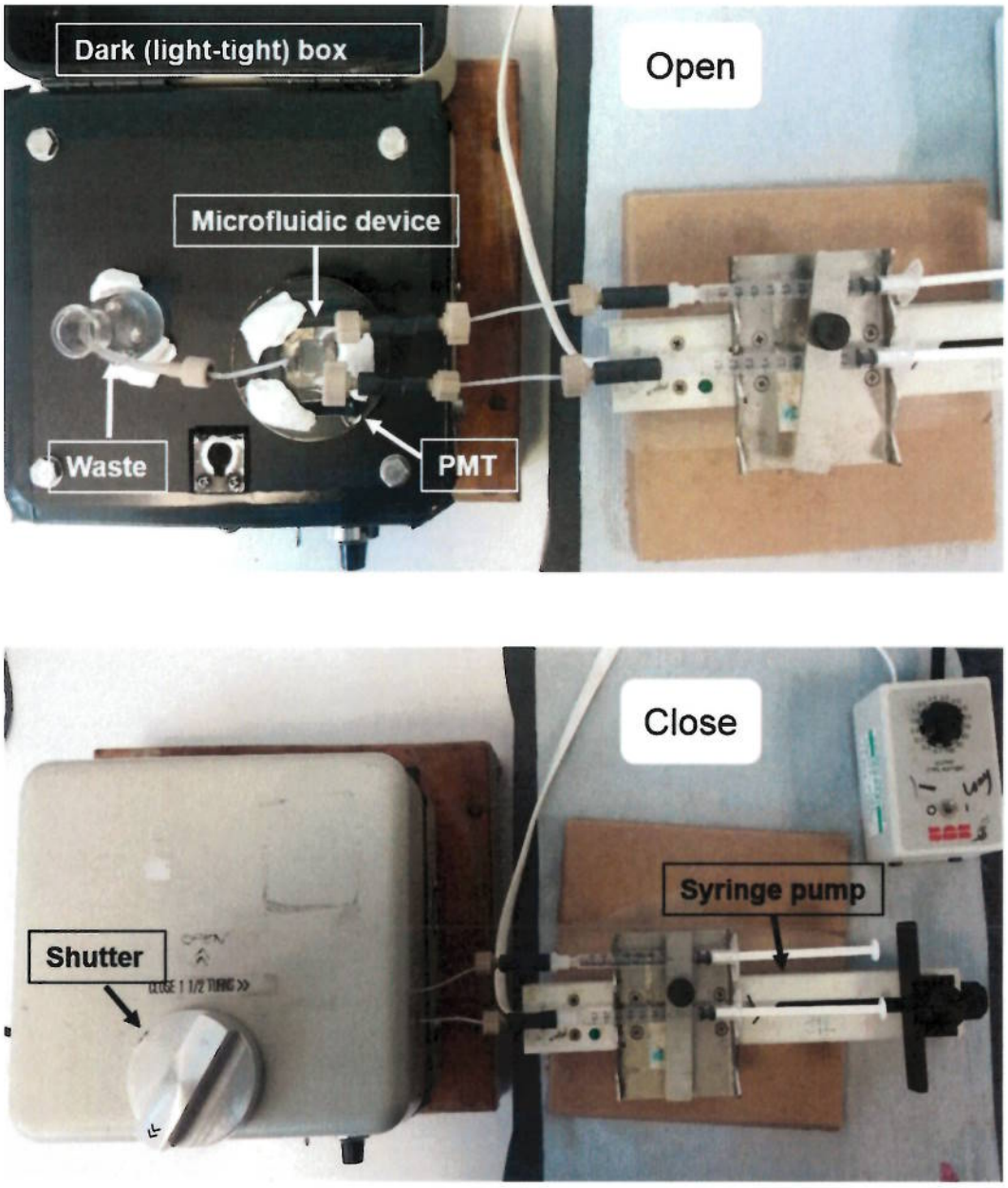

Figure 2-9: Photograph showing the portable chemiluminescence detection system designed in-house

2.7.2 Preparation of chemiluminescence reagents and oxidants

Luminol solutions: A stock solution of 50 mM luminol ($C_8H_7N_3O_2$) was prepared by dissolving (0.886g) in sodium hydroxide (NaOH) and stored for 24 h in a refrigerator to attain stability before use. The luminol solution is stable at least for one month.[272] The working solutions were prepared by appropriate dilution.

Hydrogen peroxide solutions: A 50 mM stock solution of hydrogen peroxide (H_2O_2) was prepared in ultrapure water and the corresponding working solutions were prepared daily by appropriate dilutions.

Potassium permanganate solutions: A 1 mM stock solution of potassium permanganate ($KMnO_4$) was prepared by dissolving the product in ultrapure water and stored in darkness at room temperature for one month. [255, 272]

Cerium (IV) sulphate solutions: These were freshly prepared in nitric acid or sulphuric acid.

Cerium (IV) ammonium sulphate solutions: A 50 mM stock solution of Ce(IV) solution was prepared from ammonium cerium (IV) sulphate hydrate ($Ce(NH_4)_4(SO_4)_4 \cdot 2H_2O$) in 4 M nitric acid daily. [253]

2.7.3 Analysis of environmental water samples

The applicability of the proposed microfluidic-CL method to real samples was demonstrated with recovery studies of eserine in different water samples (ultra-high

purity, tap, and river water) spiked at different concentrations. The tap water sample was obtained from the University of Hull, while the river water sample came from the River Hull.

All the samples were collected in plastic bottles, filtered and stored in a refrigerator at 4° C until analysis. Before the microfluidic-CL analysis, the SPE procedure with the C18 modified silica monolith was applied to each water sample. Furthermore, each water sample was spiked with different concentrations of eserine (1, 10, 100 and 200 $\mu g\ L^{-1}$) and analysed by the microfluidic-CL method proposed.

Chapter 3: Results and Discussion: Fabrication of Silica-based Monolith

This chapter describes the fabrication of the silica monolith, optimisation of sol-gel process and physical characteristics of the silica monoliths. The silica monolith mixtures were prepared from compositions of water-soluble polymers, silicon alkoxide, water, and acidic catalyst, as described in Section 1.5.1. The fabrication procedure is given in Section 2.4 and summarised in Table 2-4.

Silicon alkoxides (TEOS or TMOS) were used as a silica source due to their purity, price, and availability. A water-soluble polymer (PEO or F127) was used to induce phase separation between the silica, and an acidic catalyst was used to start the hydrolysis and condensation reactions. The solution mixture was transferred into a 1 or 2 mL disposable plastic syringe that was used as a mould for preparation of the monolithic silica rod.

The formed wet silica rod was washed with water to remove any possible residues and treated with a basic solution of ammonia hydroxide for 24 hours in order to generate the mesopores in the silica skeleton. This step was followed by washing and then drying at 40° C for one day and at 90° C for an additional day. The bare silica monolith rods were then transferred to a furnace and calcined at 550–650 °C for three hours to remove any remaining organic material.

The dimensions of the resulting monolith depended on the mould used. The resulting monolith exhibited about 30% shrinkage in the size of the fabricated cylindrical monoliths, which enabled easy removal of the silica rods from the moulds. A caliper was used to measure the diameter of the cylindrical monolithic rod. The cylindrical

moulds had inner diameters of 4.6 and 8.3 mm, resulting in the monoliths having outer diameters of 3.3 and 5.8 mm, respectively. The fabricated silica monoliths exhibited monolithic shapes, with white colour and glossy surfaces, as shown in Figure 3-1.

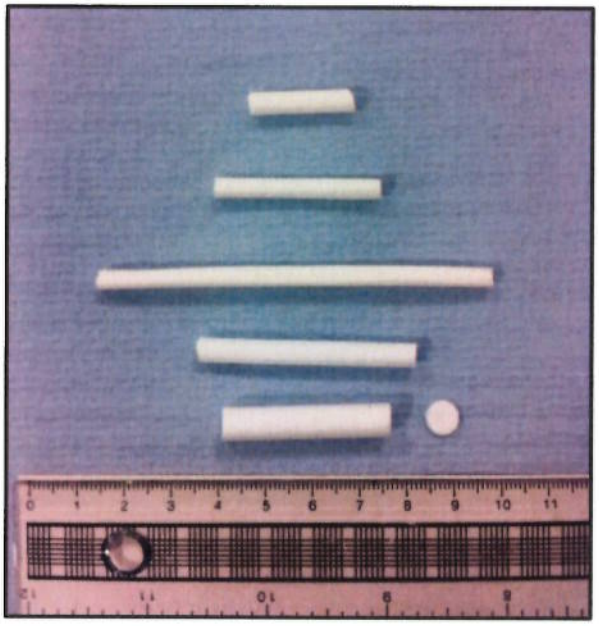

Figure 3-1: The resulting silica monoliths prepared in different cylindrical moulds

In order to study the influence of the sol-gel on the internal structure of the silica monoliths, SEM was used. The internal structures of TMOS silica monolith rods during the fabrication were obtained using SEM as shown in Figure 3-2. The SEM images of TMOS were captured after gelation, basic treatment and the calcination at 600 °C as shown in Figure 3-2 (A), (B) and (C), respectively.

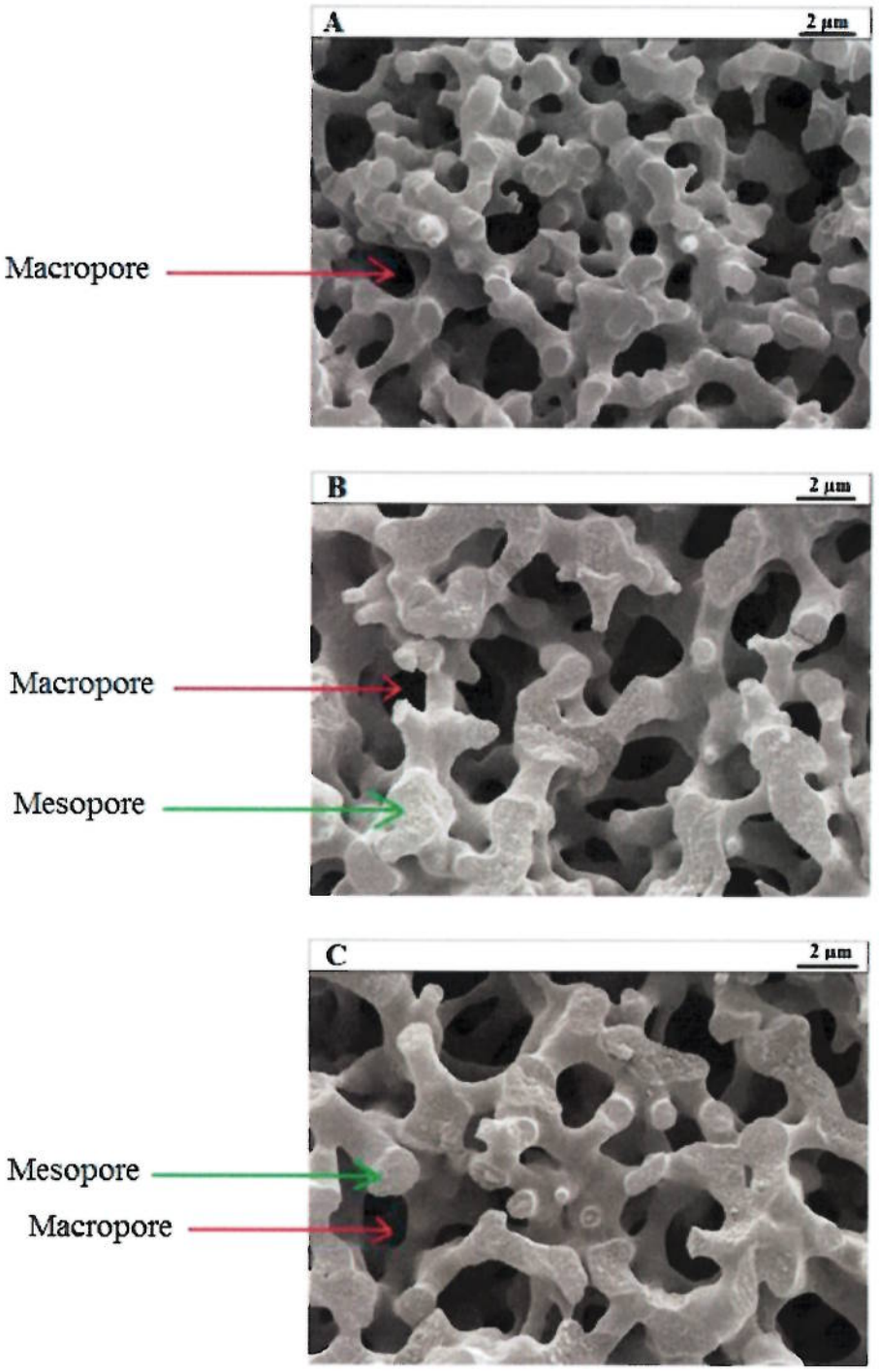

Figure 3-2: SEM micrographs of internal structure of silica monoliths, consisting of TMOS + poly (ethylene oxide) (100 kDa) + nitric acid (1 M), during the fabrication process (A) before the basic treatment with ammonia hydroxide (1 M) (B) after the basic treatment with ammonia hydroxide (1 M) (C) after the basic treatment and the calcination

The SEM micrographs reveal that the surface of the monolith is highly porous with a rigid silica backbone arranged in a continuous random geometry without any apparent regular lattice or sponge structure. It can be seen that the macropores are present and the surface of the internal structure of the silica monoliths is smooth (Figure 3-2: A). There is a clear change of the surface after the basic treatment, as it has become rougher (Figure 3-2: B). This change indicates that mesopores have been formed on the surface skeleton by a dissolution–reprecipitation process as detailed previously in Section 1.5.1.4. When the high heat treatment is applied, the organic residues are removed without causing any possible deformation on the monolithic structure (Figure 3-2: C). SEM provides actual photographs of the silica surface, but no quantitative characterisation of the pore diameter, pore volume and specific surface area. Further investigations were carried out using the Brunauer–Emmett–Teller (BET) method to evaluate the effect of the basic treatment on the internal structure of the silica monolith in next section.

3.1 Effect of the basic treatment on the structure of silica monolith

The mesopore on the monolithic silica surface are important to obtain a specific and high surface area. The surface area, pore diameter, and pore volume were obtained using BET methods, as described in Section 1.5.5.1. Before and after basic treatment of the monolith, the isotherm curves were also calculated using the BET method, as explained in Section 2.4. The physical characteristics of TMOS monoliths are listed in Table 3-1.

The specific surface area of TMOS (prepared with PEO 100 kDa) monolith after basic treatment was approximately 289.46 m^2g^{-1}, whereas the untreated TMOS monolith surface area was 47.10 m^2g^{-1} – that is lower than the basic treated TMOS and is due to the presence of mesopores. The pore diameter and pore volume are also directly proportional to the surface area, as listed in Table 3-1.

Table 3-1: The physical properties of the silica TMOS monolith before and after the basic treatment

TMOS monolith with PEO (100 kDa), HNO_3 and water	BET surface area (m^2 g^{-1})	Average pore diameter mesoporous (nm)	Pore volume (cm^3 g^{-1})
Non-treated with NH_4OH	47.10	4.68	0.026
Treated with NH_4OH	289.46	9.65	0.98

Two isotherm curves of TMOS monolithic silica rods illustrated before and after the basic treatment are shown in Figure 3-3. The isotherm curve of TMOS without the basic treatment shows as similar to the type II (non-porous or macroporous) isotherm curve as discussed in Section 1.5.5.1 (see Figure 3-3A) having strong adsorption for macroporous aborbents (pore size >50 nm). In contrast, the isotherm curve of TMOS with basic treatment shows as similar to the type IV (mesoporous) isotherm curve as discussed in Section 1.5.5.1 (Figure 3-3B) having a well-defined step at approximately p/p_0 = 0.4–0.9 for mesoporous materials (2 nm < pore size <50 nm).[164, 166, 273]

These outcomes favour the proposition that the internal pore structure of the silica-based monolithic rods increased in surface area through the formation of mesopores using the ammonia solution, as previously reported by Nakanishi *et al.*[134, 135] Hence, it is clear that the presence of the basic step is essential to the creation of mesopores in the silica monolith and increase the surface area significantly.

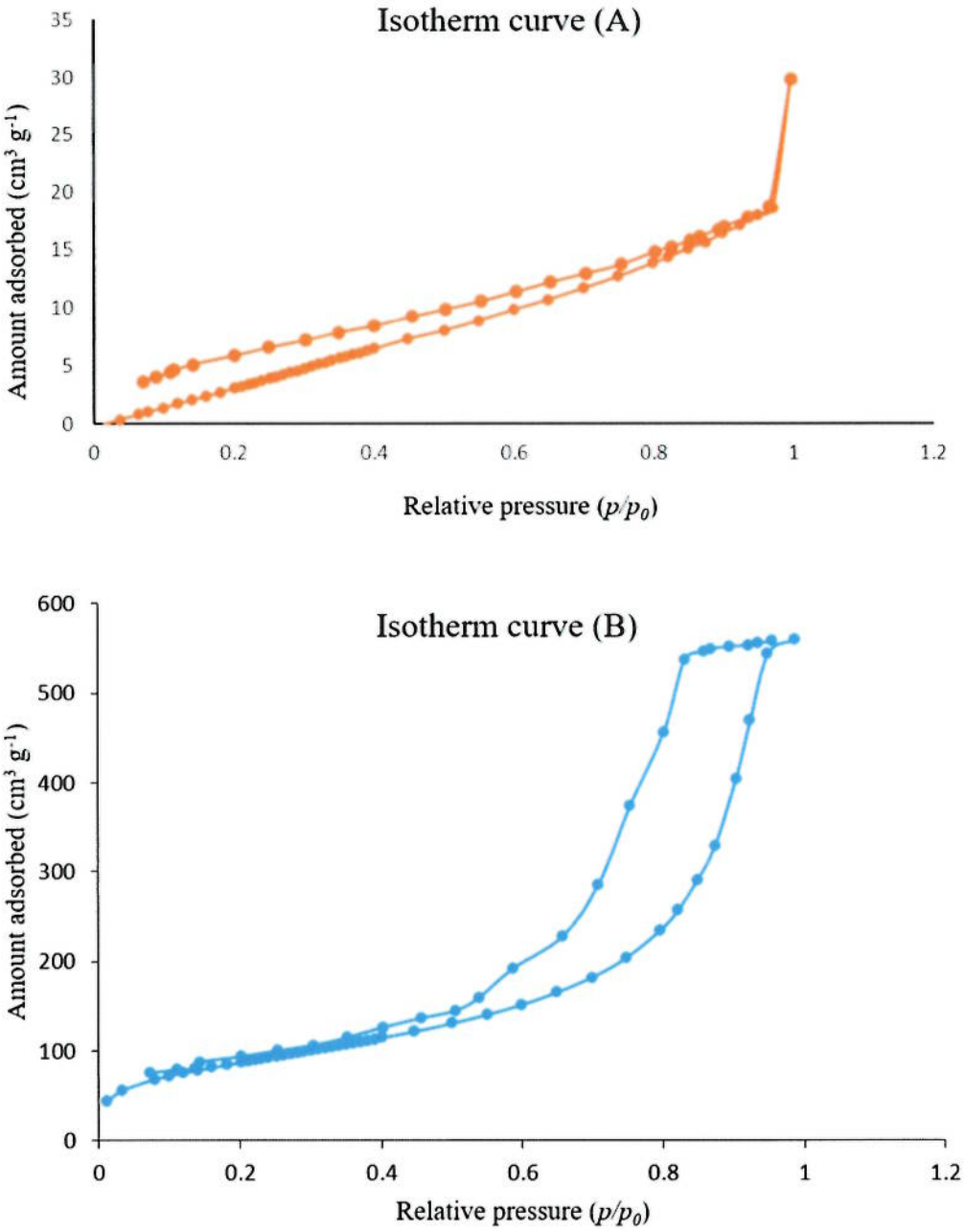

Figure 3-3: BET isotherm curves obtained for TMOS silica monolith. Isotherm (A) is for the TMOS silica monolith before the basic treatment and isotherm (B) is for the TMOS silica monolith after the basic treatment at 80 °C for 24 hours.

The period of the basic treatment will be discussed later after the optimising the starting materials.

3.2 Optimising the starting materials of silica-based monolith

The purpose of optimising the starting materials of the silica monolith was to produce a bimodal porous structure that offers a large surface area (by small mesopores), and provides easier access to the flow and reduces the pressure drop over the materials (by the macropores). Numerous applications require a large surface area to obtain a high loading capacity.

It is very difficult to expect the precursor type to be utilised for a given purpose. The reactivity of the precursor depends not only on its chemical nature, but also on the applied reaction condition.[274] Nitrogen sorption isotherm at 77 k was used to provide information about the physical properties of silica monoliths including the specific pore volume ($cm^3\ g^{-1}$), the specific surface area ($m^2\ g^{-1}$), and mesopores diameter (nm). The diameters of the macropores were measured using the SEM micrographs.[133] Table 3.2 shows a summary of the silica monolith compositions, including silicon alkoxide, water-soluble polymer, acid, and water, and their physical characterisation parameters. The RSDs of the physical characterisation parameters of three different batches of the silica-based monolith were calculated.

Table 3-2: A summary of silica monolith compositions and their physical characterisation parameters

Starting materials	BET surface area ($m^2\ g^{-1}$) ± RSD (n=3)	Average pore diameter mesopores (nm) ± RSD (n=3)	Pore volume ($cm^3\ g^{-1}$) ± RSD (n=3)	Average pore diameter macropores (μm) ± RSD (n=3)
Mon 1- TMOS, (PEO) 100kDa, HNO_3 and water	289.46 ± (4.3)	9.65 ± (1.6)	0.98 ± (0.53)	3.2 ± (0.65)
Mon 2- TMOS, (PEO) 200kDa, HNO_3 and water	315.44 ± (5.4)	7.50 ± (1.7)	0.93 ± (0.26)	2.6 ± (0.48)
Mon 3- TEOS, (PEO) 100kDa, HNO_3 and water	263.49 ± (3.5)	12.3 ± (0.84)	1.35 ± (1.2)	3.4 ± (0.82)
Mon 4- TEOS, (PEO) 200kDa, HNO_3 and water	286.60 ± (6.7)	11.62 ± (1.3)	1.28 ± (1.4)	2.9 ± (0.78)
Mon 5- TMOS, F127, CH_3CO_2H and water	366.7 ± (7.2)	7.80 ± (1.25)	0.90 ± (0.8)	1.8 ± (0.58)
Mon 6- TEOS, F127, CH_3CO_2H and water	322.2 ± (1.8)	8.45 ± (0.72)	0.97 ± (1.3)	2.2 ± (0.63)

As can be seen from the table (above), six different types of silica-based monolith have been made through the sol-gel process, as described in Section 2.4. In the monoliths (1–4), two kinds of silicon alkoxides, TMOS and TEOS, were used with two different molecular weights of polyethylene oxide (100 and 200 kDa), while TMOS and TEOS were then used with a triblock copolymer pluronic (F127) in monoliths (5 and 6).

The calculated specific surface area for the TMOS monolith in the presence of the low molecular weight of PEO (Mon 1) was found to be about 289.46 ± (4.3) $m^2\ g^{-1}$,

compared to the same silicon alkoxide in the presence of the high molecular weight of PEO (Mon 2) which offered a higher surface area of 315.44 ± (5.4) m^2 g^{-1}.

On the side of TEOS monoliths, the high molecular weight of PEO (Mon 4) obtained a surface area of 286.60 ± (6.7) m^2 g^{-1} greater than that obtained in the presence of the low molecular weight of polymer (Mon 3) with the surface area of 263.49 ± (3.5) m^2 g^{-1}. In Mon 4, the mesopores diameter and macropores diameter were 11.62 ± (1.3) nm 2.9 ± (0.78) μm, respectively. In Mon 3, the mesopore diameter and macropore diameter were 12.3 ± (0.84) nm 3.4 ± (0.82) μm, respectively.

It has been also reported that the TEOS monolith with PEO 100 kDa and PEO 200 kDa possess surface areas of 164 m^2g^{-1} and 201 m^2g^{-1}, macropores diameters of 10 μm and 4 μm, and mesopores diameters of 16 nm and 13.2 nm.[133]

Generally, the surface areas of TEOS monoliths achieved in this study were significantly more than those achieved by Fletcher *et al.* using a similar composition of starting material.[133] The increase in the surface area of TEOS monoliths of this study may be due to the longer gelation step (one day more) and double the basic treatment period as compare to Fletcher *et al.*'s experiment.[133] Increasing the molecular weight of the PEO as a starting mixture also enhances the surface area and reduces the macropore diameter, which has been also reported by Shrinivasan *et al.*[132]

Table 3-2 shows there was a slight reduction in the macropore diameter with the high molecular weight of PEO (Mon 2 and 4) compared to Mon 1 and 3, respectively. The reduction of macropores happens because of the rapid growth of the silica network before the structure of the silica monolith is frozen during the phase separation, as described in Section 1.5.1.4.

The structural morphology of the TMOS and TEOS monoliths in the presence of high molecular weight of polymer, Mon 2 and Mon 4, were compared using SEM. The SEM micrographs of the internal structure of TMOS and TEOS at different magnifications are shown in Figure 3-4.

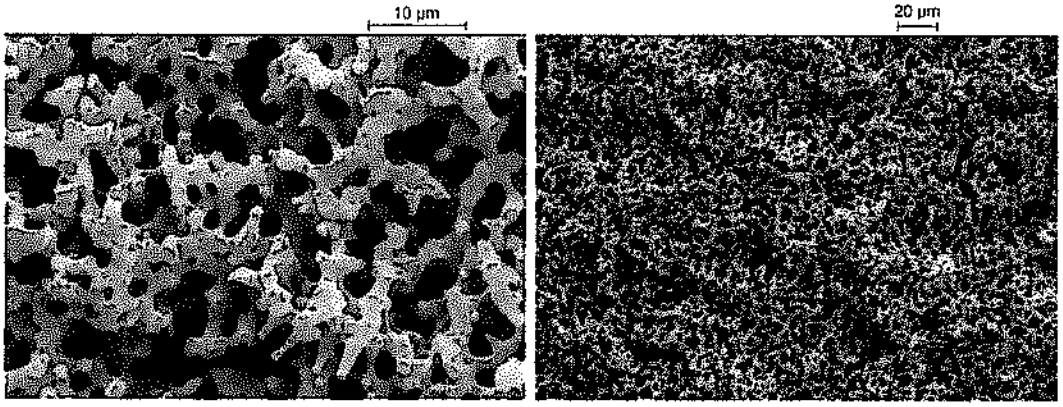

TMOS monolith (Mon 2)

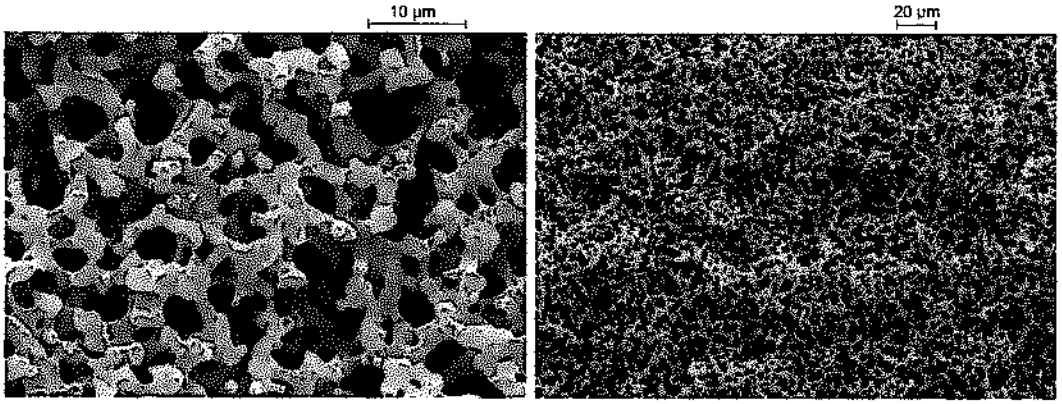

TEOS monolith (Mon 4)

Figure 3-4: SEM micrographs of internal structure of silica monoliths of TMOS and TEOS with PEO (200 kDa) at different magnifications

From the images in Figure 3-4, it was observed that there were no noticeable differences in structural morphology of both types. The general structure for both monoliths is similar. However, the data of the BET method in Table 3-2 showed

TMOS monolith (Mon 2) had a surface area of 315.44 ± (5.4) $m^2 g^{-1}$ with a mesopore diameter of 7.50 ± (1.7) nm and pore volume of 0.93 ± (0.26) $cm^3 g^{-1}$. This is 10% more than the surface area, 35% less in mesopore diameter and 27% less in the pore volume observed when compared to the TEOS monolith using the same molecular weight of PEO (Mon 4). It can be concluded from these results that TMOS monoliths with the two molecular weights of the polymer (Mon 1 and Mon 2) provide higher surface areas and smaller macropore diameter compared to the TEOS monoliths (Mon 3 and Mon 4).

In Mon 5 and 6, Triblock copolymer pluronic (F127) and acetic acid were used with silicon alkoxides (TMOS and TEOS) instead of PEO and nitric acid, respectively. From the data in Table 3-2, it was found that the TMOS monolith with F127 (Mon 5) gave a higher surface area of 366.7 ± (7.2) $m^2 g^{-1}$ and lower macropore diameter of 1.8 ± (0.58) μm compared to 287.79 $m^2 g^{-1}$ and 2.2 ± (0.63) μm for TEOS (Mon 6). Also the result of Mon 5 shows greater surface areas, compared to the surface area (205 $m^2 g^{-1}$) obtained by the other group using a similar composition for the starting material.[133]

Generally, it was observed that the total surface areas of all TMOS monoliths were higher than those of all TEOS monoliths. This is due to TMOS being more rapid in hydrolysis in the sol-gel process than TEOS. TMOS consists of smaller size SiO_2 particles in the network whereas TEOS consists of larger size SiO_2 particles in the network.[114]

The data of this study are similar to the data of Motokawa *et al.* They prepared silica monoliths with different sizes of macropores and skeleton structures. The silica

monoliths with smaller macropore size and thinner skeleton structure have higher surface area, greater efficiency, and lower back pressure.[125]

Upon quick observation of Table 3-2, Mon 5 has the highest surface area of 366 $m^2 g^{-1}$. Since the high surface area is required to increase the binding capacity of the monolith, TMOS, F127, and acetic acid were selected in the following experiments as the silica source, organic additive and catalyst, respectively.

3.3 Effect of the period of the basic treatment

Due to the effect of the basic treatment on the internal structure of the monolith it was suggested that an optimum surface area could be established by varying this treatment at different times (5, 10, 15, and 20 hr). The influence of the period of the basic treatment on the structural morphology of the TMOS-F127 monoliths was investigated by SEM, since it can provide an estimation of the diameter of the macropores. The SEM micrographs of the internal structure of the TMOS-F127 monolith for different periods of basic treatment (5, 10, 15, and 20 hr) are shown in Figure 3-5. All SEM micrographs in Figure 3-5 conclude that all monoliths have bimodal pore structure and the macropore diameters were 2–4 μm.

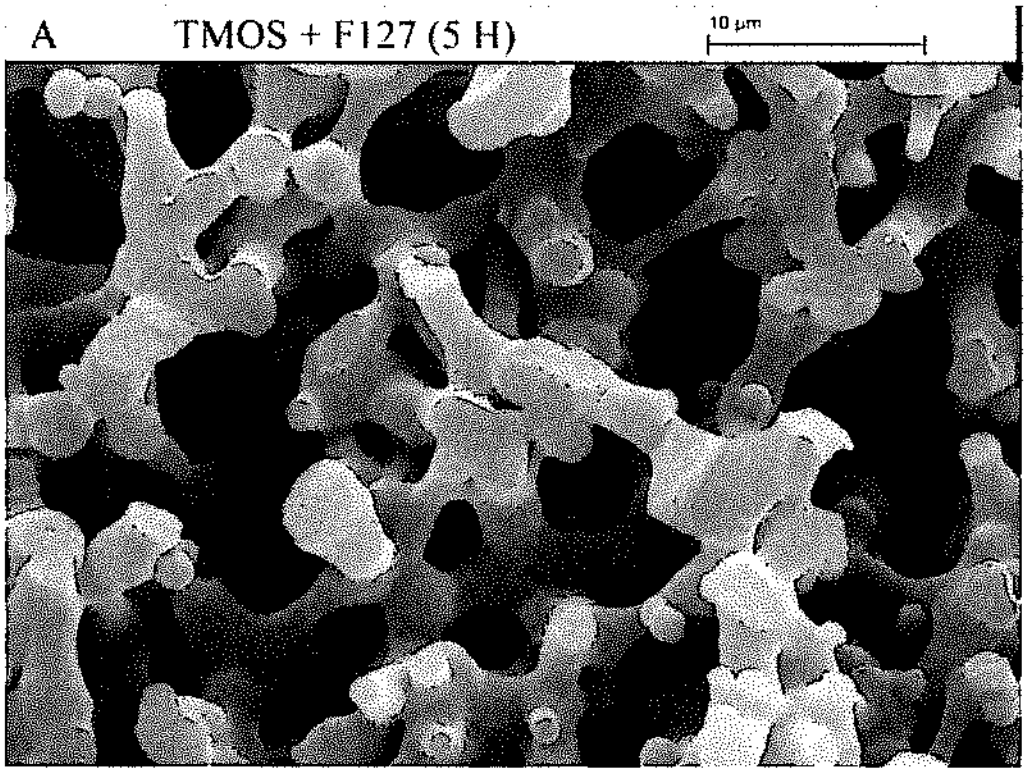
A
TMOS + F127 (5 H)
10 µm

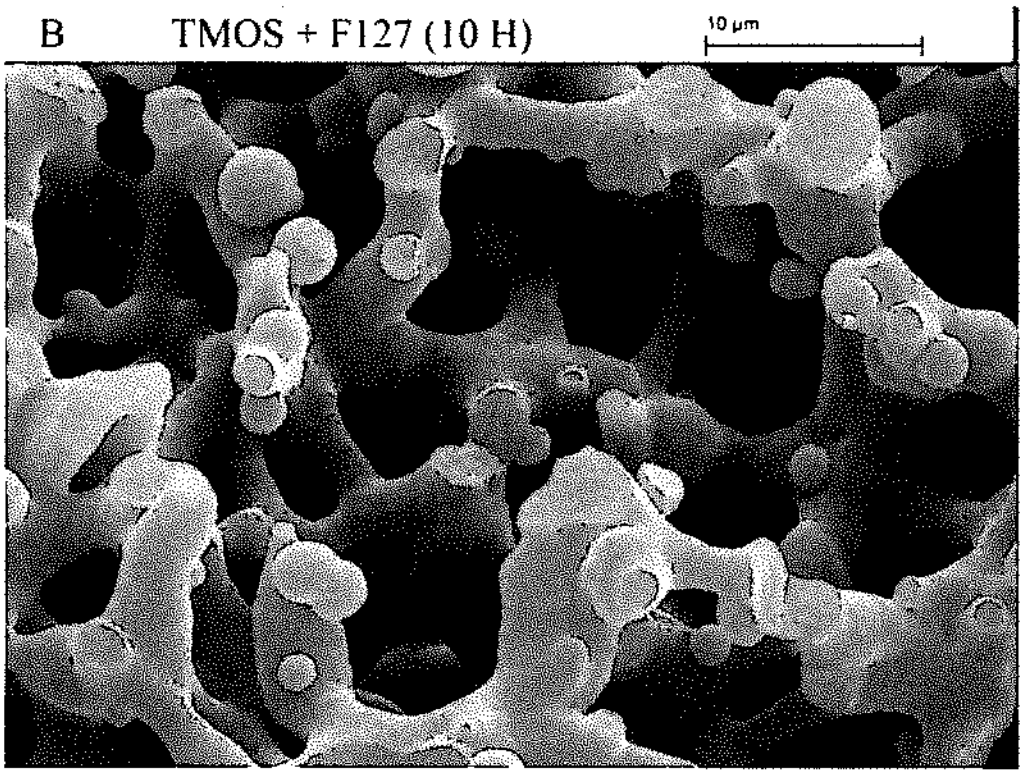
B
TMOS + F127 (10 H)
10 µm

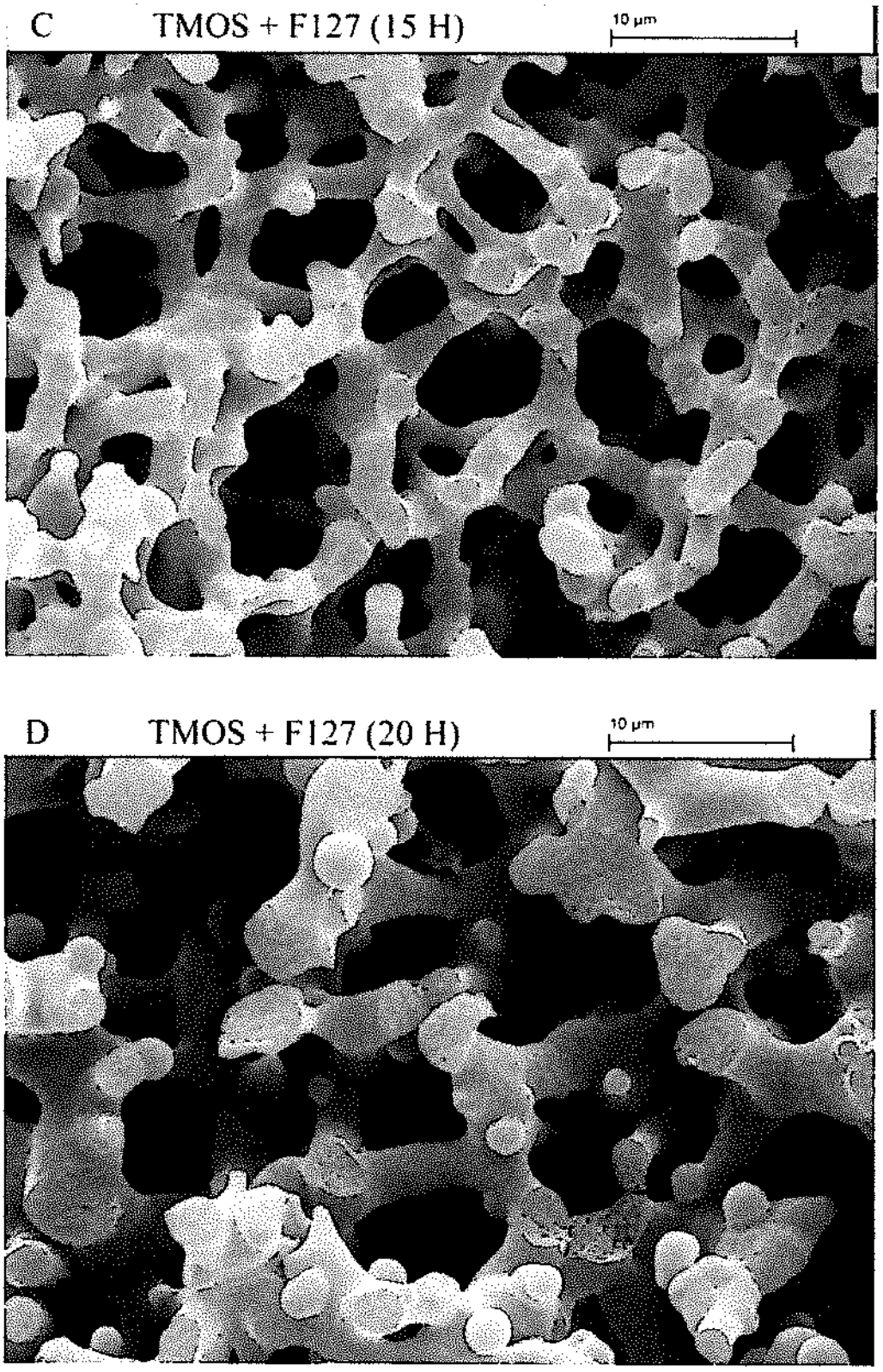

Figure 3-5: Morphology changes of the silica monolith with different time periods of ammonia hydroxide treatment. The sample was prepared from TMOS-F127.

From micrographs, it was hard to see the differences in internal structure of the TMOS-F127 monoliths from the SEM images; thus, the specific surface area and the mesopore diameter were investigated using the BET model, as shown in Table 3-3.

Table 3-3: The physical properties of the TMOS-F127 monoliths with 1 M NH_4OH treatment over different periods of time

Ammonium treatment time (h)	BET surface area (m^2 g^{-1}) ± RSD (n=3)	Average pore diameter mesoporous (nm) ± RSD (n=3)
5	219.6 ± (7.3)	12.4 ± (1.3)
10	264.2 ± (4.5)	11.65 ± (2.2)
15	295.6 ± (8.6)	10.8 ± (1.7)
20	338.60 ± (9.4)	8.67 ± (1.4)

The above table shows there has been a gradual increase in the surface area with increasing the length of time of the basic treatment. The observed increase in the surface area does not therefore appear to come from the mesopore diameter but it may be associated with the enlargement of the macropore structure resulting from the etching process. The present findings seem to be consistent with other research which indicated that an increase in mesopore diameter by dissolution/ reprecipitation would be at the expense of surface area.[110] Data from this table can be compared with Mon 5 in Table 3-2 which shows a surface area of 366.7 m^2 g^{-1} with 1 M NH_4OH treatment for 24 h. The conclusion can be drawn from the present study that the optimal period of the basic treatment was 20–24 hours.

3.4 Physical characterisation of the C18 modified silica-based monolith

Once the silica monolith was fabricated, the surface was then chemically modified by octadecyldimethylchlorosilane (C18), as detailed in Section 1.5.4. Surface modification of the monolithic silica was accomplished by continuously flowing silanisation solution through the porous monolithic silica rod inside the heat-shrinkable tube, as described in Section 2.4.2.

The structural morphology of the modified silica monolith was studied by SEM and BET methods to evaluate the influence of the surface modification of the silica monolith with C18. The SEM micrographs of the TMOS monoliths before and after modification with octadecyl groups are shown in Figure 3-6. Figure 3-6 (A) shows the SEM micrograph of the internal structure of the non-modified TMOS monolith, and (B) shows the SEM image of the C18 modified TMOS monolith.

It is apparent from these micrographs that there is a significant difference in general morphology comparing the SEM micrographs of the monolith before and after modification. The internal structure of modified TMOS monoliths appear thicker with smaller macropores.

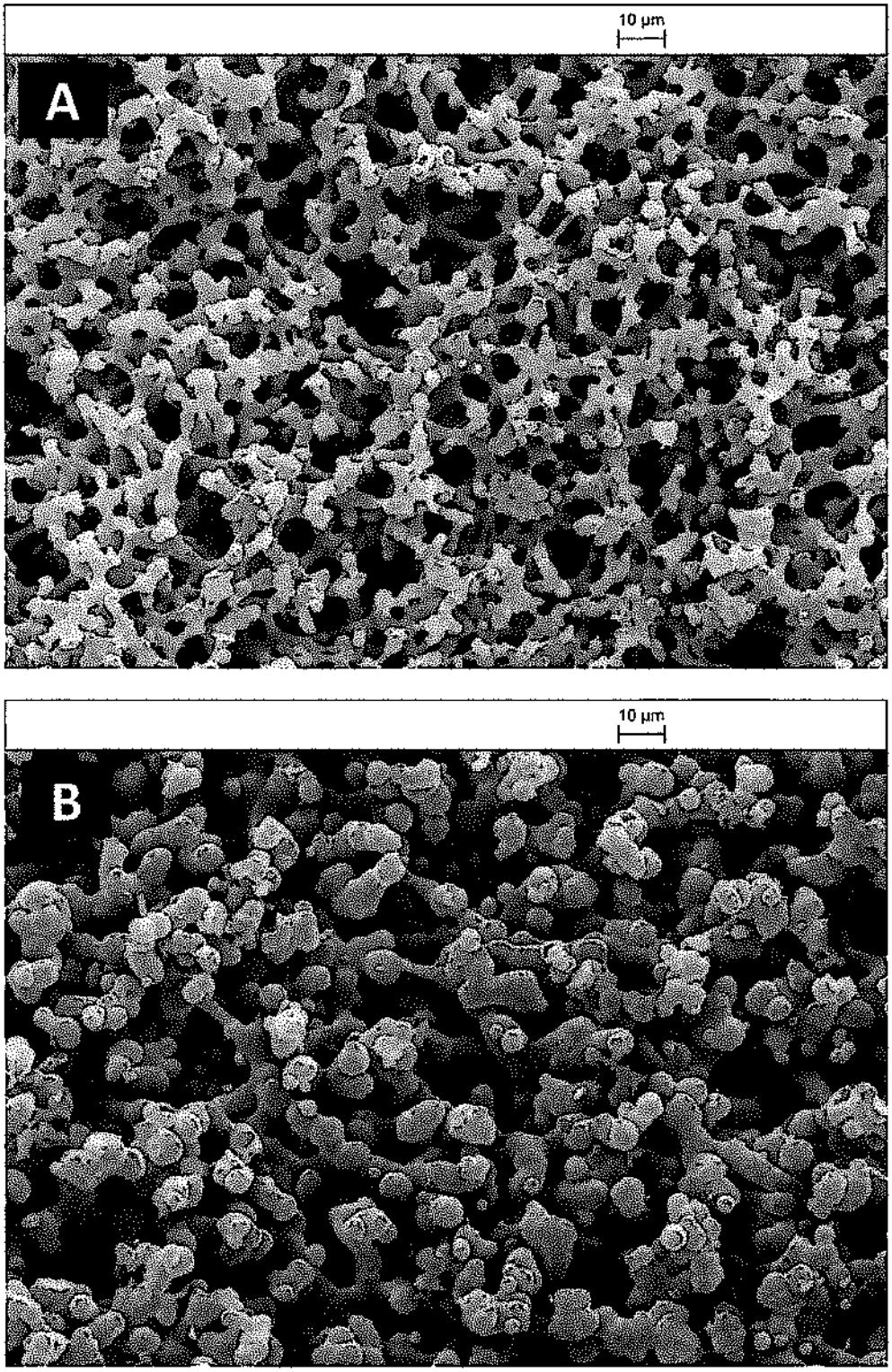

Figure 3-6: SEM micrograph of the internal structure of TMOS silica monolith; (A) non-modified monolith and (B) C18 modified monolith

Furthermore, additional examinations were carried out using the BET method to determine the change in surface area of the silica monolith after the C18 modification process. The findings of this examination found that the surface area of the C18 modified monolith decreased to 312 m^2 g^{-1}, compared to (Mon 5), in Table 3-2, previously achieved for the non-modified silica monolith.

The reason for the decrease in surface area after modification could be related to the blocking of micropore access (< 2 nm) in the silica-based monolith by the bonded phase (the alkyl chains attached to the silica surface), as described in Section 1.5.4.[54, 67] This decrease in surface area is a good indication that the modification process was successfully achieved.

3.4.1 Elemental analysis by EDX

Besides the analysis of the octadecylated silica monolith with the SEM and BET methods, the derivatisation of the silica monolith with octadecyl groups was confirmed by using energy dispersive X-ray (EDX) analysis. The EDX spectra of the non-modified silica monolith with the elements detected on the surface is shown in Figure 3-7. Quantitative EDX analysis for all elements in non-modified silica-based monoliths is shown in Table 3-4. As expected, the non-modified silica monolith is generally composed of silicon (Si), carbon (C), and oxygen (O) at 45.37%, 2.97%, and 51.5% for Si, C, and O, respectively.

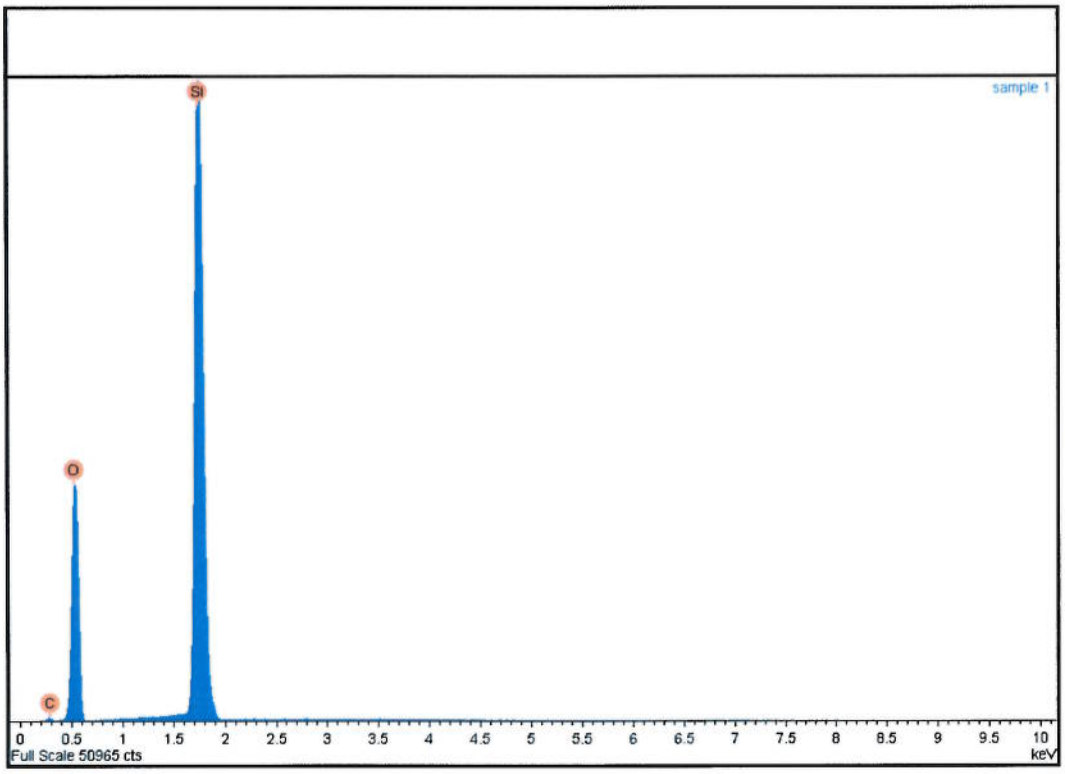

Figure 3-7: EDX spectra of non-modified silica-based monolith

Table 3-4: Quantitative EDX analysis for all elements in non-modified silica-based monolith

Spectrum	C %	O %	Si %	Cl %	Total
Non-modified silica monolith	2.97	51.5	45.37	0.00	100.00

The EDX spectra for the modified monolith with the elements detected on the surface is shown in Figure 3-8. Quantitative EDX analysis for all elements in the modified silica monolith is shown in Table 3-5. From the EDX result, it was observed that the carbon peak increases from 2.97 to 15.48% of the total elements. This was an indication of the presence of chlorodimethyloctadecylsilane.

This finding is in agreement with other research findings which showed that the degree of surface loading by the R group of the monochlorosilane (C-2 to C-18) will vary from 5 to 19% by weight as carbon for the packing material.[54, 67] Furthermore, a new peak for chlorine (Cl) appeared in the spectra. In general, this spectra exposes the presence of octadecyl groups on the surface of the silica monolith.

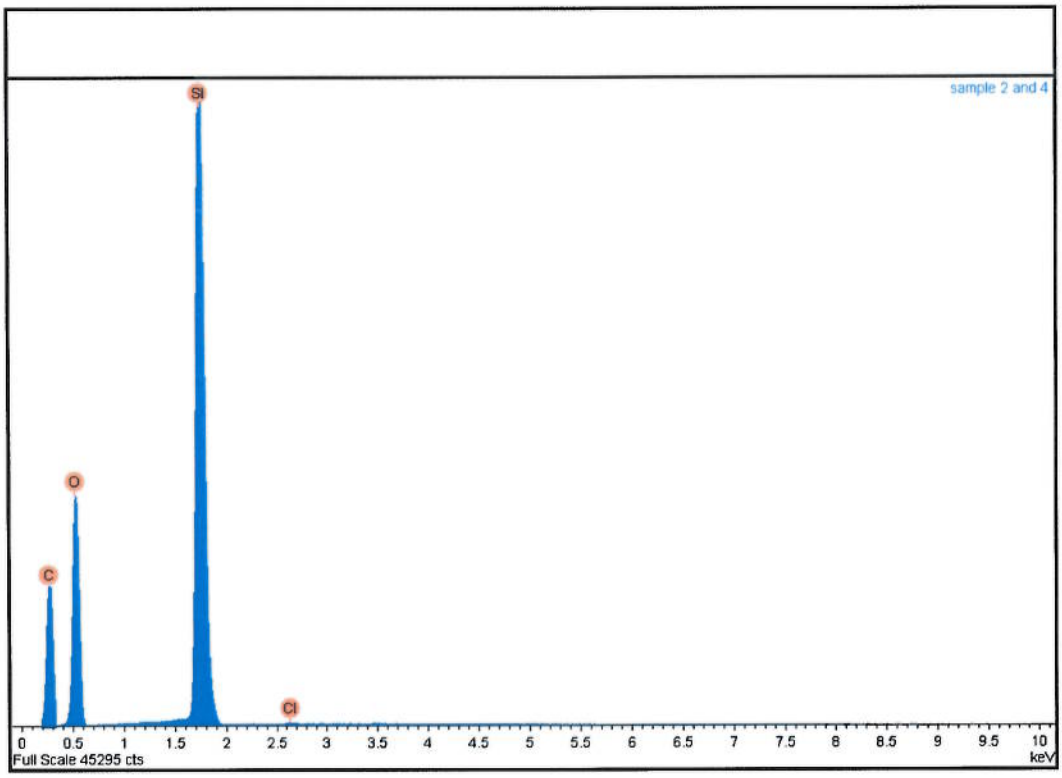

Figure 3-8: EDX spectra of modified silica-based monolith

Table 3-5: Quantitative EDX analysis for all elements in modified silica-based monolith

Spectrum	C %	O %	Si %	Cl %	Total
Modified silica monolith	15.48	44.82	39.44	0.26	100.00

The successful modification of the surface with C18 was further confirmed by using the monolith for SPE and pre-concentration of the target analyte.

3.5 Conclusion

Fabrication of a silica-based monolith using a sol-gel process was examined. The work presented here confirms previous outcomes and contributes additional evidence that fabrication of the silica monolith is related to the concentration and molecular weight of the polymer in the starting mixture, resulting in increased surface area and reduction of the macropore diameter.[120, 132, 133]

The optimising of the starting materials is essential since it has a significant influence on the internal structure of the silica monolith. For that, six different types of monolith were made. The highest surface area was obtained from the chemical composition of TMOS, F127, and acetic acid at 366 $m^2 g^{-1}$. The surface areas achieved in this work were greater than those achieved by other researchers,[133, 176, 275] although they were less than some of the popular commercial SPEs which can reach 800 $m^2 g^{-1}$.[78] These commercial columns however are usually available in a certain cartridge shape and require at least 1 to 2 ml of sample. Also, this surface area is still lower than that indicated with similar starting materials in a recent study, which was 944 $m^2 g^{-1}$.[273]

The basic treatment is the most essential step to improve the surface area of the silica monolith. Therefore, the basic treatment with ammonia solution was shown to significantly increase the surface area by converting micropore to mesopores.[131, 134]

The surface of the silica-based monolith was chemically modified by octadecyldimethylchlorosilane (C18). This modification process on the silica surface was successfully confirmed by using SEM analysis, BET method, and EDX analysis.

A new peak for chlorine (Cl) appeared in the EDX spectra. The carbon peak increased from 2.97% (in the non-modified monolith) to 15.48% (in the modified silica monolith). This finding is in agreement with other research findings which showed that the degree of surface loading by the R group of the monochlorosilane will vary from 5 to 18% by weight as carbon for the packing material.[67, 78]

Chapter 4: Results and Discussion: Applications of Silica-based Monolith for Eserine

This work involved using a C18 surface-modified silica monolith for SPE and required identifying the optimum conditions for trapping and release of pesticides in an aqueous sample. The extraction efficiency, pre-concentration, and loading capacity of the monolith were evaluated by using eserine, a type of carbamate pesticide, as a model compound.

4.1 Investigation of optimum detection wavelength for eserine

Detection wavelength is the first parameter to investigate to establish the optimum sensitivity of the test compound (eserine). Standard eserine solutions at two different concentrations (20 ppm and 2 ppm), dissolved in water, were measured by using a UV-VIS spectrometer in the 200–800 nm wavelength range. In this experiment, water was used as a base reference and a quartz cuvette was used as a sample cell. Each concentration was measured independently and showed two absorbance bands. The relationship of the eserine detection wavelengths at concentrations of 20 ppm and 2 ppm are shown in Figure. 4-1 and 4-2, respectively.

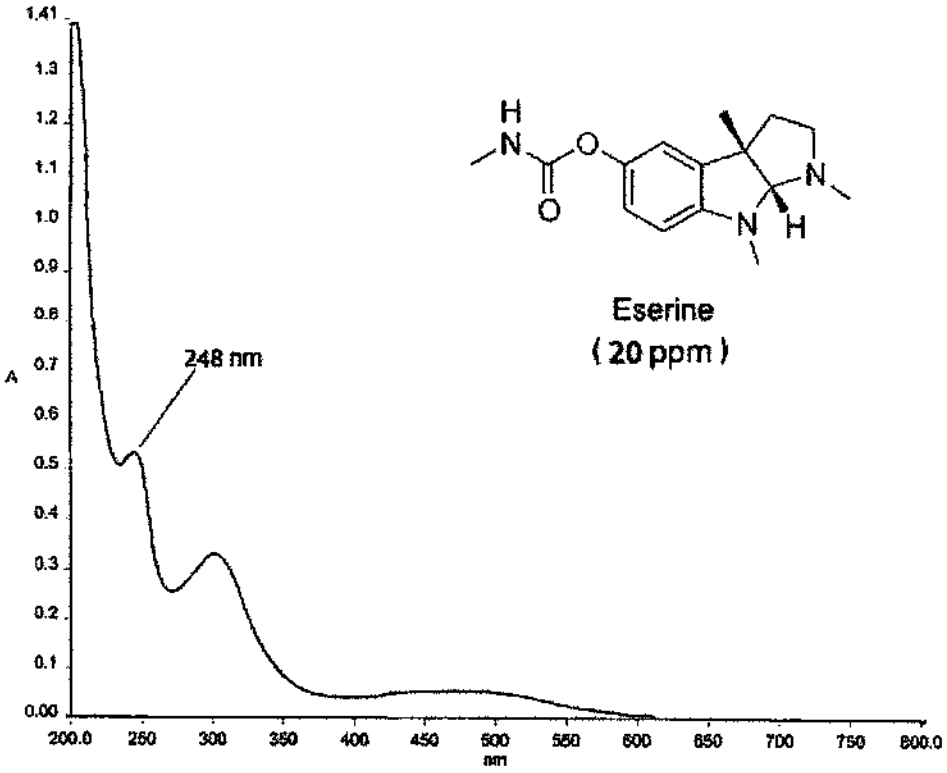

Figure 4-1: Spectra of 20 ppm of eserine detected by UV-VIS spectrometer

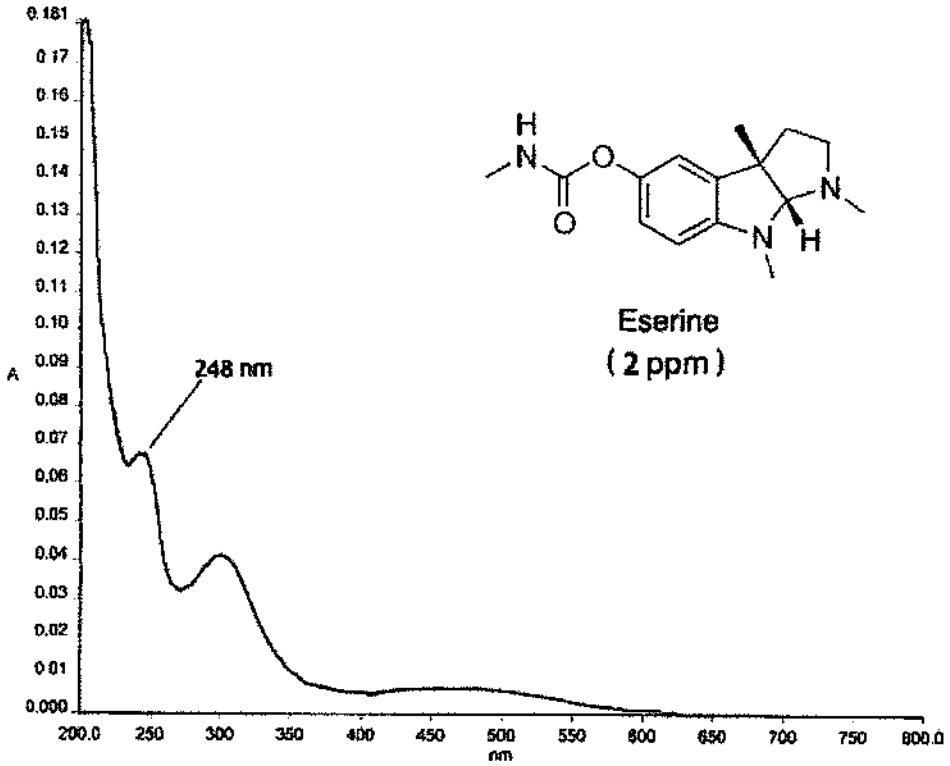

Figure 4-2: Spectra of 2 ppm of eserine detected by UV-VIS spectrometer

From the spectra in Figures 4-1 and 4-2, it is clearly shown that the eserine peaks at 248 nm, and the sample appears colourless, because it does not absorb in the visible region from 400 to 800 nm. As the concentration of the sample is proportional to absorbance by the Beer–Lambert Law (Equation 4-1), calibration will be carried out to establish the limit of detection (LOD) and limit of quantification (LOQ) in the next section, 4-2. The optimum wavelength at 248 nm was selected in the following experiments.

$$A = \varepsilon cl \qquad (4\text{-}1)$$

where (A) is the absorbance, (ε) is the molar absorptivity of the compound, (c) is the concentration of the solvent, and (l) is the path length.

4.2 Calibration curve of eserine standards

Calibration curves were used to determine the amount of analyte in the unknown samples. The calibration curves were prepared according to the procedure presented in Section 2.5.3, under the optimised conditions for a range of standard solutions of 5–100 μg mL^{-1}, at eleven concentration levels. These working standard solutions were analysed directly by HPLC-UV three consecutive times at each concentration level and the peak areas were plotted against concentration (μg mL^{-1}), as shown in Figure 4-3.

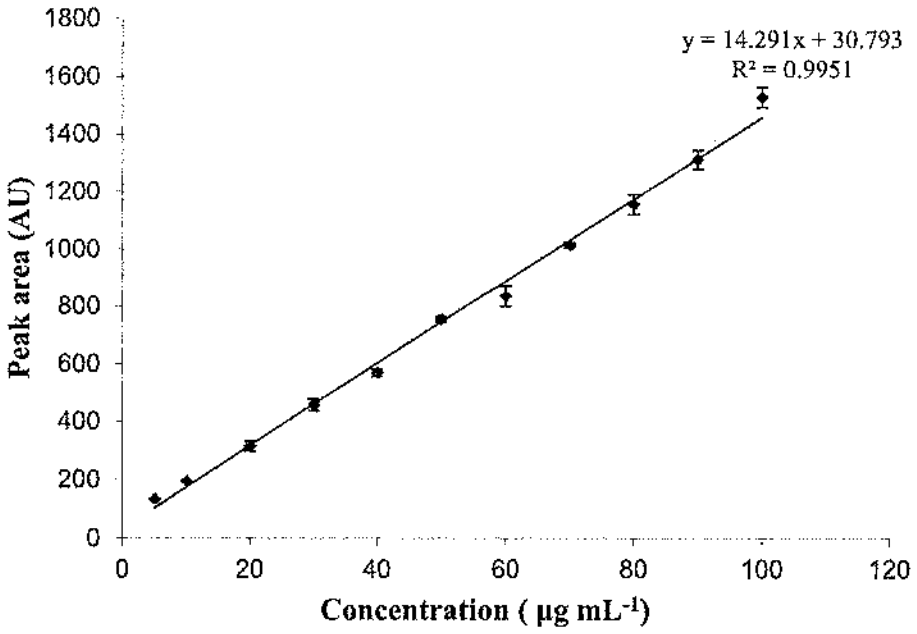

Figure 4-3: Calibration curve of eserine standard solutions with the peak areas plotted versus concentration (µg mL^{-1})

The eserine calibration curves (Figure 4.3) showed good linear regression (r^2= 0.9951) within the 5–100 µg mL^{-1} linear range. The LOD (3SD/S) and LOQ (10SD/S) for eserine were calculated using Equation 2-2 and Equation 2-3 (Section 2.5.3), respectively, from the calibration curve in Figure 4-3. The equation obtained for the calibration curve was y=14.291x +30.793. The regression equation, R^2, LOD, and LOQ of eserine are summarised in Table 4-1.

Table 4-1: Analytical figures of merit for eserine (n=3)

Compound	Regression equation	R^2	LOD (µg mL^{-1})	LOQ (µg mL^{-1})
Eserine	y= 14.291x + 30.793	0.9951	0.07035	0.23452

It can be observed that the limit of quantification of eserine (0.07035 × 1000 =70.35 μg L^{-1}) is 700 times higher, compared to the EU permissible concentration (0.1 μg L^{-1}) for individual pesticide. This reflects a limitation with using UV absorbance as an analytical method.

4.3 Effect of flow rate on the extraction efficiency

The extraction procedure is described in Section 2.5.4. Extraction recovery studies were performed with 100 μg mL^{-1} of eserine, at eight different flow rates. The flow rate of the sample solution through the C18 silica monolith is an efficient parameter to control the analysis time. It must be low enough to perform an efficient trapping, and high enough to shorten the processing time. The effect of flow rate on extraction efficiency was determined in the 20–1000 μL min^{-1} range. The extraction was performed three times for each flow rate. The effect of sample flow rate on extraction efficiency for 100 μg mL^{-1} of eserine by passing 300 μL of the sample is shown in Table 4.2.

Table 4-2: Effect of flow rate on extraction efficiency

Pesticide	Flow rate ($\mu L\ min^{-1}$)	Time (min)	Recovery (%) ± RSD (n=3)
Eserine ($100\ \mu g\ mL^{-1}$)	20	45	85.21 ± 8.64
	50	18	88.10 ± 11.73
	100	15	94.98 ± 10.60
	200	4.5	93.09 ± 6.73
	400	2.25	96.58 ± 8.57
	600	1.5	89.6 ± 10.39
	800	1.125	86.3 ± 12.9
	1000	High back pressure	

The results (Table 4.2) show that the eserine recovery in the range 100–400 $\mu L\ min^{-1}$ gave the highest extraction efficiency (more than 90%). These results were acceptable and not affected considerably by flow rate. When the flow rates are below 100 $\mu L\ min^{-1}$ or over 400 $\mu L\ min^{-1}$, the recovery date becomes worse and that may be a result of non-equilibrium between the eserine in solution and eserine bound to the modified solid phase, or overload. The higher flow rate (1 $mL\ min^{-1}$) obtained a higher backpressure, and the fitting could not withstand the facing pressure; therefore, it was excluded from the experiment. To have an effective analysis in a reasonable time, the sample flow rate of 400 $\mu L\ min^{-1}$ was selected in the following experiments. Using a flow rate at 400 $\mu L\ min^{-1}$, all the extraction procedures including conditioning, loading, washing, and elution from the octadecylated silica monolith sorbent could be completed in approximately 10 min.

4.4 Extraction efficiency of C18 silica monoliths

One of the most dynamic approaches for characterising stationary phases is a simple investigation of the efficiency of extraction, then extraction of the target analytes with the C18 silica monolith was performed. Extraction efficiency is the percentage of solute moving from one phase to the other. The extraction procedure is described in Section 2.5.4; all eluted fractions were analysed directly by a HPLC-UV detector, under conditions described in Section 2.5.1. Aliquots of 300 μL of 100 μg mL^{-1} eserine solution equivalent to 30 μg were loaded through the C18 silica monolith sorbent at the optimum flow rate of 400 μL min^{-1}. Each 300 μL aliquot was passed through the C18 monolith sorbent, then washed and eluted prior to injection into an HPLC for analysis.

Ideally, no peaks should appear in the HPLC chromatogram for the analytes during the loading and washing steps as the analytes should be trapped as a result of the hydrophobic interaction between eserine and the C18 coated silica monolith sorbent. The HPLC chromatograms for the extraction process of eserine are shown in Figure 4-4. The HPLC chromatograms of eserine standard, loading fraction, washing fraction, and elution fraction are shown in Figure 4-4 (A), (B) (C) and (D), respectively.

From the chromatogram in Figure 4-4 (A), it is apparent that the retention time of the eserine standard (100 μg mL^{-1}) was 2.10 min. After that, it can be observed that there are tiny peaks appearing at or around the same retention time as eserine in loading (B) and washing steps (C) indicating possibly a very small amount of breakthrough, although this appears to be less than 0.5%. A peak can clearly be observed at 2.20 min presenting that the eserine was eluted from the C18 monolith sorbent (D).

The results in Figure 4-4 show the validity of the extraction process using the octadecylated silica monolith sorbent for eserine, where a minimal amount of analyte is detected during the loading and washing steps because it is predominantly retained in the C18 monolith sorbent. The eserine was eluted with the same solvent as the mobile phase to decrease the noise.

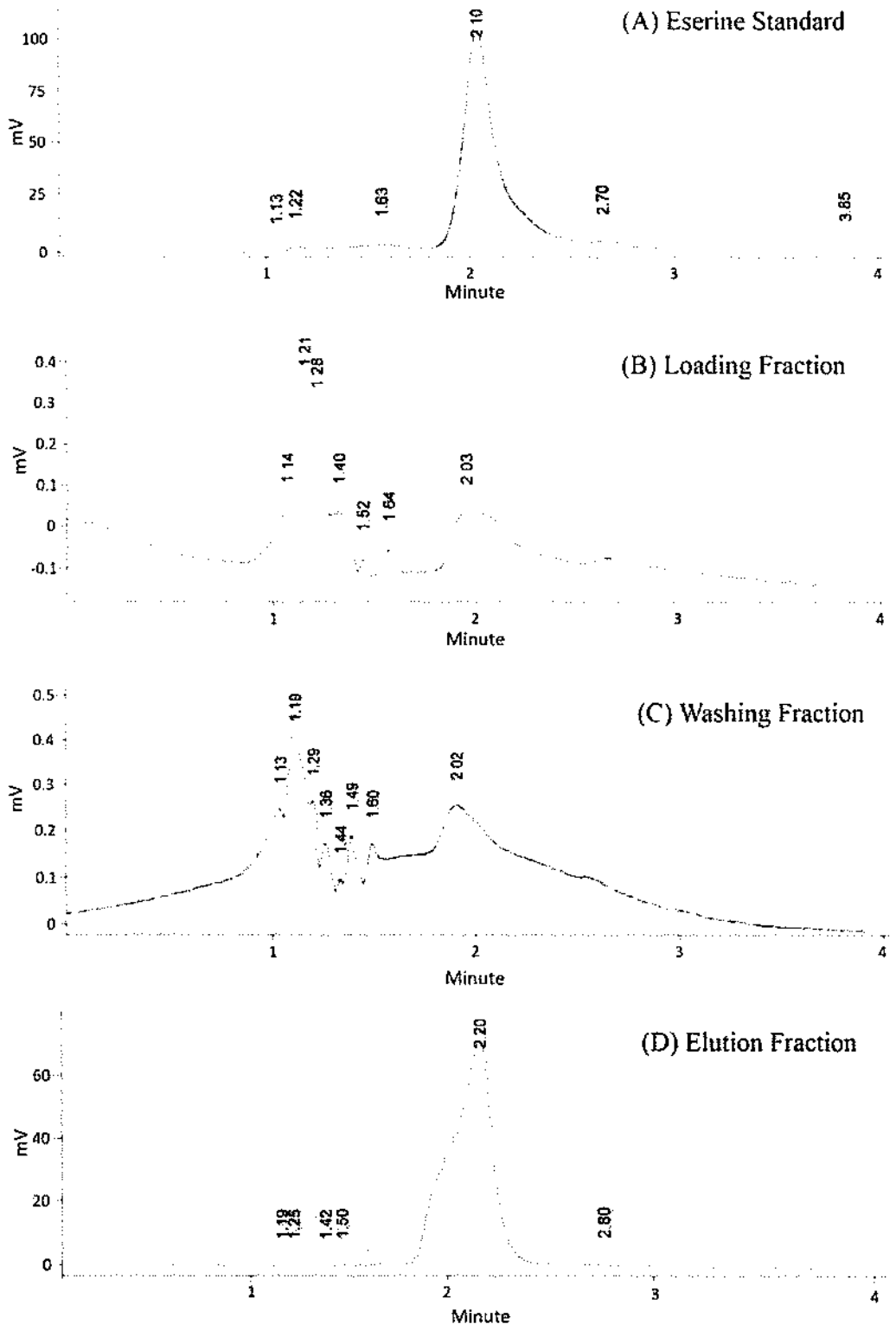

Figure 4-4: HPLC chromatogram obtained for the extraction steps. (A) The standard solution of eserine was directly injected into the HPLC, (B) The loading fraction was collected from the loading step, (C) The washing fraction and (D)

the elution fraction. The separation column was a Bio Wide Pore C18 column (5 µm, 15 cm × 2.1 mm), the mobile phase was methanol /water (60:40) (V/V) run under isocratic conditions; the UV wavelength was set at 248 nm, the injection volume was 20 µL, and the flow rate was 1 mL min^{-1}.

4.5 Evaluation of the percentage of extraction recovery

To investigate the percentage recovery for the extraction from the octadecylated silica monolith sorbent, the recovery was plotted as a bar chart for each step during the extraction procedure. The percentage recovery of eserine was measured by comparing chromatographic peak areas for the direct injection of the standard samples with those obtained from all the fractions after extraction. Each analysis was carried out in triplicate and the extraction recovery (ER) was calculated (see Equation 2-1 in Section 2.5.1) below, and defined as the percentage of the total eserine amount (n_0) measured before extraction compared with the total eserine eluted after extraction (n_{set}).

$$ER = (n_{set}/n_0) \times 100$$

For example, when the peak area of one standard of eserine sample was 1568 (n_0) and the peak area of the extracted eserine sample was 1480 (n_{set}), then the extraction recovery was approximately (1480/1568) × 100= 94.4%.

Each fraction was analysed three times and all the recovery data is shown in Table 4-3.

Table 4-3: the extraction recovery of eserine runs and the average.

	Extraction recovery (ER) (%)			
Fraction	Run 1	Run 2	Run 3	Average
Std. 100 μg mL^{-1}	100	100	100	100
Loading	0.096	0.13	0.058	0.95
Washing 1	0.001	0.005	0.048	0.018
Washing 2	0.008	0.004	0.01	0.007
Washing 3	0.054	0.066	0.073	0.064
Elution	94.35	97.48	98	96.61

The efficiency was expressed as a percentage of mean recovery (n=3) according to Equation 2-1 in Section 2.5.1. The extraction profile data presented in Figure 4-5 shows the efficient recovery of 100 μg mL^{-1} eserine from the octadecylated silica monolith sorbent at a flow rate of 400 μL min^{-1}.

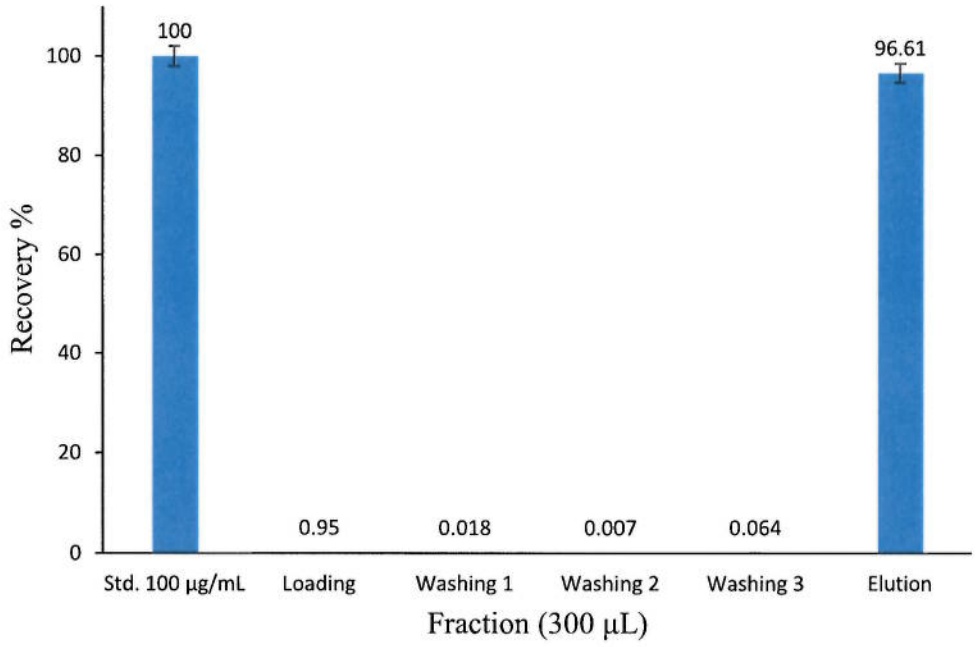

Figure 4-5: The extraction profile for 100 µg mL^{-1} of eserine using the C18 silica monolith. The average recovery percentage was obtained from three consecutive experiments (n=3) and the error bars indicate one standard deviation

The extraction efficiency performed by using the octadecylated silica monolith was 96.6%, with negligible analyte detected during the loading and washing steps. The remaining 3.4% was either retained in the C18 silica sorbent or approx. 1% lost during loading and washing steps. The modification process for silica monolith indicates a good selectivity towards eserine.

4.6 The pre-concentration study of eserine

In the extraction process the sample is usually pre-concentrated as this can expand the sensitivity of the method and reduce the detection limit. The C18 functionalised silica monolith was tested for both extraction and pre-concentration of eserine from liquid

samples. A 4 ml sample (10 μg mL^{-1}) was loaded through the C18 silica monolith sorbent at a flow rate of 400 μL min^{-1}. The analytes were eluted with 400 μL of methanol/water (60:40) at the same flow rate from the C18 silica monolithic sorbent. The pre-concentration procedure is described in Section 2.5.4; all eluted fractions were analysed directly by a HPLC-UV detector, under the conditions described in Section 2.5.1. The HPLC chromatograms for the pre-concentration process of eserine are shown in Figure 4-6.

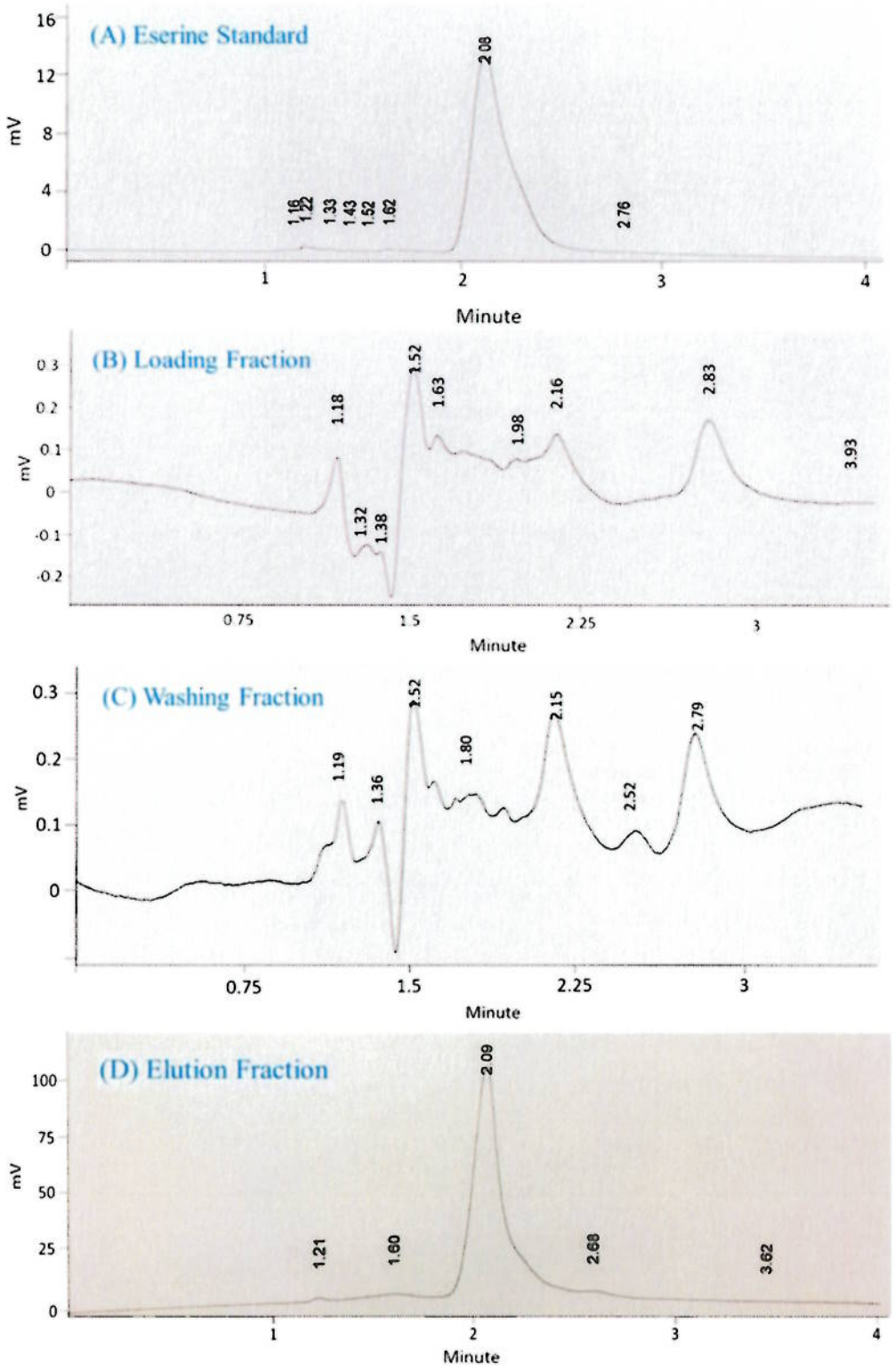

Figure 4-6: HPLC chromatogram shows the peak areas response (A) the standard solution of eserine (10 µg mL^{-1}), (B) the loading fraction, (C) the washing fraction and (D) the pre-concentrated elution fraction. The separation

column was Bio Wide Pore C18 column (5 µm, 15 cm × 2.1 mm), the mobile phase was methanol /water (60:40) (V/V) run under isocratic conditions; the UV wavelength was set at 248 nm, the injection volume was 20 µL, and the flow rate was 1 mL min^{-1}

From the chromatogram in Figure 4-6 (A), it can be seen that the retention time of the eserine standard (10 µg mL^{-1}) was 2.08 min. Then, there are no significant peaks appearing at the retention time of eserine during loading, as shown in Figure 4-6 (B). While there is a small peak observed around the retention time from the washing steps (see Figure 4-6 (B)). Afterwards, the target analyte was pre-concentrated, the peak area response was significantly increased at the retention time of 2.09 min, as shown in Figure 4-6 (D).

To investigate the pre-concentration of eserine, the peak area response was plotted in a bar chart for direct injection of the standard solution, loading, washing, and elution fractions. The pre-concentrated profile data for eserine (10 µg mL^{-1}) using the C18 functionalised silica monolith at a flow rate of 400 µL min^{-1}, is shown in Figure 4-7.

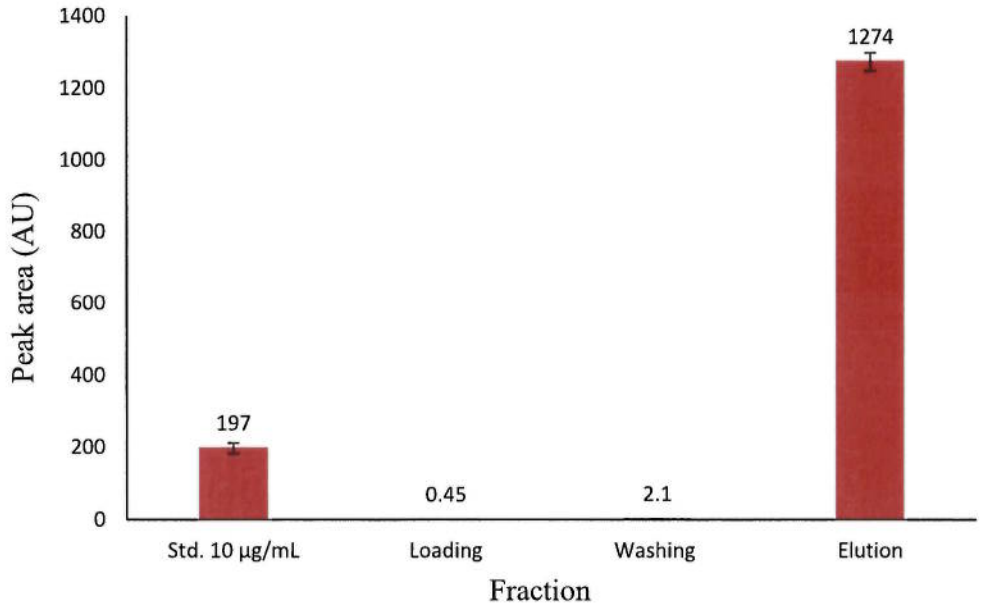

Figure 4-7: The pre-concentrated ability for 10 µg mL^{-1} of eserine using the octadecylated silica monolith. The average peak area response was obtained from HPLC three consecutive times and the error bars indicate one standard deviation.

It can be seen from the figure that the peak area response for the standard solution was 197 and after it passed through the monolith, the peak area increased to 1274. The concentration of eserine was calculated by using calibration curve equation (Section 4.2). The pre-concentration profile of 10 µg mL^{-1} eserine using the C18 –TMOS modified monolith column at flow rate 400 µL min^{-1}, is shown in Figure 4-8.

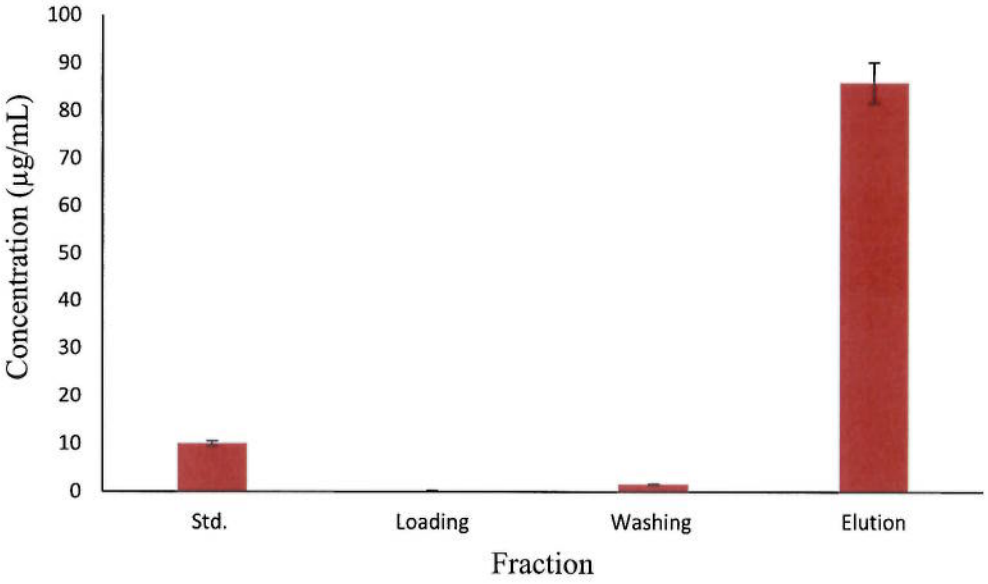

Figure 4-8: The pre-concentrated profile for eserine, (n=3). The error bar indicates one standard deviation

According to the result achieved during this experiment the C18 functionalised silica monolith has the ability to pre-concentrate the target analyte eserine where the concentration increased from 10 to 86 µg mL^{-1}. This indicates that the pre-concentration value is more than 8.5 fold and the functionalised silica monolith could be suitable for online pre-concentration purposes and provides promise to continue further work.

4.7 Loading capacity and longevity

Sample capacity is one of the important characteristics of the solid-phase extraction process. If there is not enough capacity, the target analytes will pass through the C18 silica monolith sorbent during extraction without being trapped.[151] For evaluating the monolith sorbent, breakthrough volume was established from a breakthrough curve and measured by loading the constant concentrations of the sample through the monolith sorbent. The analytes are quantitatively retained during the initial sampling phase by the sorbent, up to the point that the sample volume exceeds the retention capacity of the sorbent. Further sample entering the sorbent bed will not be quantitatively retained by the sorbent, and eventually, the concentrations of analytes entering and exiting the sampling device become identical. The point on the curve at which an arbitrary sample amount is detected at the outlet of the sampling device is the breakthrough volume (V).[70]

An assay for determining breakthrough volume was performed according to the procedure described in Section 2.5.5. A maximum loading capacity experiment was conducted to investigate the absorption performance of the C18 silica monolith. Increasing amounts of eserine were loaded into the monolith; in order to reach 'saturation', the initial eserine concentrations were increased, and the plateau values (adsorption capacity values) were obtained.

A fraction of 300 μL of a sample containing 30 μg of eserine was loaded into the C18 silica monolith fabricated from TMOS, F127, and acetic acid, at 400 μL min^{-1}. Each fraction was collected separately and measured directly by a HPLC-UV detector, under conditions described in Section 2.5.1. The breakthrough capacity curve for eserine is shown in Figure 4-8.

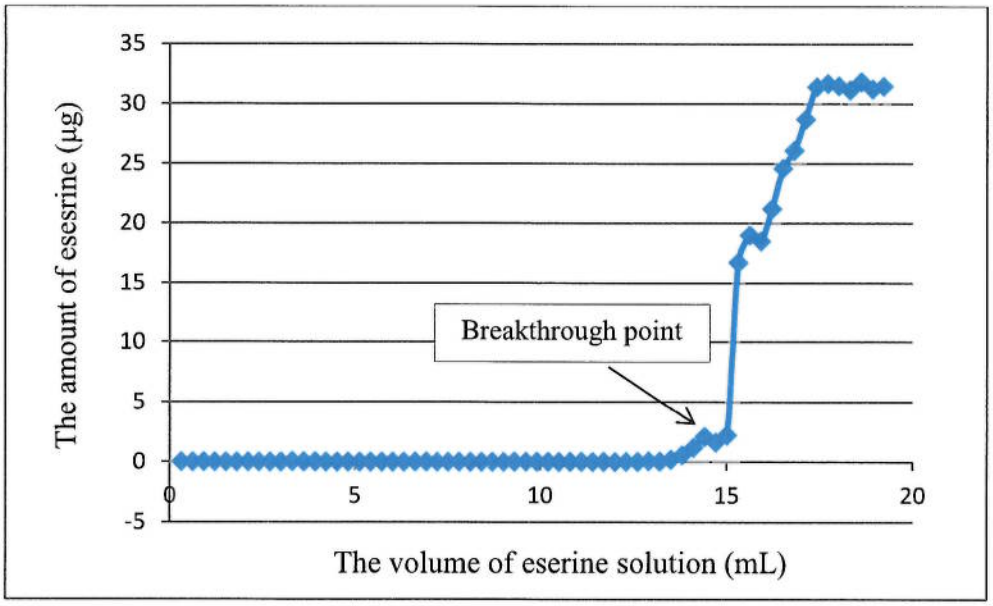

Figure 4-9: Loading capacities of a C18 silica monolith rod (78.4mg) as measured using breakthrough of eserine

As shown in Figure 4-8, the curve is steep at the breakthrough point. The eserine breakthrough in the silica monolith was saturated after 13.8 mL (46 fractions) and the loading time was 34.5 min. The capacity of the silica monolith sorbent, which weighed 78.4 mg, was calculated and found to be 17.6 µg mg^{-1} for eserine. This result of capacity is lower than the result obtained by a similar study, which shows C18-TMOS has capacity of 28 µg mg^{-1} for caffeine.[275] During a testing period of two months, more than 200 injections were carried out. There were no significant changes in the performance of the silica monolith.

The European Union Directive limits the content of individual pesticides in drinking water with a recommended limit of 0.1 mg L^{-1}, which means that a more sensitive detection technique with lower detection limits (LOD) needs to be introduced to reach the target of 0.1 mg L^{-1}. These could possibility include chemiluminescence detection methods.

4.8 Conclusion

The optimum detection wavelength of the test compound (eserine) was investigated by using a UV-VIS spectrometer. The effect of the flow rate on the extraction efficiency was studied at eight different flow rates. The efficiency of extraction for eserine from the C18 modified silica sorbent was evaluated.

The percentage recovery of the analytes of interest was measured by comparing chromatographic peak areas for the direct injection of the standard samples with those obtained by the fraction after extraction. High extraction recoveries for eserine were achieved by using the C18 silica monolith (96.58%). This SPE method offers various advantages including simplicity, a low volume of sample of 300 µL, and speed of extraction of the analyte (less than 10 min) compared to conventional SPE cartridges which require a large volume of sample from 3 to 6 mL and take more than 20 min.[276]

Furthermore, a modified silica monolith was successfully confirmed to pre-concentrate eserine from the liquid sample. This confirms that the C18 modified silica monolith has the ability to pre-concentrate the analyte of interest by 5 times. In addition, the modified silica monolith showed good capacity of 17.6 µg mg^{-1} (lower than that indicated from a previous study)[275] and offered longevity up to two months with more than 200 injections. This indicates that the functionalised silica monolith could be appropriate for the pre-concentration purposes of eserine and provides promise to be applied to real samples.

Chapter 5: Results and Discussion: Detection of Eserine by Chemiluminescence

5.1 Optimisation of chemiluminescence parameters

To select the optimum conditions for the determination of carbamate pesticides, two parameters were evaluated using a univariate approach. The key parameters optimised were pH and flow rate. These parameters were studied using the microfluidic manifold shown in Section 2.6.1, which fabricated a glass device with a serpentine manifold (206 mm length) with a channel depth of 65 μm and width of 200 μm. Reagents and sample were continuously injected into the microfluidic device which was included within the light-tight housing detailed in Section 2.7.1. A schematic of the microfluidic manifold is shown in Figure 5-1.

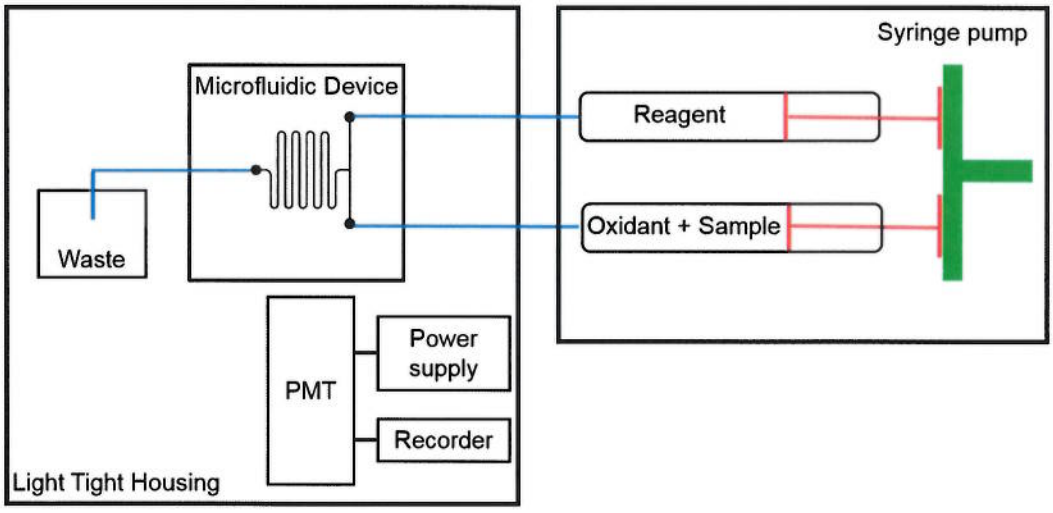

Figure 5-1: Schematic diagram of the reaction manifold used for the determination of eserine

5.1.1 Effect of pH on CL intensity

Since the CL reagent luminol required an alkaline medium, the effect of pH on the CL intensity was examined in the range of 8.5 to 12, as previous studies have shown this to be the optimum range for the luminol reaction[277-279], discussed in Section 1.8. The luminol concentration was 20 mM, the oxidant hydrogen peroxide concentration was 20 mM and the flow rate was 15 μL min^{-1}. The results of the effect of pH on CL signal are shown in Figure 5-2.

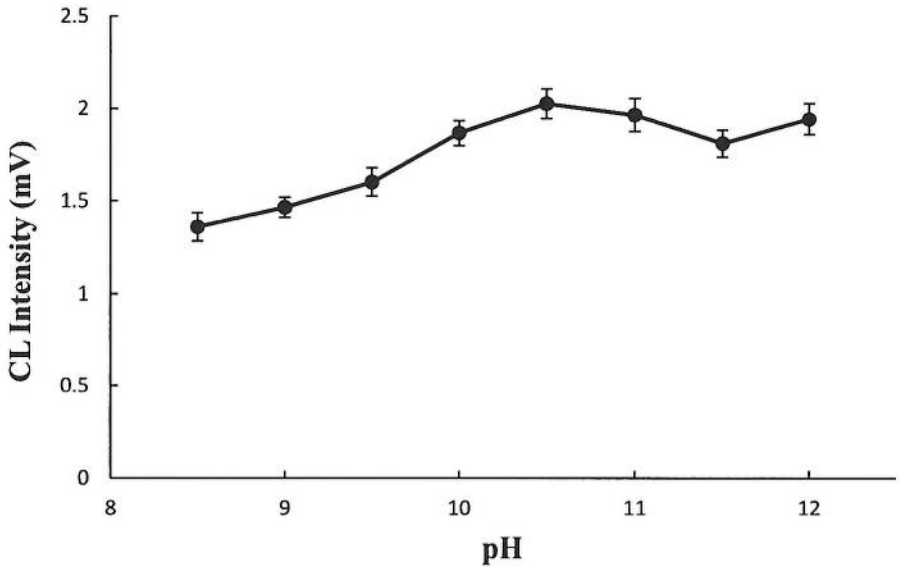

Figure 5-2: Effect of pH on the luminol chemiluminescence emission within a microfluidic device where the concentration of luminol was fixed at 20 mM, the concentration of H_2O_2 was fixed at 20 mM, and the flow rate was 15 μL min^{-1}. Error bars: one standard deviation (n=5).

As can be seen in Figure 5-2, the chemiluminescence intensity increased quite significantly from 1.36 (at pH =8.5) to 2.02 mV (at pH =10.5). The maximum chemiluminescence intensity was obtained with better reproducibility at a pH of 10.5.

Therefore, the pH was maintained at the optimal value of 10.5 for all future use in the investigation.

5.1.2 Effect of flow rate on CL intensity

The CL reagent, oxidant, and analyte were introduced into a microfluidic device at identical flow rates. Flow rate is an essential factor in the CL reaction because it is critical for maximum collection of the emitted light. Hence, the influence of flow rate on intensity was investigated in the range of 5 to 35 μL min^{-1}, with three replicates. The luminol concentration was 20 mM, the oxidant hydrogen peroxide concentration was 20 mM, and the pH was 10.5. The results of the influence of flow rate on CL signal are shown in Figure 5-3.

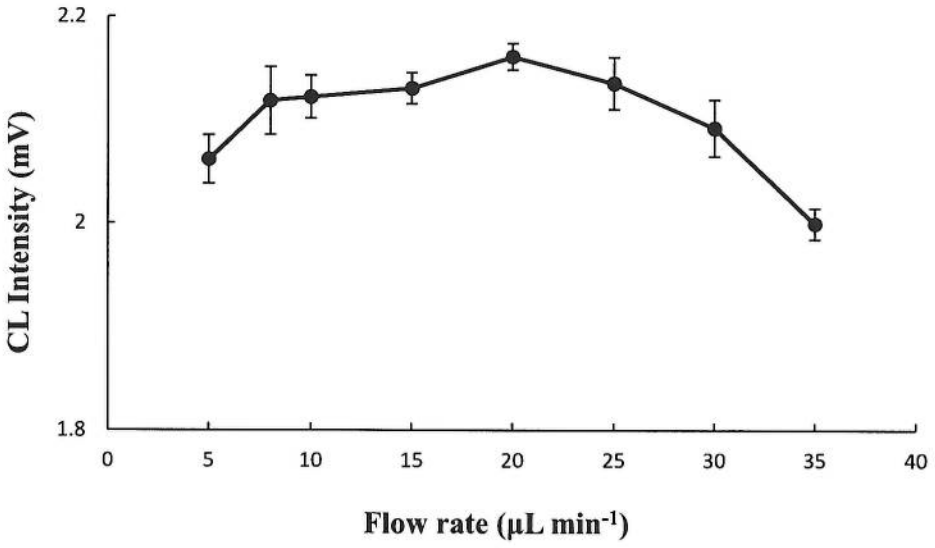

Figure 5-3: Effect of flow rate on the chemiluminescence reaction signal where the concentration of luminol was fixed at 20 mM, the concentration of H_2O_2 was fixed at 20 mM, and the pH was 10.5. Error bars: one standard deviation (n=5).

The luminol reaction is fast therefore indicating a higher flow rate is necessary. It can be seen from the above figure that the increasing amount of chemiluminescence intensity reached the highest value of 2.16 mV when the flow rate was 20 μL min^{-1}. Therefore it can be observed that the CL intensity drops at even higher flow rates. This is probably related to the light emitted before reaching the optimum position directly under the PMT. Thus the flow rate of 20 μL min^{-1} was selected as the flow rate for further experiments.

5.2 Study of different oxidants

It is essential in any analysis that the target analyte is determined under the best conditions. If this does not occur, it can result in unnecessarily low measurement precision and decreased sensitivity. High reagent concentrations can increase the chemiluminescence, but can also cause an increase in the background emission.

With regard to this, a series of experiments was performed to investigate the effect of different oxidants on the CL intensity for eserine using the flow manifold reported previously in Section 5.1. The following four oxidants – potassium permanganate ($KMnO_4$), hydrogen peroxide (H_2O_2), cerium (IV) sulphate ($Ce(SO_4)_2$), and cerium (IV) ammonium sulphate ($Ce(NH_4)_4(SO_4)_4 \cdot 2H_2O$) were studied. Luminol was used as a chemiluminescence reagent with potassium permanganate and hydrogen peroxide in an alkaline medium. Nitric and sulphuric acid were used as the oxidation medium for cerium (IV) sulphate, whereas nitric was used for cerium (IV) ammonium sulphate.

5.2.1 Effect of potassium permanganate

Potassium permanganate was employed as an oxidant in the CL luminol reaction. The influence of the potassium permanganate concentration on the CL intensity was evaluated ranging from 0.1 to 1 mM, with three replicates. The concentration of luminol, the flow rate, and the pH were 20 mM, 20 µL min-1, and 10.5, respectively. The effects of potassium permanganate concentration on CL signal are shown in Figure 5-4.

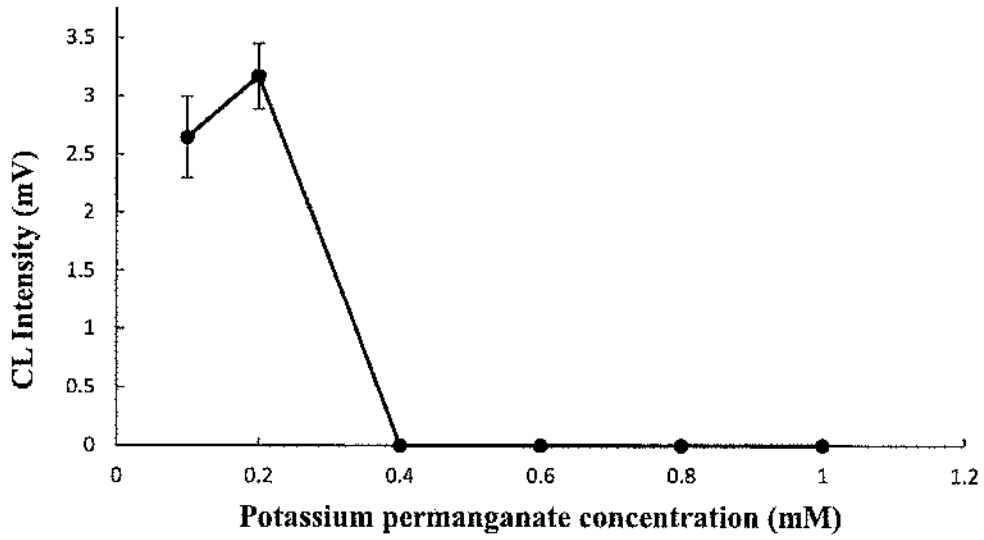

Figure 5-4: Effect of potassium permanganate concentration on the CL intensity where the concentration of luminol was fixed at 20 mM, the flow rate was 20 µL min^{-1}, and the pH was 10.5. Error bars: one standard deviation (n=5).

The results from experiments demonstrate that the two lowest potassium permanganate concentrations (0.1 and 0.2 mM) showed an increase in the CL intensity from 2.64 ± (0.35) to 3.17 ± (0.28) mV. However, when the concentration of $KMnO_4$ was higher than 0.2 mM, no CL signal and blockages in the narrow microfluidic channel were observed. This is probably due to the formation of insoluble MnO_2 in the microchannel.[280] Microscope images of the blocked microfluidic at different magnifications are shown in Figure 5-5.

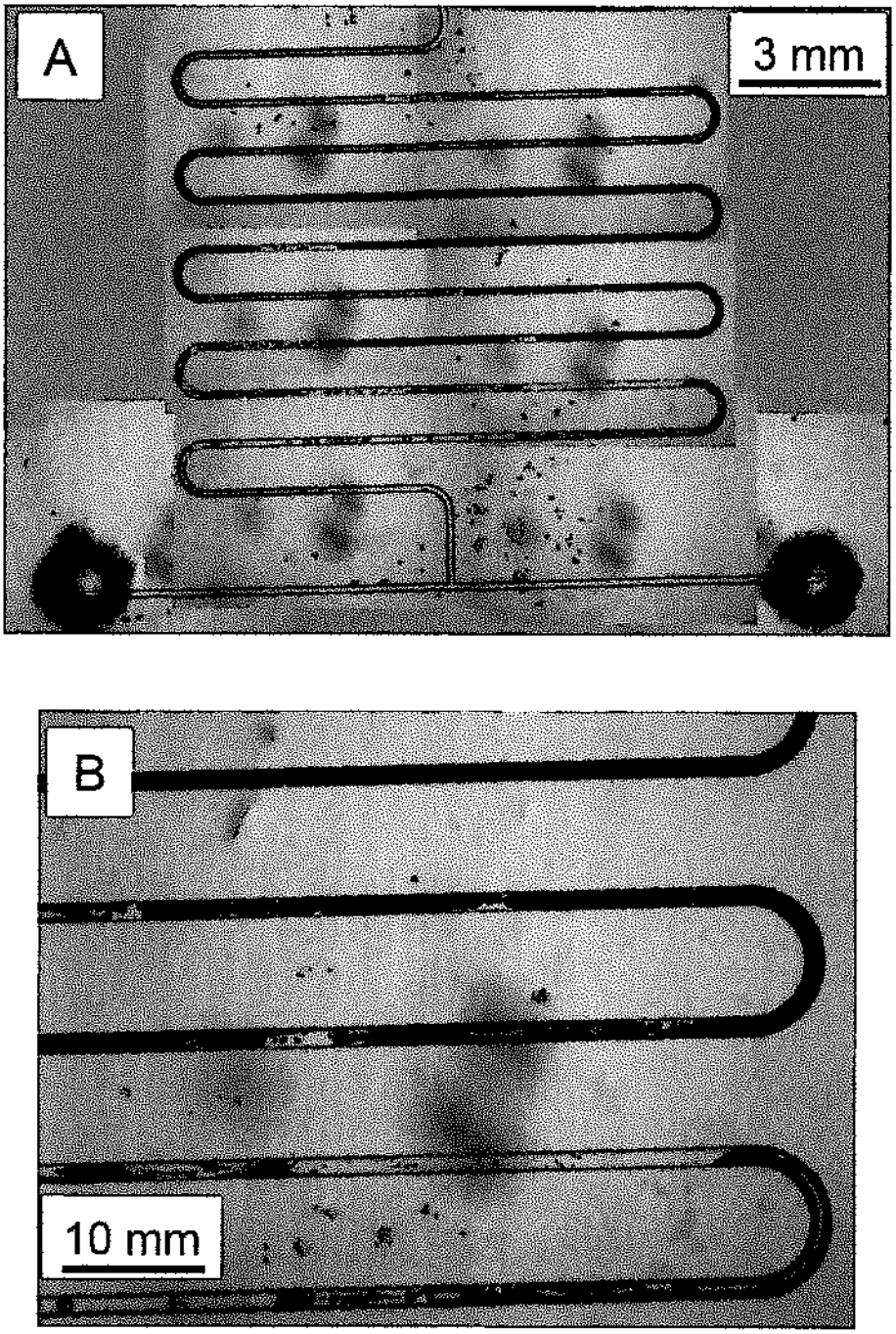

Figure 5-5: Microscope images of the blocked microfluidic channel with $KMnO_4$. (A) magnification at 3mm and (B) magnification at 10mm

5.2.2 Effect of concentrations of hydrogen peroxide

The effect of hydrogen peroxide concentration on the chemiluminescence signal was investigated over the range 1 to 50 mM, with three replicates. The luminol concentration was held constant at 20 mM with a flow rate of 20 μL min^{-1}. The results of the effect of hydrogen peroxide concentration on the CL signal are shown in Figure 5-6.

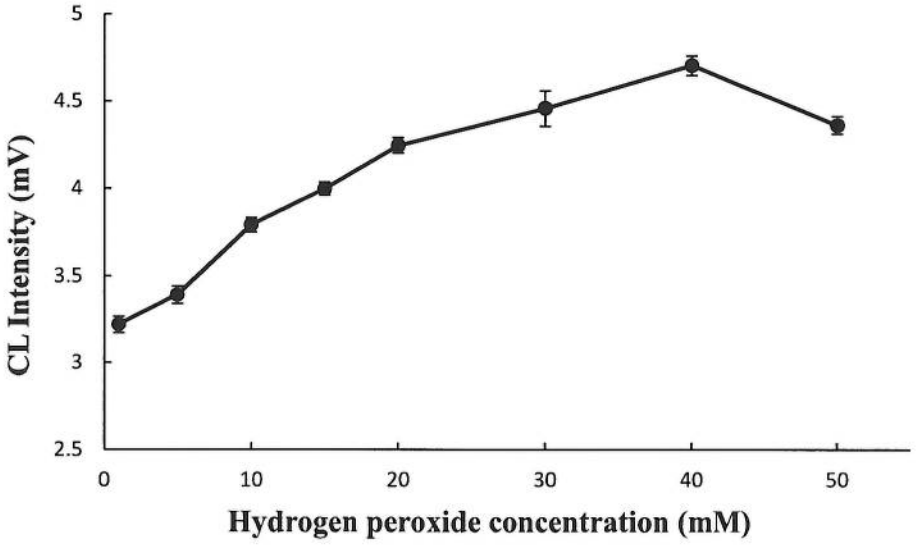

Figure 5-6: Effect of the hydrogen peroxide concentration on the CL emission where the concentration of luminol was at 20 mM, the flow rate was 20 μL min-1, and the pH was 10.5. Error bars: one standard deviation (n=5).

As can be seen from the graph, the CL intensity increased slightly by increasing the concentration of hydrogen peroxide from 1 to 40 mM; above the concentration of 40 mM, the CL signal decreased. The values of intensity were 3.2–4.7 mV. Therefore,

for the experiments, the concentration of hydrogen peroxide was maintained at the optimal value of 40 mM and gave a CL intensity of 4.7 mV.

5.2.3 Effect of cerium (IV) sulphate

Cerium (IV) sulphate is not readily soluble in water, but is stable in dilute acid. Nitric acid (HNO_3) and sulphuric acid (H_2SO_4) were used to dilute cerium (IV) sulphate. The effect of Ce(IV) concentration on the CL response of eserine was examined in the range of 1 to 50 mM, with three replicates. The concentrations of eserine and acids were 10 ppm and 1 M, respectively. The results of the effect of Ce(IV) concentration on the CL intensity are shown in Figure 5-7.

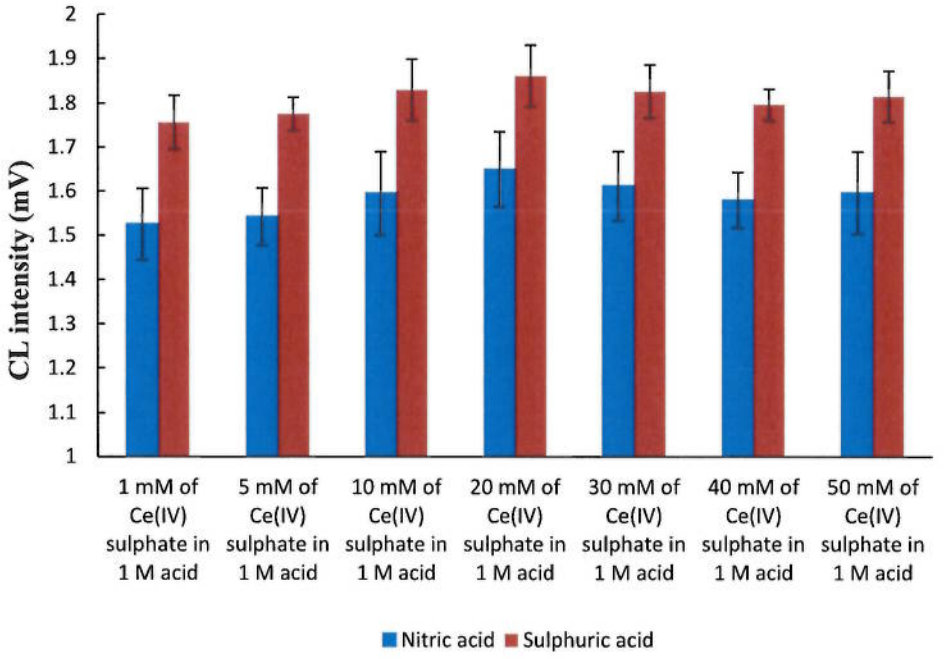

Figure 5-7: Effect of cerium (IV) sulphate concentration on the CL intensity, where the concentration of eserine was 10 ppm and the concentrations of HNO_3 and H_2SO_4 were 1 M. Error bars: one standard deviation (n=5).

From the figure, there are small changes in the CL emission signal with an increasing concentration of Ce(IV). The intensity range was 1.52–1.86 mV. The highest chemiluminescence intensity was 1.86 ± (0.28) mV when the concentration of Ce(IV) was at 20 mM, prepared in H_2SO_4. Therefore, sulphuric acid is shown to be a better reagent medium compared to nitric acid.

5.2.4 Effect of Cerium(IV) ammonium sulphate

The effect of cerium(IV) ammonium sulphate concentration on the CL response of eserine was examined in the range of 1–50 mM, with three replicates. Here, rhodamine 6G was used as a sensitiser to enhance the CL emission that resulted from the chemical reaction of Ce(IV) with a carbamate pesticide.[253] Two different concentrations of rhodamine 6G (0.5 and 1 mM) were used in this experiment. The concentration of eserine was kept constant at 10 ppm. The effect of cerium(IV) ammonium sulphate concentration on the CL intensity are shown in Figure 5-8.

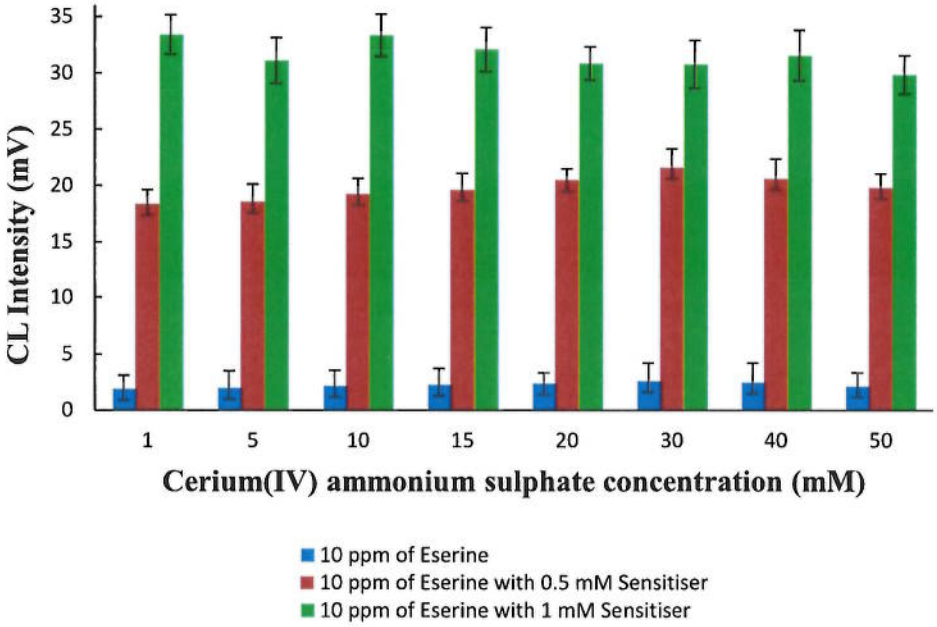

Figure 5-8: The effect of cerium (IV) ammonium sulphate concentration on the CL intensity where the concentration of eserine was 10 ppm. Error bars: one standard deviation (n=5).

From the figure, it was found that the chemical reaction between the different concentrations of the oxidant Ce(IV) (1–50 mM) and eserine gives a CL intensity in the range of 1.86–2.58 mV. The maximum CL signal was 2.58 observed with 30 mM of Ce(IV) at 2.58 mV.

When 0.5 mM of rhodamine 6G was used with eserine, the chemical reaction obtained a CL intensity in the range of 18.35–21.62 mV. These intensity values are more than 70% compared to the intensity without a sensitiser. Again, 30 mM of Ce(IV) achieved the highest intensity value at 21.62 mV among the range of concentrations.

The result of experiments with 1 mM rhodamine 6G of demonstrates that the intensity increased compared to the result that was obtained with 0.5 mM of rhodamine 6G.

However, the maximum emission intensity (33.4 mV) was found at the lowest concentration of oxidant (1 mM). This result is a contrast to the results that were obtained from the chemical reaction without a sensitiser and with 0.5 mM rhodamine 6G. Therefore, a 30 mM of Ce(IV) with 0.5 mM of sensitiser were selected for further experiments.

5.2.5 Selection of the oxidant

To select the oxidant system that will provide the maximum CL intensity in the reaction with eserine, four strong oxidants with different concentrations and oxidation media were examined as described in previous sections.

By comparing the results of the four oxidants, it was found that potassium permanganate produced a blockage problem in the microfluidic and it was excluded as an oxidant. The oxidation system cerium(IV) ammonium sulphate in 1 M acid, either nitric or sulphuric, obtained a very low CL intensity in all examined oxidant concentrations. Cerium (IV) ammonium sulphate and hydrogen peroxide provided high CL emission signals, the CL signal obtained by Ce(IV) being 4.6 times higher. Hence, 30 mM of Ce(IV) and 40 mM of H_2O_2 were both selected for subsequent experiments.

5.3 Effect of the concentrations of luminol

As the CL reagent, the concentration of luminol was an essential factor which affected the CL intensity. The effect of the concentration of luminol on the chemiluminescence signal was investigated in the range of 1–50 mM, with three replicates. The optimum pH at 10.5 was used, again the optimum hydrogen peroxide concentration was 40 mM with a flow rate of 20 μL min^{-1}. The influence of the luminol concentration on the chemiluminescence emission is illustrated in Figure 5-9.

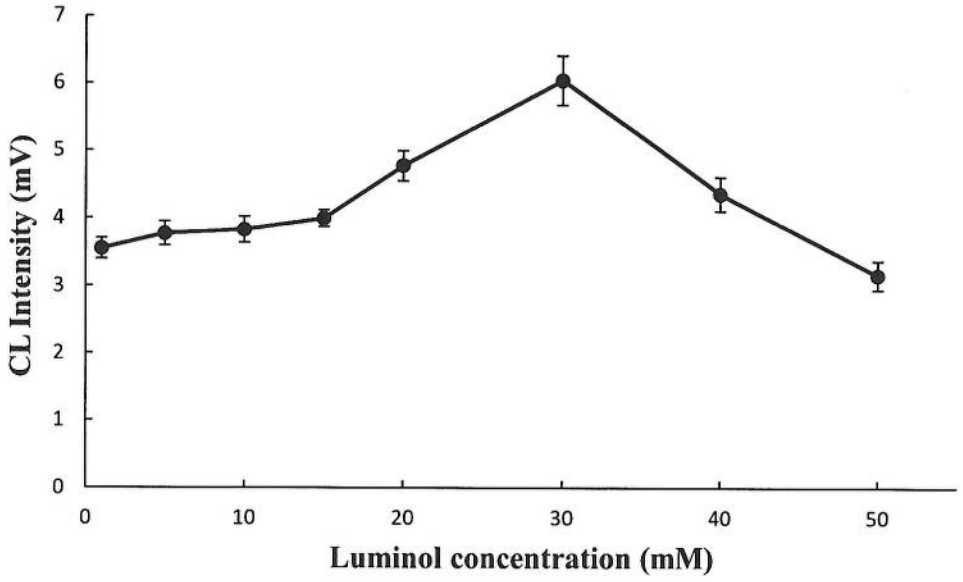

Figure 5-9: Effect of the concentration of luminol on the CL emission where the pH was fixed at 10.5 and the concentration of hydrogen peroxide was 40 mM. Error bars: one standard deviation (n=5).

As can be seen from the figure, the CL intensity increased with the increase in the concentration of luminol and reached a maximum intensity of 6.04 mV at 30 mM and then followed a decline. Numerous studies proposed that the CL emission signal improved linearly with a rise in the concentration of luminol, which attains its highest

intensity at a certain concentration.[281-283] Above this certain concentration, the CL signal decreased. Luminol is a highly sensitive molecule and any variations in the solution can significantly influence the performance of CL analysis. Therefore, a concentration of 30 mM luminol solution provided the highest CL intensity and it was employed in the following experiments.

5.4 Enhancement of the chemiluminescence signal

To improve the CL intensity and the sensitivity, the influence of a reflective surface applied above the microfluidic device was studied. It was important that the surface provided a reproducible response. Foil and black tape were chosen as the reflective surface in this investigation. The results of the influence of reflective surfaces on CL response is illustrated in Figure 5-10.

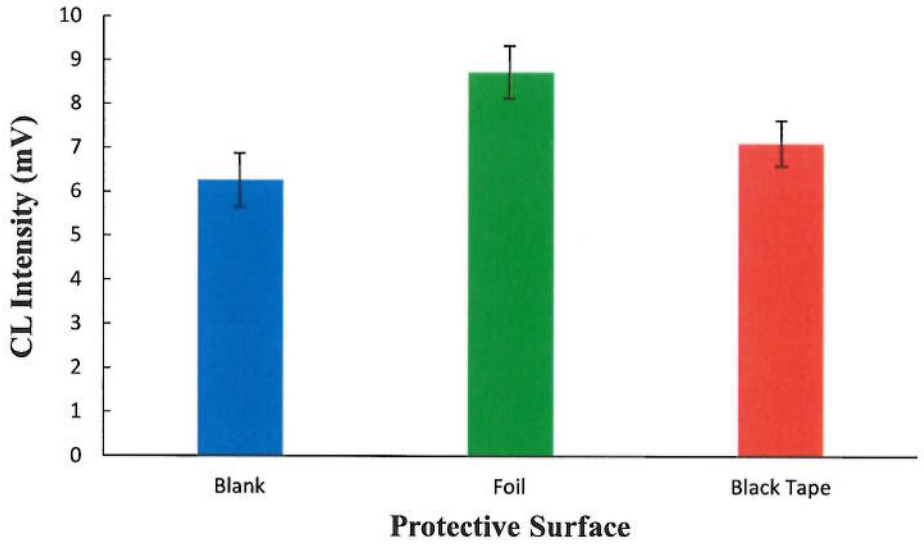

Figure 5-10: The influence of protective surfaces above the microfluidic device on the CL response where the concentrations of luminol and hydrogen peroxide were 30 mM and 40 mM, respectively. Error bars: one standard deviation (n=5).

From the bar charts in the Figure 5-10, it was observed that the CL signal that resulted from the chemical reaction was enhanced when foil was placed on top of the chip. This surface improved the intensity to 8.72 ± (0.6) mV and was selected as the optimum option.

5.5 Effect of the methanol percentage

In the extraction process, the analyte of interest (eserine) was eluted from the C18 silica monolithic sorbent with methanol/water (60:40) (V/V), as described in Section 2.5.4. Pulgarin *et al.* found that there was a reduction in the CL intensity as the ethanol contact increased when they determined carbaryl pesticides.[253]

As a result of that, the effect of the methanol percentage was investigated in the range of 5% to 60% methanol/water. The two best oxidants, 30 mM of Ce(IV) ammonium sulphate and 40 mM of hydrogen peroxide, were used for studying the influence of methanol on the CL signal. A 10 ppm solution of eserine was prepared in the selected methanol percentage ranges. The influence of the methanol percentage in eserine solution with Ce(IV) on the CL signal is illustrated in Figure 5-11.

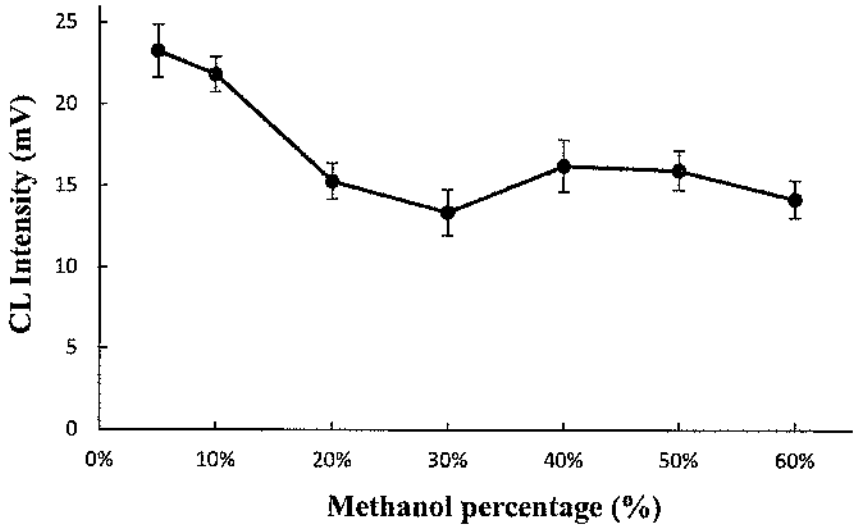

Figure 5-11: The effect of MeOH percentage in eserine solution with Ce(IV) on the CL signal where the concentrations of eserine, Ce(IV), and rhodamine 6G were 10 ppm, 30 mM, and 0.5 mM, respectively. Error bars: one standard deviation (n=5).

It can be seen from the graph that the CL signal decreased when the percentage of alcohol increased. The required percentage for the extraction (60%) showed the second lowest CL intensity among the range of percentages. Data from this figure can be compared with the data in Figure 5-8 which shows the optimum highest intensity at 21.62 mV is greater than the CL intensity that was observed in the percentage methanol range from 20% to 60%. However, the findings of these experiments show that the efficiency of the chemical reaction is impacted by methanol in the presence of the oxidation system Ce(IV). Therefore, Ce(IV) was ruled out as oxidant in further investigation.

The influence of the methanol percentage was investigated again, in the range of 5% to 60% MeOH/H_2O, in the presence of the oxidant hydrogen peroxide. The

concentration of H_2O_2, luminol, and eserine were kept constant at 40 mM, 30 mM, and 10 ppm, respectively. The effect of changing the methanol percentage in eserine solution with luminol-H_2O_2 on the CL signal is illustrated in Figure 5-12.

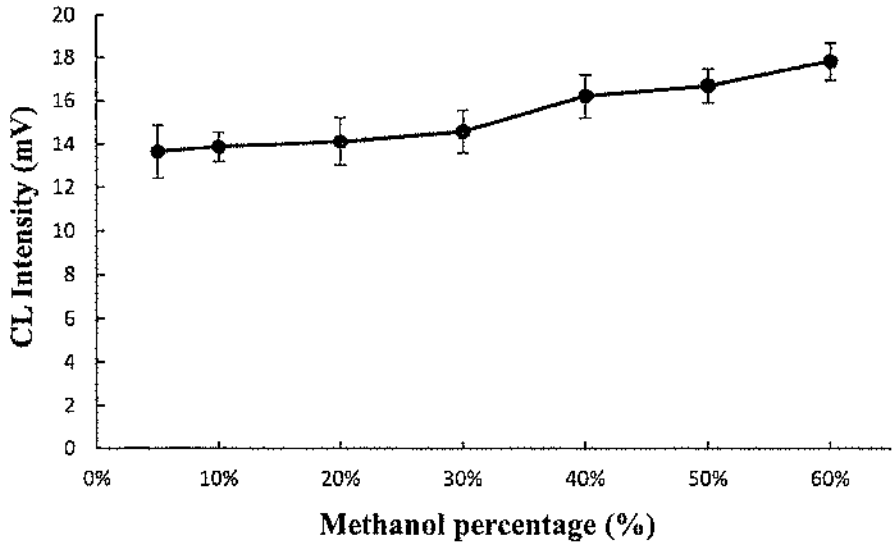

Figure 5-12: The effect of MeOH percentage in eserine solution with luminol-H_2O_2 on the CL signal where the concentrations of eserine, luminol, and H_2O_2 were 10 ppm, 30 mM, and 40 mM, respectively. Error bars: one standard deviation (n=5).

This result clearly demonstrates the effect of the MeOH percentage on the CL emission signal. Increasing the alcohol percentage in the eserine solution leads to improvement in the CL intensity. In addition, 60% of MeOH provided the maximum intensity and indicated very promising results for subsequent experiments.

To obtain a background reference for the CL reaction, a further experiment was conducted. All the previous optimum parameters required for the luminol-H_2O_2 chemiluminescence reaction were involved in this investigation. Here, 40 mM of the oxidant H_2O_2 was prepared in the elution solvent, MeOH/H_2O (60:40) (V/V), where

the concentration of luminol was kept at 30 mM. The result of the background reference experiment is shown in Table 5-1.

Table 5-1: The result of the background reference experiment. One standard deviation (n=5).

CL intensity (mV)	SD (±)	RSD (%)
21.081	0.318	1.51

The working parameters found for the constituents of the luminol reaction for the determination of eserine are summarised in Table 5-2.

Table 5-2: A summary of the optimum values of all the CL parameters studied within a microfluidic device for the determination of eserine

Variable	Studied range	Optimum value
pH	8.5–12	10.5
Flow rate ($\mu L\ min^{-1}$)	5–35	20
Hydrogen peroxide concentration (mM)	1–50	40
Luminol concentration (mM)	1–50	30
Methanol percentage (%)	5–60	60
Reflective surface	Blank, foil, and black tape	Foil

5.6 Analysis of eserine sample using chemiluminescence

5.6.1 Calibration curve

Under the optimum experimental conditions summarised in Table 5-2, the linearity of CL intensity was established from nine concentrations over the range 1×10^{-4} to 1×10^{4} μg L^{-1} for eserine, using the microfluidic device. The reagents and standards were continuously introduced into the microfluidic device and the response continuously measured over two minute intervals, with an average of 5 readings taken during this time. A linear calibration curve was obtained by plotting the chemiluminescence intensity versus eserine concentration: $y = (a \pm s_a) + (b \pm s_b) \cdot C$, where y is the chemiluminescence signal (mV) and C is the eserine concentration (μg L^{-1}), as presented in Figure 5-13.[284]

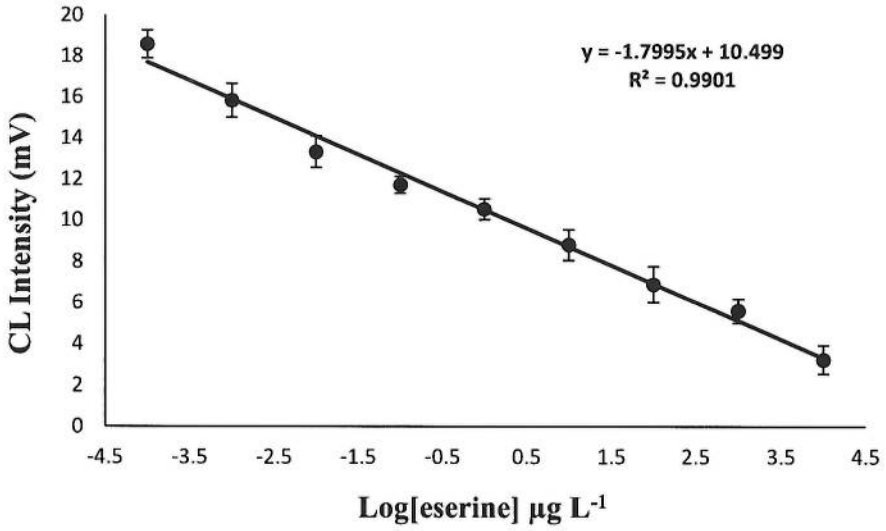

Figure 5-13: Calibration curve showing how the CL intensity changes with the increase in concentration of eserine. Error bars: one standard deviation (n=5).

As can be seen from Figure 5-13, there has been a gradual reduction in the CL intensity as the eserine concentration increases. This result can be explained by the fact that some pesticides, especially carbamate, can act as both inhibitors of the CL emission and as substances that are easily oxidised and act as interferents in the luminol reaction, being indirectly determined by calculating the reduction resulted in the CL emission, as discussed in the literature in Section 1.8.6.1. The calibration curve was obtained again by plotting the change/difference of chemiluminescence intensities (Δ CL_I) against the concentration of eserine concentration, as illustrated in Figure 5-14. Where Δ CL_I the change/difference between the background intensity (Table 5-1) and the analyte intensity.

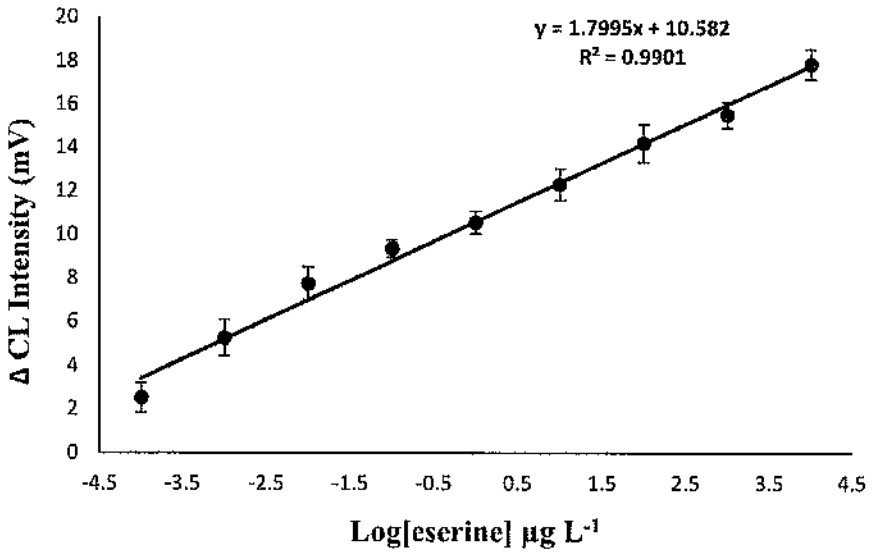

Figure 5-14: Calibrations for the determination of eserine using the luminol-H_2O_2 chemiluminescence reaction. Error bars: one standard deviation (n=5).

It can be observed that the calibration curve for the target analytes in the range 10^{-4} to 10^{4} µg L^{-1} showed a good coefficient of determination (R^2=0.9901). The LOD (3SD/S)

and LOQ (10SD/S) for eserine were calculated using Equation 2-2 and Equation 2-3 (in Section 2.5.3), respectively. The precision performance of the method was investigated in terms of repeatability (intra-day) and reproducibility (inter-day) at different concentration levels of eserine such as 1 μg L^{-1}, 10 μg L^{-1}, and 100 μg L^{-1}. For repeatability studies, the standards of eserine were prepared and measured for five replicates on the same day. The same process was repeated in five replicates on different days for reproducibility studies. The calibration date of CL intensity versus the concentrations of eserine is summarised in Table 5-3.

Table 5-3: Analytical figures of merit for eserine determination by CL. (n=5)

Regression equation	$Ic_L = 1.7995\ C + 10.582$
Correlation coefficient (r)	0.9950
Linear dynamic range (μg L^{-1})	1×10^{-4} - 1×10^{4}
LOD (μg L^{-1})	0.057
LOQ (μg L^{-1})	0.466
Repeatability (Eserine concentration, % RSD)	1 μg L^{-1}, 2.6% 10 μg L^{-1}, 1.8% 100 μg L^{-1}, 5.8%
Reproducibility (Eserine concentration, % RSD)	1 μg L^{-1}, 4.5% 10 μg L^{-1}, 6.2% 100 μg L^{-1}, 8.4%

From Table 5-3 it was found that the proposed method obtained LOD up to 0.057 μg L^{-1} and a LOQ of 0.466 μg L^{-1} of eserine. The LOD obtained for this method is below

the EU maximum residue limits (MRLs) of individual carbamate pesticides in drinking water 0.1 μg L^{-1}.[25]

The equation obtained for the calibration curve was:

$$Ic_L = 1.7995\ C + 10.582$$

Where, Ic_L is the chemiluminescence intensity (mV)

C is the concentration of eserine (μg L^{-1})

This equation can be utilised for the quantitative determination of eserine in real samples. Therefore, the sensitivity of the method (defined as slope of calibration graph) was found to be 1.8% per 1 μg L^{-1}. The relative standard deviation (RSD) was always below 10% over the range studied.

5.6.2 Comparison with other studies

To the researcher's knowledge, no one has described the microfluidic-CL method for the determination of carbamate pesticides in the literature. The comparison of the LOD between the proposed method with the previously cited published studies found in the literature, based on carbamate pesticide determination by chemiluminescence, is presented in Table 5-4. Some methods provide higher sensitivity and/or lower LOD values than those achieved by the traditional FIA-CL method.

Table 5-4: Analytical performance of FIA-CL applied to the determination of carbamates in water samples

Carbamates	LOD	Flow rate ($mL\ min^{-1}$)	Pesticide (mL)	DR	Comments	Ref.
Carbaryl	28.7 $ng\ mL^{-1}$	6.3	2	50–2000 $ng\ mL^{-1}$	Carbaryl-Ce(IV)-rhodamine 6G system	253
Carbaryl	47.7 $\mu g\ L^{-1}$	1.5	0.6	100–4024 $\mu g\ L^{-1}$	Luminol-H2O2-Co(II)	257
Carbaryl	4.9 $ng\ mL^{-1}$	3–5	0.7	5–100 $ng\ mL^{-1}$	Carbaryl-luminol-KMnO4-OH− system	254
Carbofuran	0.02 $\mu g\ mL$	4	0.5	0.06–0.5 $\mu g\ mL^{-1}$	KMnO4-luminol-NaOH	255
Pirimicarb	0.12 $\mu g\ L^{-1}$	1	0.35	4.25-30.75 $\mu g\ L^{-1}$	Luminol-H2O2-HRP	258
Propoxur	5 $ng\ L^{-1}$	1.2–1.4	2.35	0.05–5 $\mu g\ mL^{-1}$	MA-$Ru(bpy)^{3}{}_{3}$ system	285

Although some reported articles gave greater sensitivity and/or lower LOD than that obtained by the proposed method, they used large amounts of sample and reagent. The benefits of the proposed μFIA system over the traditional flow are minimum waste production, minimum sample and reagent consumption, and small size of the instrument.

In contrast to previous reports found in the literature on conventional FIA for carbamate pesticide determination based on the same substrate [257], the optimum reagent flow rate of this method is 20 μL min^{-1} whereas that of the conventional FIA system is 1.5 mL min^{-1} indicating that by using the microfluidic device, the reagent consumption can be reduced 75 times.

Regarding the substrate and pesticide consumption used in both systems, it is clear that the proposed system requires 300 μL of substrate and 300 μL of pesticide (in 15 mins for ten runs) while the traditional system uses more 5 mL of substrate injection volume and 2 mL of pesticide (for one run). This implies that the traditional FI system consumes larger substrate and pesticide volumes than those consumed by the μFIA system.

From these results, it was clearly demonstrated that the proposed method provided a cleaner analytical method with minimal use of sample and chemical reagent as well as reduced waste generation, which could be considered to be more environmentally friendly.

5.6.3 Eserine determination in real samples

In order to illustrate the usefulness of the proposed microfluidic-CL method for the analysis of eserine for real samples, recovery experiments were carried out on different types of water. The samples were treated and prepared as described in Section 2.7.3. Different water samples (UHP, tap, and river water) were spiked at four different levels (1, 10, 100 and 200 μg L^{-1}) of eserine. The SPE procedure with the C18 modified silica monolith was applied to each water sample before the microfluidic-CL analysis. The result of the CL intensity of different eserine samples is shown in Figure 5-15.

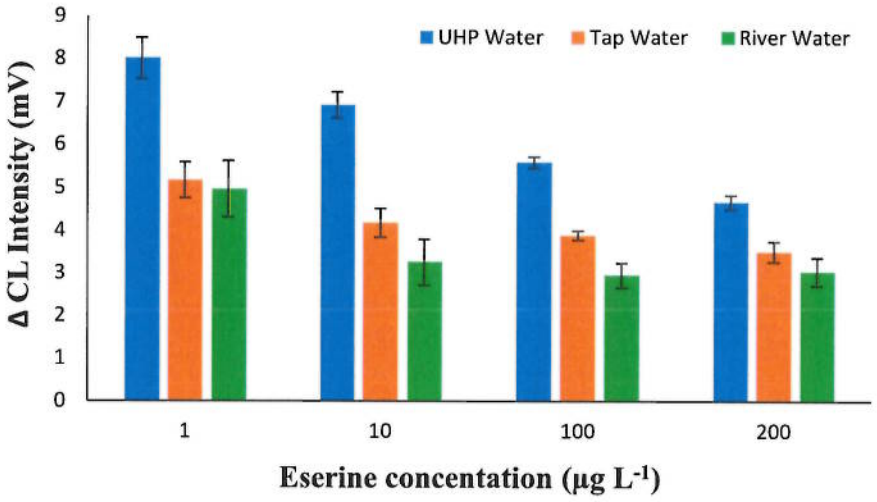

Figure 5-15: The CL intensity of different concentration of eserine samples (n=5)

From the bar charts in Figure 5-15, it is clearly showed that a gradual decrease in the difference in chemiluminescence intensities (Δ CL_I) as the concentration of eserine increases in real samples, this is as explained by the fact that carbamate can act as both inhibitors of the CL emission and interferent in the luminol reaction with H_2O_2. [254, 255]

Here, eserine has a negative effect on CL resulting in a depression in the CL signal, as discussed in Section 1.8.6.1.

In addition, the UHP water shows better CL intensity in the range 30–50% compared to tap and river water. There is a clear trend of decreasing the CL intensity as the concentration of eserine increases in UHP water. The CL intensity for 1, 10, 100, and 200 μg L^{-1} of eserine in UHP water were 8, 6.92, 5.58, and 4.67 mV, respectively. Whereas in tap water the trend is still present but less clear and the CL intensity for 1, 10, 100, and 200 μg L^{-1} of eserine were 5.17, 4.18, 3.98, and 3.5 mV, respectively. In the case of river water the CL intensity for 1, 10, 100, and 200 μg L^{-1} of eserine were 4.96, 3.25, 2.98, and 3 mV, respectively, and the trend is even less clear.

The data for eserine determination in water samples is shown in Table 5-5.

Table 5-5: Determination of eserine added to different kinds of waters (n=5)

Water sample	Add concentration ($\mu g\ L^{-1}$)	Found concentration ($\mu g\ L^{-1}$)[a]	Recovery (%)
Ultra-high purity (UHP) water	1	1.15 ± 0.07	115 ± 6
	10	12.5 ± 0.55	125.7 ± 4.4
	100	114.1 ± 2.9	114.1 ± 2.5
	200	196.6 ± 7	98.2 ± 3.6
		Average recovery 113.25 ± 4	
Tap water (TW)	1	0.7 ± 0.06	70.6± 8.5
	10	7.1 ± 0.62	71.5 ± 8.7
	100	74.3 ± 2.45	74.3 ± 3.2
	200	137.2 ± 10.3	68.6 ± 7.5
		Average recovery 71.25 ± 7	
River water (RW)	1	0.67 ± 0.09	67.6 ± 14
	10	5.46 ± 1.03	54.6 ± 18
	100	55.1 ± 6.2	55.1 ± 11
	200	117.2 ± 14.6	58.6 ± 12
		Average recovery 59 ± 13.75	

[a] Mean of five determinations ± ST

As can be seen from the table, the recovery for 1, 10, 100, and 200 $\mu g\ L^{-1}$ of UHP water were 115%, 125.7%, 114.1%, and 98.2%, respectively. Therefore, the average recovery for UHP water was 113.25% with an RSD of 4% (n=5). The recovery for 1, 10, 100, and 200 $\mu g\ L^{-1}$ of tap water were 70.6%, 71.5%, 74.3%, and 68.6%, respectively. Therefore the average recovery of tap water was found to be 71.25% with RSD of 7 %. The main reason for the decreasing recovery of eserine in tap water is

possibly an ionic interference in the luminol reaction, since ionic interferents will be significant in tap water.

In addition, the recovery for 1, 10, 100, and 200 μg L^{-1} of river water were 67.6%, 54.6%, 55.1%, and 58.6%, respectively. The average recovery of river water was found to be 59 % with RSD of 13.75%. These results for the recoveries were satisfactory except for river water, possibly this is due to the result of both ionic and organic compounds which are typically present in river water. They could also provide a potential source of interference on the luminol reaction. River water often contains high amounts of humic acids, which have several functional groups such as phenolic hydroxyl, carboxylic, carbonyl and quinone groups (see Figure 5-16). Humic acid is one of the predominant species occurring in natural waters, which decreases the analytical signal owing to oxidant consumption and/or retardation of the kinetically controlled luminescent oxidation reaction of carbamate pesticides. [251, 286]

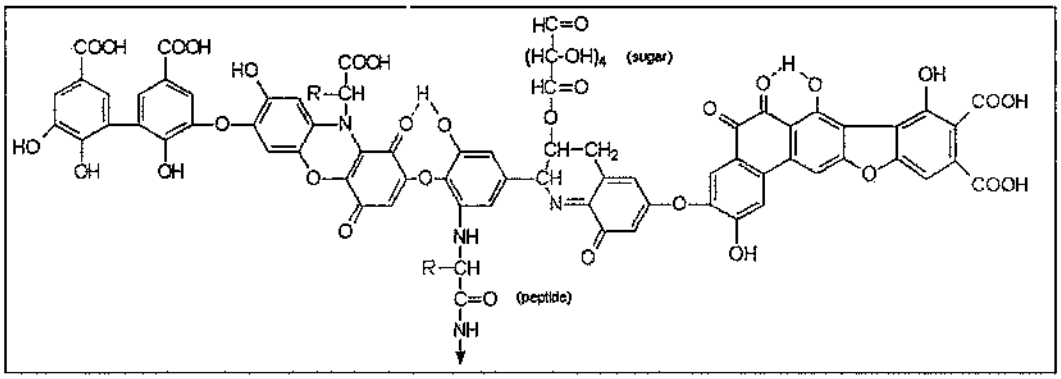

Figure 5-16: Model structure of humic acid [287]

This will need further investigation which was not possible with the timescale of this project. On the other hand, in routine pesticide residue analysis the acceptable range for recovery is usually between 60% and 140%, which shows that the proposed method provides considerable improvement and could be successfully employed for the determination of eserine in drinking water.[254, 255, 288]

5.7 Conclusion

The optimisation of chemiluminescence parameters for the determination of carbamate pesticides was investigated using the microfluidic manifold. Reagents and sample were continuously injected into the microfluidic device which was enclosed within the light-tight housing. The optimum pH and flow rate were at 10.5 and 20 μL min^{-1}, respectively.

The chemical reaction on the chemiluminescence occurs between the CL reagent and an oxidant in the presence of some cofactors. Various choices of oxidants that were used previously with carbamate, according to the literature, were tested with the selected model compound. Potassium permanganate gave blockage problems in the microfluidic, whereas cerium (IV) ammonium sulphate showed a very low CL intensity. Enhancement of the CL signal was investigated by using a protective surface above the chip. The influence of the concentration of luminol and methanol were evaluated in this study.

Under optimal conditions, a calibration curve over nine concentrations of eserine with a detection limit of 0.057 μg L^{-1} was successfully achieved. This detection limit is below the limit established for a single pesticide (0.1 μg L^{-1}) according to the European Directive on the quality of water for human consumption.[25] Comparing this with other CL techniques for the determination of carbamate pesticides, high sensitivity has been provided for a small sample volume.

The applicability of the proposed microfluidic-CL method for the analysis of eserine in real samples was demonstrated with recovery studies using different water samples.

The average recoveries for UHP water, tap water, and river water were 113.25% with an RSD of 4%, 71.25% with an RSD of 7%, and 59% with an RSD of 13.75%, respectively. The proposed method shows good recoveries in compliance with the EU guidelines for routine analysis.[254, 255, 288]

Chapter 6: Conclusions

The determination of carbamates in environmental water becomes an essential analytical demand for drinking water quality and to reduce human exposure. The determination of trace and ultra-trace pesticides in complex matrices is always a challenge to analytical chemists. In response to this challenge, the current work focused on the development of a novel analytical device capable of monitoring and detecting eserine in environmental water with a high sensitively CL technique. This approach could provide the benefits of miniaturisation for sample preparation and measurement.

In this chapter, the research work is divided into the following four sections:

1) Fabrication of silica-based monolithic columns by using sol-gel process

2) Extraction and pre-concentration of carbamate pesticide (eserine) from environmental water samples using the C18 silica-based monolith

3) Combination of the microfluidic methodology with chemiluminescence to measure and ultra-trace the eserine in small volumes of real water samples

4) The major outcomes and achievements of this research will be summarised.

6.1 Fabrication of silica-based monolithic columns

In the last years, the number of applications of monolithic materials, such as SPE sorbent, has increased and become a high-interest research area, especially for the extraction of small molecules such as pesticides. Silica-based monolithic rods were fabricated using the sol-gel formation process. Six different types of silica-based monoliths were prepared in order to obtain the highest specific surface area. Many applications require a large surface area owing to achieve a high loading capacity. All the silica monolith specimens exhibited a bimodal porous structure containing macropores and mesopores.

The basic treatment with ammonia solution led to an increase in the surface area of the silica-based monolith by converting micropores to mesopores. The influence of the basic treatment time (5, 10, 15, and 20 hours) on the internal structure of the silica-based monolith was evaluated. This study has demonstrated that increasing the period of the basic treatment resulted in a gradual increase in the surface area. The conclusion can be drawn from the present study that the optimal period for the basic treatment was 20–24 hours.

All TMOS monoliths showed a higher surface area compared to all TEOS monoliths. Therefore, the high molecular weight of PEO (Mon 2) obtained a surface area of 315.44 $m^2 g^{-1}$ greater than that obtained in the presence of the low molecular weight of the polymer (Mon 1) with the surface area of 289.46 $m^2 g^{-1}$. The highest surface area was obtained from the chemical composition of TMOS, F127, and acetic acid at 366 $m^2 g^{-1}$.

The silica-based monolith has been chemically modified with octadecyl groups, and this process was evaluated by using SEM analysis, BET method, and EDX analysis. A new peak for chlorine (Cl) appeared in the EDX spectra. The carbon peak increased from 2.97% (in the non-modified monolith) to 15.48% (in the modified silica monolith). The result from this study presented a slight decrease in the surface area from 366 to 312 $m^2 g^{-1}$.

6.2 Extraction and pre-concentration of carbamate pesticide (eserine)

The C18-TMOS monolith (RP mode) inside the heat-shrinkable tubes was investigated for its use in achieving SPE for eserine. A sample flow rate of 400 μL min^{-1} was selected. By using a flow rate at 400 μL min^{-1}, all the extraction procedures including conditioning, loading, washing, and elution from the octadecylated silica monolith sorbent could be completed in approximately 10 min.

The efficiency of extraction eserine from the C18 modified silica sorbent was evaluated. The percentage recovery of the target analytes was calculated by comparing chromatographic peak areas for the direct injection of the standard samples with those obtained by the fraction after extraction. The results showed that high extraction recoveries for eserine were achieved by using the C18 silica monolith (96.58%).

The C18 modified monolithic column has the ability to pre-concentrate the target analyte eserine where the concentration increased from 10 to 86 μg mL^{-1}. Therefore, the modified silica monolith showed a good capacity to 17.6 μg mg^{-1} and offered longevity up to two months with more than 200 injections.

6.3 Combination of the microfluidic methodology with chemiluminescence

It is essential in any analysis that the target analyte is determined under the best conditions. If this does not occur, it can result in unnecessarily low measurement precision and can also decrease the sensitivity. The optimisation of chemiluminescence parameters for the determination of carbamate pesticides was investigated using the microfluidic manifold. The optimum pH was 10.5 over the range (8–12.5), whereas the optimum flow rate was 20 μL min^{-1} over the range (5-35 μL min^{-1}).

Several oxidants that were used previously with carbamate, according to the literature, were tested with eserine in a microfluidic-CL system. Potassium permanganate oxidant gave blockage problems in the microfluidic and cerium (IV) ammonium sulphate showed a very low CL intensity, so both were excluded as oxidants. Cerium (IV) ammonium sulphate and hydrogen peroxide provided high CL emission signals, the CL signal obtained by Ce(IV) being 4.6 times higher. Therefore, 30 mM of Ce(IV) and 40 mM of H_2O_2 were both selected for subsequent experiment for investigating the effect of the methanol percentage in the CL intensity. The optimum concentration of luminol was 30 mM over the range (1–50 mM).

Under the optimal conditions, a linear relationship between CL intensity and the eserine concentration was obtained over the concentration range 1×10^{-4} to 1×10^{4} μg L^{-1} with a good coefficient of determination (R^2=0.9901). The limit of detection (LOD) was 0.057 μg L^{-1} and this is below the legal limits (0.1 μg L^{-1}) established by the European Union for drinking water.[25] The limit of quantification (LOQ) was 0.466 μg L^{-1}. The sensitivity of the method was found to be 1.8% per 1 μg L^{-1}. Intra-day and inter-day coefficients of variation were below 10% over the range studied.

The applicability of the proposed microfluidic-CL method for the analysis of eserine in real samples was demonstrated with recovery studies using different water samples. The average recoveries for UHP water, tap water, and river water were 113.25% with an RSD of 4%, 71.25% with an RSD of 7%, and 59% with an RSD of 13.75%, respectively. The recovery for 1, 10, 100, and 200 μg L^{-1} of tap water were 70.6%, 71.5%, 74.3%, and 68.6%, respectively. The proposed method provides good recoveries in compliance with the EU guidelines for routine analysis.

Chapter 7: Future work

It is suggested that further study should be carried out in optimisation of the selected starting materials of the monolith (TMOS-F127), the temperature of the thermal decomposition step, or ammonia solution concentration in order to further increase the total surface area and produce mesopores with narrow pore size distribution.

In addition, the findings of this research show that although fabrication of the silica-based monolith was a long-term process, which took almost one week and was relatively tedious, it had high porosity, was not affected by organic solvent, and exhibited high surface area.

Moreover, the silica-based monolith offers high permeability, allowing high flow, and lower backpressure; furthermore, the procedure to prepare the silica-based monolith was reproducible. Thus, it would be useful to examine alternative techniques to increase the speed of the fabrication process of the silica-based monolith.

Further work to the SPE system could focus on the extraction of additional members of the carbamate pesticide group, such as carbaryl, carbofuran, and pirimicarb, from environmental water samples by using the C18 silica monolith.

It is suggested that further study could be carried out in microfluidic device by using black tube which support transmission of the pushed liquid inside the channels and also enhance the chemiluminescence signal. Future studies on the current topic would employ experimental design software for the optimisation of the chemiluminescence parameters saving both time and labour.

Further research should be done to investigate the effect of humic acids on the chemiluminescence signal by the process of extraction and using standard addition technique. There is abundant room for further progress in studying the interference of elements with the signal of chemiluminescence. This is an important issue for future research in preparing a multimode solid phase extraction system that would utilise both hydrophobic interactions and ion exchange.

Further work could include a primary off line extraction step, silica monolith disk will be placed in the bottom of luer lock syringe. The fluid would be pulled through the syringe by a vacuum pump. This pump will run long enough to extract sufficient pesticides from approx. 1 L of drinking water sample. The volume of the eluent would be 3 mL this will be taken up in a luer lock syringe for manual injection onto the microfluidic device. The syringe can be removed and replaced by a peristaltic pump after the sample is loaded. The monolith loaded with pesticide from the sample is then washed with 1 mL water, followed by elution with MeOH/H_2O (60:40).

Further work on this miniaturised analysis system could include a silica monolith sorbent inside a glass microchip. This would attempt to integrate pre-concentration and detection steps into a single unified device, such that drinking water could be injected into the inlet for pre-concentration, elution, then mixing with the necessary reagents and detected by CL.

The sample would be passed through (inlet 1) whereas the chemiluminescence reagent luminol and the oxidant hydrogen peroxide were separately passed through the other two channels (inlet 2 and 3). During the loading and washing steps the valve in Position (A) enabling the sample to be passed to outlet 1. Whereas in the elution step the valve in Position (B) to allow eluted pesticides to mix with chemiluminescence

reagent luminol and the oxidant hydrogen peroxide in serpentine channel. The chip design will require careful consideration of channel dimensions to prevent an excessive back pressure and back flushing of sample or regents. The potential design for a primary off line extraction step and an integrated microfluidic device is shown in Figure 7-1.

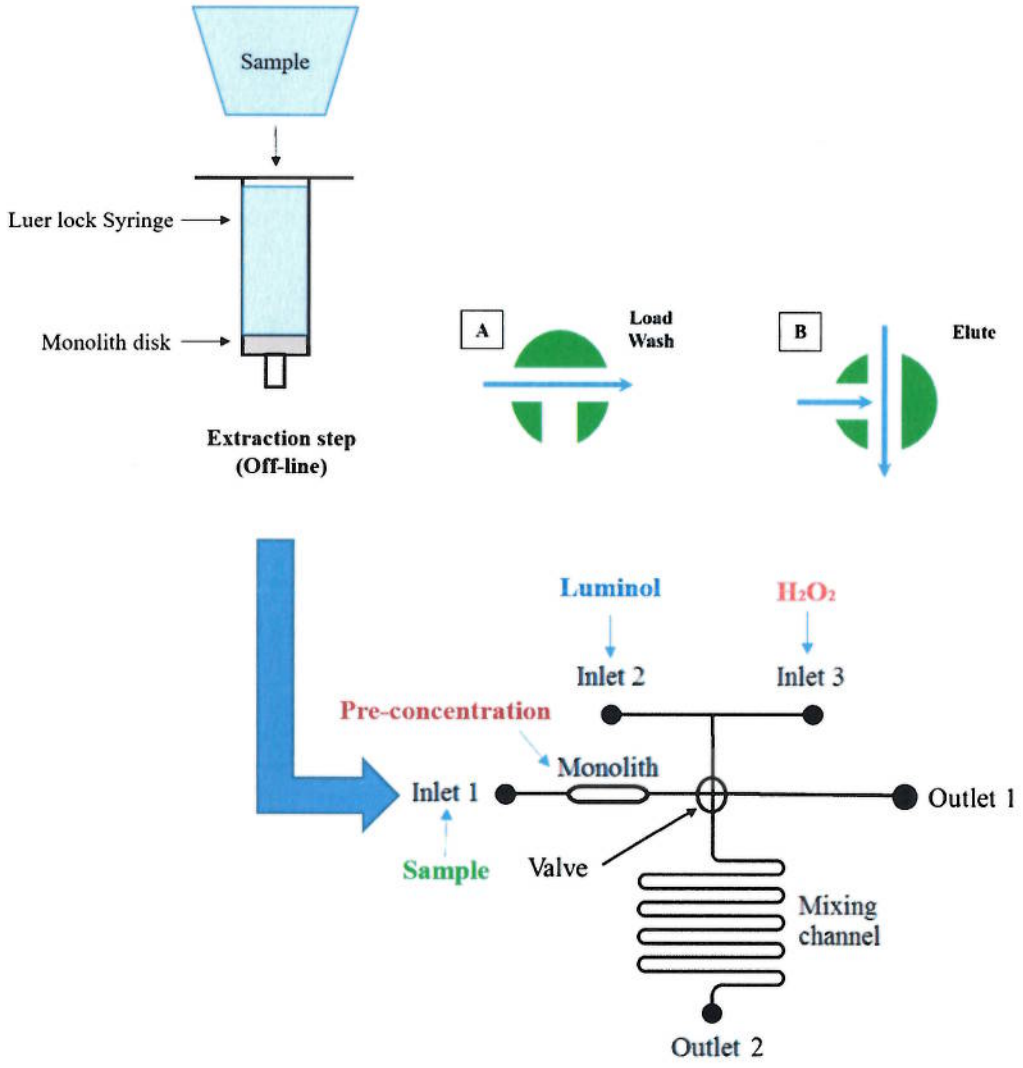

Figure 7-1: Potential designs for a primary off line extraction step and an integrated microfluidic device

Chapter 8: References

1 A. M. Rodrigues, V. Ferreira, V. V. Cardoso, E. Ferreira, and M. J. Benoliel, *Journal of Chromatography A*, 2007, **1150**, 267.

2 L. M. Nollet and H. S. Rathore, 'Handbook of pesticides: methods of pesticide residues analysis', CRC Press, 2009.

3 A. Malik, E. Grohmann, and R. Akhtar, 'Environmental Deterioration and Human Health', Springer Netherlands, 2014.

4 R. Krieger, 'Hayes' handbook of pesticide toxicology', Academic press, 2010.

5 R. Carson, 'Silent spring', Fawcett Crest., 1962.

6 J. L. Tadeo, 'Analysis of pesticides in food and environmental samples', CRC Press, 2008.

7 G. W. Ware and D. M. Whitacre, 'The pesticide book', MeisterPro Information Resources, 2004.

8 F. Group, in 'World Pesticides. World Pesticides Industry Study with Forecasts for 2014 & 2019 Study # 2664', 2010.

9 A. Grube, D. Donaldson, T. Kiely, and L. Wu, *US EPA, Washington, DC*, 2011.

10 D. Pimentel and R. Peshin, 'Integrated Pest Management: Pesticide Problems, Vol. 3', Springer Science & Business Media, 2014.

11 F. Group, in 'World Pesticides Industry Study with Forecasts for 2016 & 2021, Study No.2902, 2012.'.

12 J. Fenik, M. Tankiewicz, and M. Biziuk, *TrAC Trends in Analytical Chemistry*, 2011, **30**, 814.

13 WHO, 'The impact of pesticides on health: Preventing intentional and unintentional deaths from pesticide poisoning', Geneva: WHO, 2004.

14 J. George and Y. Shukla, *Journal of Proteomics*, 2011, **74**, 2713.

15 S. Mostafalou and M. Abdollahi, *Toxicology and Applied Pharmacology*, 2013, **268**, 157.

16 M. F. F. Bernardes, M. Pazin, L. C. Pereira, and D. J. Dorta, in 'Impact of Pesticides on Environmental and Human Health', 2015.

17 M. Gavrilescu, *Engineering in Life Sciences*, 2005, **5**, 497.

18 R. L. Kellogg, R. F. Nehring, A. Grube, D. W. Goss, and S. Plotkin, 'Environmental indicators of pesticide leaching and runoff from farm fields', Springer, 2002.

19 T. Goto, Y. Ito, H. Oka, I. Saito, H. Matsumoto, and H. Nakazawa, *Analytica Chimica Acta*, 2003, **487**, 201.

20 A. F. Hernández, T. Parrón, A. M. Tsatsakis, M. Requena, R. Alarcón, and O. López-Guarnido, *Toxicology*, 2013, **307**, 136.

21 S. Bingham, *Environment Agency, UK*, 2007.

22 C. A. Laetz, D. H. Baldwin, T. K. Collier, V. Hebert, J. D. Stark, and N. L. Scholz, *Environmental Health Perspectives*, 2009, **117**, 348.

23 H. Zeliger, 'Human toxicology of chemical mixtures. Toxic consequences beyond the impact of one-component product and environmental exposures', Amsterdam: Elsevier, 2011.

24 H. Filik and S. D. Çekiç, *Pesticides in the Modern World–Trends in Pesticides Analysis, InTech, Croatia*, 2011, 247.
25 E. D. W. Guideline, *Brussels, November*, 1998.
26 J. L. López-Paz and M. Catalá-Icardo, *Analytical Letters*, 2011, **44**, 146.
27 P. P. Worsfold, A. Townshend, and C. C. Poole, 'Encyclopedia of Analytical Sciences', Academic Press, 2004.
28 R. Carabias - Martínez, C. García - Hermida, E. Rodríguez - Gonzalo, and L. Ruano - Miguel, *Journal of Separation Science*, 2005, **28**, 2130.
29 T. A. Msagati and B. B. Mamba, *Physics and Chemistry of the Earth, Parts A/B/C*, 2012, **50**, 149.
30 J. Vichapong, R. Burakham, S. Srijaranai, and K. Grudpan, *Talanta*, 2011, **84**, 1253.
31 M. Asensio - Ramos, J. Hernández - Borges, G. González - Hernández, and M. Á. Rodríguez - Delgado, *Electrophoresis*, 2012, **33**, 2184.
32 L. Marle and G. M. Greenway, *TrAC Trends in Analytical Chemistry*, 2005, **24**, 795.
33 A. Rios, A. Escarpa, and B. Simonet, 'Miniaturization of analytical systems: principles, designs and applications', John Wiley and Sons, 2009.
34 L. Zhang, S. Liu, X. Cui, C. Pan, A. Zhang, and F. Chen, *Central European Journal of Chemistry*, 2012, **10**, 900.
35 G. H. Tan and M.-K. Chai, 'Sample Preparation in the Analysis of Pesticides Residue in Food by Chromatographic Techniques', INTECH Open Access Publisher, 2011.
36 J. Pawliszyn and H. L. Lord, 'Handbook of sample preparation', Wiley, 2010.
37 S. S. Caldas, A. Demoliner, F. P. Costa, M. G. D'Oca, and E. G. Primel, *Journal of the Brazilian Chemical Society*, 2010, **21**, 642.
38 J. Stocka, M. Tankiewicz, M. Biziuk, and J. Namieśnik, *International Journal of Molecular Sciences*, 2011, **12**, 7785.
39 P. Lucci, D. Pacetti, N. G. Frega, and O. Núñez, 'Current trends in sample treatment techniques for environmental and food analysis', INTECH Open Access Publisher, 2012.
40 H. S. Rathore and L. M. Nollet, 'Pesticides: Evaluation of Environmental Pollution', CRC Press, 2012.
41 P. Patnaik, 'Handbook of environmental analysis: chemical pollutants in air, water, soil, and solid wastes', CRC Press, 2010.
42 L. M. Nollet, 'Chromatographic analysis of the environment', CRC Press, 2005.
43 M. Kuster, M. L. de Alda, and D. Barceló, *Mass Spectrometry Reviews*, 2006, **25**, 900.
44 M. Petrovic, M. Farré, M. L. De Alda, S. Perez, C. Postigo, M. Köck, J. Radjenovic, M. Gros, and D. Barcelo, *Journal of Chromatography A*, 2010, **1217**, 4004.
45 L. Mariño-Repizo, F. Kero, V. Vandell, A. Senior, M. I. Sanz-Ferramola, S. Cerutti, and J. Raba, *Food chemistry*, 2015, **172**, 663.
46 M. J. Gómez, M. Petrović, A. R. Fernández-Alba, and D. Barceló, *Journal of Chromatography A*, 2006, **1114**, 224.
47 M. J. Telepchak, G. Chaney, and T. F. August, 'Forensic and clinical applications of solid phase extraction', Springer, 2004.
48 S. Dahane, M. D. G. García, A. U. Moreno, M. M. Galera, M. d. M. S. Viciana, and A. Derdour, *Microchimica Acta*, 2015, **182**, 95.
49 C. F. Poole, *Trac Trends in Analytical Chemistry*, 2003, **22**, 362.

50 A. Żwir-Ferenc and M. Biziuk, *Polish Journal of Environmental Studies*, 2006, **15**, 677.
51 L. R. Snyder, J. J. Kirkland, and J. W. Dolan, 'Introduction to modern liquid chromatography', John Wiley & Sons, 2011.
52 D. Barceló, *Analyst*, 1991, **116**, 681.
53 J. S. Fritz and M. Macka, *Journal of Chromatography A*, 2000, **902**, 137.
54 N. J. Simpson, 'Solid-phase extraction: principles, techniques, and applications', CRC press, 2000.
55 J. Pawliszyn, 'Sampling and sample preparation for field and laboratory: fundamentals and new directions in sample preparation', Elsevier, 2002.
56 S. Rodriguez-Mozaz, M. J. L. de Alda, and D. Barceló, *Journal of Chromatography A*, 2007, **1152**, 97.
57 F. Rodriguez-Plasencia, F. Navarro-Villoslada, L. Pérez-Arribas, M. Leon-Gonzalez, and L. Polo-Díez, *Journal of Chromatography A*, 1997, **760**, 314.
58 Y.-Y. Zhou, S.-W. Wang, K.-N. Kim, J.-H. Li, and X.-P. Yan, *Talanta*, 2006, **69**, 970.
59 P. Lucci and O. Núñez, *Journal of Separation Science*, 2014, **37**, 2929.
60 R. Sasano, T. Hamada, M. Kurano, and M. Furuno, *Journal of Chromatography A*, 2000, **896**, 41.
61 B. Cavaliere, M. Monteleone, A. Naccarato, G. Sindona, and A. Tagarelli, *Journal of Chromatography A*, 2012, **1257**, 149.
62 N. Ochiai, K. Sasamoto, H. Kanda, and S. Nakamura, *Journal of Chromatography A*, 2006, **1130**, 83.
63 Q. Wu, G. Zhao, C. Feng, C. Wang, and Z. Wang, *Journal of Chromatography A*, 2011, **1218**, 7936.
64 M. Mena, P. Martınez-Ruiz, A. Revicjo, and J. Pingarron, *Analytica Chimica Acta*, 2002, **451**, 297.
65 J. Płotka-Wasylka, N. Szczepańska, M. de la Guardia, and J. Namieśnik, *TrAC Trends in Analytical Chemistry*, 2015, **73**, 19.
66 S. Hansen, S. Pedersen-Bjergaard, and K. Rasmussen, 'Introduction to pharmaceutical chemical analysis', John Wiley & Sons, 2011.
67 E. M. Thurman and M. S. Mills, 'Solid-phase extraction: principles and practice', Wiley New York, 1998.
68 G. D. Christian, 'Analytical chemistry', John Wiley and Sons, 2004.
69 J. R. Dean, 'Extraction methods for environmental analysis', John Wiley Chichester, 1998.
70 C. F. Poole, A. D. Gunatilleka, and R. Sethuraman, *Journal of Chromatography A*, 2000, **885**, 17.
71 S. Mitra, 'Sample preparation techniques in analytical chemistry', John Wiley & Sons, 2004.
72 S. C. Moldoveanu and V. David, 'Modern Sample Preparation for Chromatography', Elsevier, 2014.
73 J. S. Fritz, 'Analytical solid-phase extraction', Wiley-Vch, 1999.
74 V. Berezkin and A. Townshend, *Analytica Chimica Acta*, 1990, **237**, 512.
75 H. Braus, F. Middleton, and G. Walton, *Analytical Chemistry*, 1951, **23**, 1160.
76 E. Abel, F. Pollard, P. Uden, and G. Nickless, *Journal of Chromatography A*, 1966, **22**, 23.
77 J. Riley and D. Taylor, *Analytica Chimica Acta*, 1969, **46**, 307.
78 M.-C. Hennion, *Journal of Chromatography A*, 1999, **856**, 3.

79 M. Leon-Gonzalez and L. Perez-Arribas, *Journal of Chromatography A*, 2000, **902**, 3.
80 D. Allen and Z. El Rassi, *Electrophoresis*, 2003, **24**, 3962.
81 A.-M. Siouffi, *Journal of Chromatography A*, 2003, **1000**, 801.
82 H. Minakuchi, K. Nakanishi, N. Soga, N. Ishizuka, and N. Tanaka, *Journal of Chromatography A*, 1998, **797**, 121.
83 T. Nema, E. Chan, and P. Ho, *Talanta*, 2010, **82**, 488.
84 J. S. Fritz, P. J. Dumont, and L. W. Schmidt, *Journal of Chromatography A*, 1995, **691**, 133.
85 N. Tanaka and H. Kobayashi, *Analytical and Bioanalytical Chemistry*, 2003, **376**, 298.
86 S. Hjerten, J.-L. Liao, and R. Zhang, *Journal of Chromatography A*, 1989, **473**, 273.
87 F. Svec and J. M. Fréchet, *Analytical Chemistry*, 1992, **64**, 820.
88 H. Minakuchi, K. Nakanishi, N. Soga, N. Ishizuka, and N. Tanaka, *Analytical Chemistry*, 1996, **68**, 3498.
89 S. M. Fields, *Analytical Chemistry*, 1996, **68**, 2709.
90 J. F. Kennedy and G. O. Phillips, 'Cellulosics: Materials for Selective Separations and Other Technologies:[International Conference on Selective Purification and Separation Processes: the Role of Cellulosic Materials, Cellucon 92, Held at the North East Wales Institute of Higher Education, Wreham, Wales]', Ellis Horwood, 1993.
91 K. K. Unger, N. Tanaka, and E. Machtejevas, *Wiley-VCH, Weinheim*, 2011, **15**, 16.
92 K. K. Unger, R. Skudas, and M. M. Schulte, *Journal of Chromatography A*, 2008, **1184**, 393.
93 G. Guiochon, *Journal of Chromatography A*, 2007, **1168**, 101.
94 W. Li, D. P. Fries, and A. Malik, *Journal of Chromatography A*, 2004, **1044**, 23.
95 H. Oberacher and C. G. Huber, *TrAC Trends in Analytical Chemistry*, 2002, **21**, 166.
96 M. Jonnada, R. Rathnasekara, and Z. El Rassi, *Electrophoresis*, 2015, **36**, 76.
97 H. Zou, X. Huang, M. Ye, and Q. Luo, *Journal of Chromatography A*, 2002, **954**, 5.
98 A. Kurganov, *Analytica Chimica Acta*, 2013, **775**, 25.
99 S. El Deeb, *Chromatographia*, 2011, **74**, 681.
100 R. Asiaie, X. Huang, D. Farnan, and C. Horvath, *Journal of Chromatography A*, 1998, **806**, 251.
101 T. Adam, K. K. Unger, M. M. Dittmann, and G. P. Rozing, *Journal of Chromatography A*, 2000, **887**, 327.
102 M. T. Dulay, R. P. Kulkarni, and R. N. Zare, *Analytical Chemistry*, 1998, **70**, 5103.
103 Q. Tang, B. Xin, and M. L. Lee, *Journal of Chromatography A*, 1999, **837**, 35.
104 G. S. Chirica and V. T. Remcho, *Electrophoresis*, 2000, **21**, 3093.
105 L. Roed, E. Lundanes, and T. Greibrokk, *Journal of Chromatography A*, 2000, **890**, 347.
106 K. Cabrera, D. Lubda, H.-M. Eggenweiler, H. Minakuchi, and K. Nakanishi, *Journal of High Resolution Chromatography*, 2000, **23**, 93.

107 K. Miyamoto, T. Hara, H. Kobayashi, H. Morisaka, D. Tokuda, K. Horie, K. Koduki, S. Makino, O. Núñez, and C. Yang, *Analytical Chemistry*, 2008, **80**, 8741.
108 S. Miyazaki, M. Takahashi, M. Ohira, H. Terashima, K. Morisato, K. Nakanishi, T. Ikegami, K. Miyabe, and N. Tanaka, *Journal of Chromatography A*, 2011, **1218**, 1988.
109 K. B. Spilstead, S. J. Haswell, N. W. Barnett, X. A. Conlan, P. G. Stevenson, and P. S. Francis, *Analytical Methods*, 2015, **7**, 4908.
110 K. Nakanishi, *Journal of Porous Materials*, 1997, **4**, 67.
111 O. Núñez, K. Nakanishi, and N. Tanaka, *Journal of Chromatography A*, 2008, **1191**, 231.
112 R. Takahashi, S. Sato, T. Sodesawa, and T. Azuma, *Journal of Sol-gel Science and Technology*, 2004, **31**, 373.
113 K. Nakanishi, H. Minakuchi, N. Soga, and N. Tanaka, *Journal of Sol-gel Science and Technology*, 1998, **13**, 163.
114 P. Wagh, R. Begag, G. Pajonk, A. V. Rao, and D. Haranath, *Materials Chemistry and Physics*, 1999, **57**, 214.
115 J. H. Harreld, T. Ebina, N. Tsubo, and G. Stucky, *Journal of Non-Crystalline Solids*, 2002, **298**, 241.
116 N. Ishizuka, H. Kobayashi, H. Minakuchi, K. Nakanishi, K. Hirao, K. Hosoya, T. Ikegami, and N. Tanaka, *Journal of Chromatography A*, 2002, **960**, 85.
117 A. Frolova, M. Chukhlieb, A. Drobot, A. Kryshtal, L. Loginova, and A. Boichenko, *Open Surface Science Journal*, 2009, **1**, 40.
118 K. Nakanishi and N. Soga, *Journal of Non-Crystalline Solids*, 1992, **139**, 1.
119 J. Martin, B. Hosticka, C. Lattimer, and P. Norris, *Journal of Non-Crystalline Solids*, 2001, **285**, 222.
120 N. Tanaka, H. Kobayashi, N. Ishizuka, H. Minakuchi, K. Nakanishi, K. Hosoya, and T. Ikegami, *Journal of Chromatography A*, 2002, **965**, 35.
121 Z.-G. Shi, Y.-Q. Feng, L. Xu, S.-L. Da, and Y.-Y. Ren, *Microporous and Mesoporous Materials*, 2004, **68**, 55.
122 C. J. Brinker and G. W. Scherer, 'Sol-gel science: the physics and chemistry of sol-gel processing', Academic press, 2013.
123 L. L. Hench, 'Sol-gel silica: properties, processing and technology transfer', William Andrew, 1998.
124 K. Sinkó, *Materials*, 2010, **3**, 704.
125 M. Motokawa, H. Kobayashi, N. Ishizuka, H. Minakuchi, K. Nakanishi, H. Jinnai, K. Hosoya, T. Ikegami, and N. Tanaka, *Journal of Chromatography A*, 2002, **961**, 53.
126 H. M. Kirker, D. Meyers, and S. Chaudhuri, *J. Non-Cryst. Solids*, 1998, **225**, 14.
127 M.-A. Einarsrud, M. B. Kirkedelen, E. Nilsen, K. Mortensen, and J. Samseth, *Journal of Non-Crystalline Solids*, 1998, **231**, 10.
128 M.-A. Einarsrud, E. Nilsen, A. Rigacci, G. M. Pajonk, S. Buathier, D. Valette, M. Durant, B. Chevalier, P. Nitz, and F. Ehrburger-Dolle, *Journal of Non-Crystalline Solids*, 2001, **285**, 1.
129 S. Dai, Y. Ju, H. Gao, J. Lin, S. Pennycook, and C. Barnes, *Chem. Commun.*, 2000, 243.
130 G. Reichenauer, *Journal of Non-Crystalline Solids*, 2004, **350**, 189.
131 N. Ishizuka, H. Minakuchi, K. Nakanishi, K. Hirao, and N. Tanaka, *Colloids and Surfaces A: Physicochemical and Engineering Aspects*, 2001, **187**, 273.

132 S. Shrinivasan, M. C. Breadmore, B. Hosticka, J. P. Landers, and P. M. Norris, *Journal of Non-Crystalline Solids*, 2004, **350**, 391.
133 P. D. Fletcher, S. J. Haswell, P. He, S. M. Kelly, and A. Mansfield, *Journal of Porous Materials*, 2011, **18**, 501.
134 R. Takahashi, K. Nakanishi, and N. Soga, *Faraday Discussions*, 1995, **101**, 249.
135 K. Nakanishi, R. Takahashi, T. Nagakane, K. Kitayama, N. Koheiya, H. Shikata, and N. Soga, *Journal of Sol-gel Science and Technology*, 2000, **17**, 191.
136 K. Nakanishi, H. Minakuchi, N. Soga, and N. Tanaka, *Journal of Sol-Gel Science and Technology*, 1997, **8**, 547.
137 G. Puy, R. Roux, C. Demesmay, J.-L. Rocca, J. Iapichella, A. Galarneau, and D. Brunel, *Journal of Chromatography A*, 2007, **1160**, 150.
138 A. Galarneau, J. Iapichella, D. Brunel, F. Fajula, Z. Bayram - Hahn, K. Unger, G. Puy, C. Demesmay, and J. L. Rocca, *Journal of Separation Science*, 2006, **29**, 844.
139 R. Takahashi, K. Nakanishi, and N. Soga, *Journal of Sol-gel Science and Technology*, 2005, **33**, 159.
140 K. Cabrera, *Journal of Separation Science*, 2004, **27**, 843.
141 M. Yoo, D. Hage, and P. Wang, *St Albans: ILM*, 2010.
142 M. Al-Bokari, D. Cherrak, and G. Guiochon, *Journal of Chromatography A*, 2002, **975**, 275.
143 H. Kobayashi, T. Ikegami, H. Kimura, T. HARA, D. TOKUDA, and N. TANAKA, *Analytical Sciences*, 2006, **22**, 491.
144 D. E. Raynie, *Analytical Chemistry*, 2006, **78**, 3997.
145 N. Fontanals, R. Marcé, and F. Borrull, *Journal of Chromatography A*, 2007, **1152**, 14.
146 T. Nema, E. C. Chan, and P. C. Ho, *Journal of Pharmaceutical and Biomedical Analysis*, 2014, **87**, 130.
147 A. Namera, A. Nakamoto, T. Saito, and S. Miyazaki, *Journal of Separation Science*, 2011, **34**, 901.
148 S. Xie, F. Svec, and J. M. Fréchet, *Chemistry of Materials*, 1998, **10**, 4072.
149 C. Yu, M. H. Davey, F. Svec, and J. M. Fréchet, *Analytical Chemistry*, 2001, **73**, 5088.
150 A. Namera and T. Saito, *TrAC Trends in Analytical Chemistry*, 2013, **45**, 182.
151 Y. Shintani, X. Zhou, M. Furuno, H. Minakuchi, and K. Nakanishi, *Journal of Chromatography A*, 2003, **985**, 351.
152 L. Jia, N. Tanaka, and S. Terabe, *Journal of Chromatography A*, 2004, **1053**, 71.
153 J. Bones, K. Thomas, P. N. Nesterenko, and B. Paull, *Talanta*, 2006, **70**, 1117.
154 S. Yu, J. Geng, P. Zhou, J. Wang, A. Feng, X. Chen, H. Tong, and J. Hu, *Analytica Chimica Acta*, 2008, **611**, 173.
155 J. Hu, X. Li, Y. Cai, and H. Han, *Journal of Separation Science*, 2009, **32**, 2759.
156 T. Kumazawa, C. Hasegawa, X.-P. Lee, and K. Sato, *Forensic Toxicology*, 2010, **28**, 61.
157 A. Nakamoto, A. Namera, M. Nishida, M. Yashiki, T. Kuramoto, Y. Takei, M. Furuno, H. Minakuchi, K. Nakanishi, and K. Kimura, *Forensic Toxicology*, 2006, **24**, 75.

158 S. Miyazaki, K. Morisato, N. Ishizuka, H. Minakuchi, Y. Shintani, M. Furuno, and K. Nakanishi, *Journal of Chromatography A*, 2004, **1043**, 19.
159 L. Xu and H. K. Lee, *Journal of Chromatography A*, 2009, **1216**, 5483.
160 T. Saito, R. Yamamoto, S. Inoue, I. Kishiyama, S. Miyazaki, A. Nakamoto, M. Nishida, A. Namera, and S. Inokuchi, *Journal of Chromatography B*, 2008, **867**, 99.
161 F. Naoto, *Journal of Chromatography Separation Techniques*, 2012.
162 T. Nema, E. Chan, and P. Ho, *Journal of Mass Spectrometry*, 2011, **46**, 891.
163 T. Nema, E. C. Chan, and P. C. Ho, *Journal of Separation Science*, 2011, **34**, 1041.
164 P. Jal, S. Patel, and B. Mishra, *Talanta*, 2004, **62**, 1005.
165 C. Yang, T. Ikegami, T. Hara, and N. Tanaka, *Journal of Chromatography A*, 2006, **1130**, 175.
166 N. Kanellopoulos, 'Nanoporous materials: Advanced techniques for characterization, modeling, and processing', CRC Press, 2011.
167 K. S. Sing, *Pure and applied chemistry*, 1985, **57**, 603.
168 B. Mattiasson, A. Kumar, and I. Y. Galeaev, 'Macroporous polymers: production properties and biotechnological/biomedical applications', CRC Press, 2009.
169 F. Svec, *Journal of Chromatography A*, 2012, **1228**, 250.
170 I. Nischang, *Journal of Chromatography A*, 2013, **1287**, 39.
171 P. Jandera, *Journal of Chromatography A*, 2013, **1313**, 37.
172 X. Huang and D. Yuan, *Critical Reviews in Analytical Chemistry*, 2012, **42**, 38.
173 F. C. Leinweber and U. Tallarek, *Journal of Chromatography A*, 2003, **1006**, 207.
174 I. Nischang, I. Teasdale, and O. Brüggemann, *Analytical and Bioanalytical Chemistry*, 2011, **400**, 2289.
175 I. Nischang, I. Teasdale, and O. Brüggemann, *Journal of Chromatography A*, 2010, **1217**, 7514.
176 E. S. Alzahrani, 'Investigation of monolithic materials for protein sample preparation', University of Hull, 2012.
177 S. Xie, R. W. Allington, J. M. Fréchet, and F. Svec, in 'Porous polymer monoliths: an alternative to classical beads', 2002.
178 I. M. Lazar, L. Li, Y. Yang, and B. L. Karger, *Electrophoresis*, 2003, **24**, 3655.
179 M. Kele and G. Guiochon, *Journal of Chromatography A*, 2002, **960**, 19.
180 S. L. Cohen and B. T. Chait, *Analytical Chemistry*, 1996, **68**, 31.
181 E. C. Peters, F. Svec, J. M. Fréchet, C. Viklund, and K. Irgum, *Macromolecules*, 1999, **32**, 6377.
182 V. Samanidou, A. Ioannou, and I. Papadoyannis, *Journal of Chromatography B*, 2004, **809**, 175.
183 K. Cabrera, G. Wieland, D. Lubda, K. Nakanishi, N. Soga, H. Minakuchi, and K. K. Unger, *TrAC Trends in Analytical Chemistry*, 1998, **17**, 50.
184 A. Gambero, L. T. Kubota, Y. Gushikem, C. Airoldi, J. M. Granjeiro, E. M. Taga, and E. F. Alcântara, *Journal of Colloid and Interface Science*, 1997, **185**, 313.
185 Y. Ueki, T. Umemura, J. Li, T. Odake, and K.-i. Tsunoda, *Analytical Chemistry*, 2004, **76**, 7007.
186 E. Alzahrani and K. Welham, *Analyst*, 2012, **137**, 4751.

187 C. Viklund, E. Pontén, B. Glad, K. Irgum, P. Hörstedt, and F. Svec, *Chemistry of Materials*, 1997, **9**, 463.
188 F. Svec, *Journal of Chromatography A*, 2010, **1217**, 902.
189 A. Namera, A. Nakamoto, M. Nishida, T. Saito, I. Kishiyama, S. Miyazaki, M. Yahata, M. Yashiki, and M. Nagao, *Journal of Chromatography A*, 2008, **1208**, 71.
190 D. Luo, F. Chen, K. Xiao, and Y.-Q. Feng, *Talanta*, 2009, **77**, 1701.
191 J. C. Jokerst, J. M. Emory, and C. S. Henry, *Analyst*, 2012, **137**, 24.
192 K. Rogers, *Analytica Chimica Acta*, 2006, **568**, 222.
193 A. Hulanicki, S. Glab, and F. Ingman, *Pure and Applied Chemistry*, 1991, **63**, 1247.
194 A. Manz, E. Verpoorte, D. E. Raymond, C. S. Effenhauser, N. Burggraf, and H. M. Widmer, Micro Total Analysis Systems, 1995, p. 5.
195 P. K. Sekhar, E. L. Brosha, R. Mukundan, and F. H. Garzon, *The Electrochemical Society Interface*, 2010, **19**, 35.
196 J. Ŗuzicka and E. Hansen, *Analytica Chimica Acta*, 1975, **78**, 145.
197 A. Roda, 'Chemiluminescence and bioluminescence: past, present and future', Royal Society of Chemistry, 2011.
198 M. Trojanowicz, 'Advances in flow analysis', John Wiley & Sons, 2008.
199 M. Miró and E. H. Hansen, *Analytica Chimica Acta*, 2007, **600**, 46.
200 A. Manz, N. Graber, and H. á. Widmer, *Sensors and Actuators B: Chemical*, 1990, **1**, 244.
201 A. W. Chow, *AIChE Journal*, 2002, **48**, 1590.
202 G. M. Whitesides, *Nature*, 2006, **442**, 368.
203 H.-F. Li and J.-M. Lin, *Analytical and Bioanalytical Chemistry*, 2009, **393**, 555.
204 G. Chen, Y. Lin, and J. Wang, *Talanta*, 2006, **68**, 497.
205 F. H. Labeed and H. O. Fatoyinbo, 'Microfluidics in Detection Science: Lab-on-a-chip Technologies', Royal Society of Chemistry, 2014.
206 P. N. Nge, C. I. Rogers, and A. T. Woolley, *Chemical Reviews*, 2013, **113**, 2550.
207 D. R. Reyes, D. Iossifidis, P.-A. Auroux, and A. Manz, *Analytical Chemistry*, 2002, **74**, 2623.
208 J. Pihl, J. Sinclair, M. Karlsson, and O. Orwar, *Materials Today*, 2005, **8**, 46.
209 D. Kim and A. E. Herr, *Biomicrofluidics*, 2013, **7**, 041501.
210 C. W. Price, D. C. Leslie, and J. P. Landers, *Lab on a Chip*, 2009, **9**, 2484.
211 K. F. Jensen, *MRS bulletin*, 2006, **31**, 101.
212 U. M. Attia, S. Marson, and J. R. Alcock, *Microfluidics and Nanofluidics*, 2009, **7**, 1.
213 R. Pelton, *TrAC Trends in Analytical Chemistry*, 2009, **28**, 925.
214 S.-E. Ong, S. Zhang, H. Du, and Y. Fu, *Front Biosci*, 2008, **13**, 2757.
215 A. Smirnova, K. Mawatari, A. Hibara, M. A. Proskurnin, and T. Kitamori, *Analytica Chimica Acta*, 2006, **558**, 69.
216 A. Smirnova, K. Shimura, A. Hibara, M. A. Proskurnin, and T. Kitamori, *Analytical Sciences*, 2007, **23**, 103.
217 A. Smirnova, K. Shimura, A. Hibara, M. A. Proskurnin, and T. Kitamori, *Journal of Separation Science*, 2008, **31**, 904.
218 T. McCreedy, *TrAC Trends in Analytical Chemistry*, 2000, **19**, 396.
219 G. S. Fiorini and D. T. Chiu, *BioTechniques*, 2005, **38**, 429.

220 S.-J. J. Lee and N. Sundararajan, 'Microfabrication for microfluidics', Artech House, 2010.
221 A. Webster, J. Greenman, and S. J. Haswell, *Journal of Chemical Technology and Biotechnology*, 2011, **86**, 10.
222 L. Marle, 'Miniaturised analytical systems with chemiluminescence detection for environmental applications', University of Hull, 2006.
223 A. Manz, N. Pamme, D. Iossifidis, and D. Lossifidis, 'Bioanalytical chemistry', World Scientific, 2004.
224 S. Haeberle and R. Zengerle, *Lab on a Chip*, 2007, **7**, 1094.
225 L. Marton and C. Marton, 'Fluid Dynamics. Methods of Experimental Physics, Volume 18', Elsevier Science & Technology, 1981.
226 H. A. Stone, A. D. Stroock, and A. Ajdari, *Annu. Rev. Fluid Mech.*, 2004, **36**, 381.
227 P. Atkins and J. de Paula, 'Elements of Physical Chemistry', Oxford University Press, 2005.
228 X. Zhang and S. Haswell, in 'Micro-fluidic and lab-on-a-chip technology', 2007.
229 J. C. Gertsch, S. D. Noblitt, D. M. Cropek, and C. S. Henry, *Analytical Chemistry*, 2010, **82**, 3426.
230 N. Hudson, A. Baker, and D. Reynolds, *River Research and Applications*, 2007, **23**, 631.
231 R. R. Hood, C. Shao, D. M. Omiatek, W. N. Vreeland, and D. L. DeVoe, *Pharmaceutical Research*, 2013, **30**, 1597.
232 R. Hood, W. Vreeland, and D. DeVoe, *Lab on a Chip*, 2014, **14**, 3359.
233 P. Yáñez-Sedeño, L. Agüí, R. Villalonga, and J. Pingarrón, *Analytica Chimica Acta*, 2014, **823**, 1.
234 E. K. Sackmann, A. L. Fulton, and D. J. Beebe, *Nature*, 2014, **507**, 181.
235 A. J. Mach, O. B. Adeyiga, and D. Di Carlo, *Lab on a Chip*, 2013, **13**, 1011.
236 M. Bowden, M. Sequiera, J. P. Krog, P. Gravesen, and D. Diamond, *Journal of Environmental Monitoring*, 2002, **4**, 767.
237 M. Bowden, M. Sequeira, J. P. Krog, P. Gravesen, and D. Diamond, *Analyst*, 2002, **127**, 1.
238 C. M. McGraw, S. E. Stitzel, J. Cleary, C. Slater, and D. Diamond, *Talanta*, 2007, **71**, 1180.
239 Y. Ueno, T. Horiuchi, O. Niwa, H.-S. Zhou, T. Yamada, and I. Honma, *Sensors and Actuators B: Chemical*, 2003, **95**, 282.
240 E. Iannone, 'Labs on chip: Principles, design and technology', CRC Press, 2014.
241 A. M. Garcia-Campana, 'Chemiluminescence in analytical chemistry', CRC Press, 2001.
242 D. C. Harris, 'Quantitative chemical analysis', Macmillan, 2010.
243 T. H. Fereja, A. Hymete, and T. Gunasekaran, *ISRN Spectroscopy*, 2013, **2013**.
244 J. R. Totter, in 'Bioluminescence and chemiluminescence: Basic chemistry and analytical applications: Edited by Marlene A. DeLuca and William D. McElroy, Academic Press, New York/London, 1981, 782 pp. $44.00', 1981.
245 D. Christodouleas, C. Fotakis, A. Economou, K. Papadopoulos, M. Timotheou-Potamia, and A. Calokerinos, *Analytical Letters*, 2011, **44**, 176.
246 M. Sauer, J. Hofkens, and J. Enderlein, 'Handbook of fluorescence spectroscopy and imaging: from ensemble to single molecules', John Wiley & Sons, 2010.

247 E. Tyrrell, 'Development of a microfluidic based analytical system for copper monitoring in environmental water samples', Dublin City University, 2005.
248 J. Xie, M. Demarteau, R. Wagner, E. May, J. Zhang, M. Ruiz-Oses, X. Liang, I. Ben-Zvi, K. Attenkofer, and S. Schubert, SPIE Optical Engineering+ Applications, 2013, p. 884705.
249 Y. Gou, R. Eisert, and J. Pawliszyn, *Journal of Chromatography A*, 2000, **873**, 137.
250 X. Wang, J.-M. Lin, M.-L. Liu, and X.-L. Cheng, *TrAC Trends in Analytical Chemistry*, 2009, **28**, 75.
251 A. Waseem, M. Yaqoob, and A. Nabi, *Luminescence*, 2007, **22**, 349.
252 M. Palomeque, J. G. Bautista, M. C. Icardo, J. G. Mateo, and J. M. Calatayud, *Analytica Chimica Acta*, 2004, **512**, 149.
253 J. A. M. Pulgarín, A. A. Molina, and P. F. López, *Talanta*, 2006, **68**, 586.
254 J. F. Huertas-Pérez, A. M. García-Campaña, L. Gámiz-Gracia, A. González-Casado, and M. del Olmo Iruela, *Analytica Chimica Acta*, 2004, **524**, 161.
255 J. F. Huertas-Pérez, L. Gámiz-Gracia, A. M. García-Campaña, A. González-Casado, and J. L. M. Vidal, *Talanta*, 2005, **65**, 980.
256 L. Nollet and H. Rathore, 2010.
257 A. Waseem, M. Yaqoob, A. Nabi, and M. A. Siddiqui, *International Journal of Environmental and Analytical Chemistry*, 2007, **87**, 825.
258 A. N. Diaz, V. Bracho, M. Algarra, and F. Garcia Sanchez, *Analytical Letters*, 2008, **41**, 3210.
259 L. J. Nelstrop, P. A. Greenwood, and G. M. Greenway, *Lab on a Chip*, 2001, **1**, 138.
260 X.-J. Huang, Q.-S. Pu, and Z.-L. Fang, *Analyst*, 2001, **126**, 281.
261 K. TSUKAGOSHI, M. HASHIMOTO, R. NAKAJIMA, and A. ARAI, *Analytical Sciences*, 2000, **16**, 1111.
262 X. Y. H. J. N. WANG and L. C. J. C. REN, 2004.
263 A. M. Jorgensen, K. B. Mogensen, J. P. Kutter, and O. Geschke, *Sensors and Actuators B: Chemical*, 2003, **90**, 15.
264 L. Marle and G. M. Greenway, *Analytica Chimica Acta*, 2005, **548**, 20.
265 W. Som-Aum, H. Li, J. Liu, and J.-M. Lin, *Analyst*, 2008, **133**, 1169.
266 G. W. Kang and W. J. Cheong, *BULLETIN-KOREAN CHEMICAL SOCIETY*, 2006, **27**, 1459.
267 H. Zhong, F. L. Hastings, and F. P. Hain, *Journal of Agricultural and Food Chemistry*, 1994, **42**, 949.
268 M. T. Ahmed and S. M. Ismail, *Pesticide Science*, 1995, **44**, 197.
269 S. Samadi, H. Sereshti, and Y. Assadi, *Journal of Chromatography A*, 2012, **1219**, 61.
270 S. Haswell, *Analyst*, 1997, **122**, 1R.
271 P. Watts and S. J. Haswell, *Chemical Society Reviews*, 2005, **34**, 235.
272 J. F. Huertas-Pérez and A. M. García-Campaña, *Analytica Chimica Acta*, 2008, **630**, 194.
273 J. Guo, Y. Lu, and R. Whiting, *Bull. Korean Chem. Soc*, 2013, **34**, 447.
274 J. L. Gurav, I.-K. Jung, H.-H. Park, E. S. Kang, and D. Y. Nadargi, *Journal of Nanomaterials*, 2010, **2010**, 23.
275 A. K. Khattab, 'Fabrication, functionalization and characterization of silica monolith for forensic chemistry applications', University of Hull, 2014.
276 S. Zhou, H. Chen, B. Wu, C. Ma, and Y. Ye, *Microchimica Acta*, 2012, **176**, 419.

277 J. Lee and H. Seliger, *Photochemistry and Photobiology*, 1972, **15**, 227.
278 X. Liu, A. Li, C. Wu, and J. Lu, *Analytical Letters*, 2007, **40**, 2737.
279 J. Wang, C. Zhang, H. Wang, F. Yang, and X. Zhang, *Talanta*, 2001, **54**, 1185.
280 J. L. Adcock, P. S. Francis, and N. W. Barnett, *Analytica Chimica Acta*, 2007, **601**, 36.
281 P. Khan, D. Idrees, M. A. Moxley, J. A. Corbett, F. Ahmad, G. von Figura, W. S. Sly, A. Waheed, and M. I. Hassan, *Applied Biochemistry and Biotechnology*, 2014, **173**, 333.
282 H. Chen, F. Gao, R. He, and D. Cui, *Journal of Colloid and Interface Science*, 2007, **315**, 158.
283 H. C. Yao, X. F. Yang, and H. Li, *Journal of the Chinese Chemical Society*, 2007, **54**, 949.
284 C. Gómez-Benito, S. Meseguer-Lloret, and S. Torres-Cartas, *International Journal of Environmental Analytical Chemistry*, 2013, **93**, 152.
285 T. Pérez-Ruiz, C. Martínez-Lozano, and M. D. García, *Analytica Chimica Acta*, 2007, **584**, 275.
286 G. Z. Tsogas, D. L. Giokas, P. G. Nikolakopoulos, A. G. Vlessidis, and N. P. Evmiridis, *Analytica Chimica Acta*, 2006, **573**, 354.
287 F. J. Stevenson, 'Humus chemistry: genesis, composition, reactions', John Wiley & Sons, 1994.
288 D. Hamilton, A. Ambrus, R. Dieterle, A. Felsot, C. Harris, P. Holland, A. Katayama, N. Kurihara, J. Linders, and J. Unsworth, *Pure and Applied Chemistry*, 2003, **75**, 1123.

Chapter 9: Presentations and Conferences

J.S. Algethami, S.J. Haswell, "Pesticide pre-concentration using functionalised silica monoliths for environmental field analysis", The 38th International Symposium on Environmental Analytical Chemistry (ISEAC38), Lausanne, Switzerland (2014).

J.S. Algethami, S.J. Haswell, "Pesticide pre-concentration using functionalised silica monoliths for environmental field analysis", Chemistry Colloquium, University of Hull, United Kingdom (2014).

J.S. Algethami, S.J. Haswell, "Development of functionalised silica monoliths for environmental analysis in the field", The 6th Saudi Scientific International Conference, Brunel University, United Kingdom (2012).

J.S. Algethami, S.J. Haswell, "Development of functionalised silica monolith structures for the separation of compounds of environmental important", Chemistry Colloquium, University of Hull, United Kingdom (2013).

- Conference attended, The 18th International Symposium on Bioluminescence and Chemiluminescence (ISBC2014), University of Uppsala, Sweden (2014).

- Conference attended, Analytical Research Forum (ARF), Durham University, United Kingdom (2012).

- Symposium attended, Royal Society of Chemistry (RSC) Awards Symposium, University of Hull, United Kingdom (2012).